UNIVERSITÀ DEGLI STUDI DI UDINE
hic sunt futura

www.uniud.it

Corso di dottorato di ricerca in:

Scienze Biomediche e Biotecnologiche

in convenzione con Centro di Riferimento Oncologico di Aviano (CRO) IRCCS

Ciclo 31°

Transcriptome analysis identifies ETV6-NTRK3 and PTCH1-GLI1 as novel gene fusions involved in Gastrointestinal Stromal Tumors and Myoepithelial Tumors

Dottoranda
Dominga Racanelli

Supervisore
Dott.ssa Roberta Maestro

Anno 2019

INDEX

ABSTRACT

Gastrointestinal Stromal Tumors (GIST) are the most common mesenchymal tumors of the gastrointestinal tract. They feature, for the vast majority, *KIT* or *PDGFRA* mutations; less frequently *BRAF*, *KRAS*, *PIK3CA*, *NF1* or *SDH* alterations. In about 10% of all GIST no distinct genetic alteration has been identified and this subset of tumors, defined as 'quadruple negative GIST', feature an overall poor response to standard treatments. In an attempt to better define 'quadruple negative GIST' pathobiology we investigate the possible involvement of fusion genes. RNA-sequencing followed by fusion gene analysis was performed in a series of 5 such tumors. Intriguingly, an *ETV6-NTRK3* fusion was detected in one case. Stemming from our results, other GIST cases with the *ETV6-NTRK3* fusion have been identified and included in a clinical trial with Larotrectinib, a novel drug targeting NTRK proteins, demonstrating a good response.

Myoepithelial tumors (MyoT) are an uncommon heterogeneous group of tumors of uncertain differentiation. *EWSR1*, *FUS* or *PLAG1* fusion genes (with different partners) and *SMARCB1* deletions are genetic alterations already described in these tumors. A significant fraction of them still remain "orphan" of genetic marker due to the absence of known fusions. We performed RNA-sequencing and fusion gene detection in a series of 7 such tumors in order to identify novel fusion transcripts involved in their pathogenesis. Intriguingly one case turned out to express a *PTCH1-GLI1* fusion that involved, respectively, the receptor and the nuclear effector of the Hedgehog (HH) pathway. This chimera worked as a hyperactive GLI1 allele by inducing HH canonical target genes and sustaining GLI1 autoregolatory loop.

Finally, in an attempt to both dissect molecular diversity of MyoT and the closely related entity Extraskeletal Myxoid Chondrosarcoma (EMC) and to possible better define MyoT pathobiology, RNA-sequencing profiling was extended on a set of 12 EMC samples. Transcriptome profiles of the two entities were then compared. Overall, our results indicate that MyoT are a heterogeneous group of tumors that represent a distinct entity compared to EMC. Functional analysis with different bioinformatic tools suggested that, although heterogeneous, MyoT relied on common biologic signatures namely the activation of Hedgehog and WNT pathways.

INTRODUCTION

1. SARCOMA

Sarcomas are a highly heterogeneous group of malignancies of mesenchymal nature. They are conventionally classified into two broad categories: i) soft tissue sarcomas (STS) that include tumors with histological resemblance to fat, muscle, nerve sheath and blood vessels and ii) sarcomas of the bone. Indeed, diversification within these two groups includes more than 50 histological subtypes (Fletcher et al., 2013). Clinicopathological classification of sarcomas is largely based on cell morphology, lineage of differentiation and site of origin (Brenca and Maestro, 2015).

1.1 Epidemiology of sarcoma

Sarcomas are rare, representing about 1% of all malignant neoplasms in the adult but accounting for > 10% of pediatric tumors (Mackall et al., 2002). As regard STS, the estimated incidence in the United States and Europe is between 3 and 4 per 100.000 (Miettinen, 2016). However the true incidence of STS is considered to be underestimated, as the diagnosis of sarcoma may be complex and some sarcomas are likely misdiagnosed (Hui, 2016).

1.2 Genetics of sarcoma

Cancer cytogenetics allowed the identification of the first chromosomal marker in a tumor in 1960s with the detection of Philadelphia chromosome; then the advent of chromosome banding, in the 1970s, paved the way for the detection of chromosomal aberrations in hematologic malignancies (Miettinen, 2016). As regarding sarcoma cytogenetics, only in the early 1980s the description of a specific chromosome rearrangement, in Ewing sarcoma, introduced genetic approaches for studying chromosome changes in other tumors of mesenchymal origin (Aurias et al., 1983; Miettinen, 2016).
Genetic classification distinguishes sarcomas into two main groups: i) tumors with non-specific genetic alterations and complex unbalanced karyotype (Antonescu, 2006; Lauer and Gardner, 2013); ii) tumors with relatively simple karyotype, characterized by specific genetic aberrations including chromosomal translocations, amplifications or oncogenic mutations.

1.2.1 Complex-karyotype sarcoma

About half of STS are characterized by complex and unbalanced genetic changes such as chromosome gains and losses, nonreciprocal unbalanced translocations, chromosome markers, high inter and intratumor heterogeneity and, sometimes, chromothripsis (Antonescu, 2006; Bridge, 2014; Lauer and Gardner, 2013). This category can be further divided into: i) tumors that harbour a reproducible pattern of genomic rearrangements and/or involved chromosomal breakpoints that allow accurate nosology when associated to

other clinicohistopathologic features; ii) tumors with a high degree of genomic complexity and instability for which genetic approaches are not used (Bridge, 2014).

The recent sequencing effort of The Cancer Genome Atlas (TCGA) provided a detailed genomic and molecular landscape of 196 complex-karyotype sarcoma samples belonging to five subtypes namely dedifferentiated liposarcoma, leiomyosarcoma, undifferentiated pleomorphic sarcoma, myxofibrosarcoma and malignant peripheral nerve sheath tumor (Abeshouse et al., 2017). Overall, analyzed tumors were characterized predominantly by somatic copy number alterations that were more common in sarcoma if compared to most other tumor types profiled by the TCGA consortium. Genes belonging to the MDM2-p53 and the p16-CDK4-RB1 pathways resulted more frequently affected. Mutation burden was low (1.06 per Mb) and TP53, ATRX and RB1 were the only significantly mutated genes. In this study, sarcomas were also investigated for potential driver mutations in known oncogenes and tumor suppressors: 67% resulted to contain at least one variant in a gene known to be involved in cancer progression, although few in known cancer hotspots (Abeshouse et al., 2017).

1.2.2 Simple-karyotype sarcoma

Oncogenic mutations

The archetypical simple-karyotype sarcoma harbouring specific oncogenic mutations is gastrointestinal stromal tumor (GIST, about 1/3 of all STS), discussed in detail in chapter 2. Another example in this category is represented by tumors that feature SMARCB1/INI1 loss of expression, in particular malignant rhabdoid tumor (Lee et al., 2012) and epithelioid sarcoma (Modena et al., 2005). Different molecular mechanisms of SMARCB1/INI1 loss of expression have been described and include *SMARCB1* mutations (frameshift, nonsense or splice site), whole-gene deletions, promoter methylation or overexpression of targeting miRNAs (Miettinen, 2016).

Translocations

Approximately one third of all sarcomas (Borden et al., 2003; Bridge and Cushman-Vokoun, 2011) are characterized by specific recurrent chromosomal translocations that most commonly result in the production of a highly specific fusion gene. Translocations can be reciprocal or nonreciprocal/unbalanced. They often represent the only karyotype aberration in a sarcoma case and thus have been supposed the initiating oncogenic event (Julia A. Bridge and Cushman-Vokoun 2011). A role in tumor maintenance has also been recognized, as a tumor-specific translocation is present throughout the clinical course of the sarcoma (Bridge, 2008). A summary of sarcoma-associated fusion genes is provided in table 1.

Table 1. Sarcoma-associated fusion genes (Brenca and Maestro, 2015)

TUMOR	GENE FUSION	CYTOGENETIC ABERRATION	APPROXIMATE PREVALENCE	FUNCTION
Adipocytic tumors				
Lipoma	EBF1-LOC204010	t(5;12)(q33;q14)	NA	NA
	HMGA2-CXCR7	t(2;12)(q37;q14)	HMGA2 fusions: 30%	Putative TF
	HMGA2-EBF1	t(5;12)(q33;q14)		TF
	HMGA2-LHFP	t(12;13)(q14;q13)		TF
	HMGA2-LPP	t(3;12)(q28;q14)		TF
	HMGA2-NFIB	t(9;12)(p22;q14)		Putative TF
	HMGA2-PPAP2B	t(1;12)(p32;q14)		Putative TF
	HMGA1-LPP	t(3;6)(q27;p21)	10%	TF
	LPP-C12orf9	t(3;12)(q28;14)	NA	NA
Lipoblastoma	COL1A2-PLAG1	t(7;8)(q21q12)	PLAG1 fusions: 80%	TF
	HAS2-PLAG1	del(8)(q12q24)		TF
	PLAG1-RAD51L1	t(8;14)(q12;q24)		TF
	COL3A1/PLAG1	t(2;8)(q31;q12.1)		TF
Chondroid lipoma	C11orf95-MKL2	t(11;16)(q13;p13)	NA	NA
Myxoid/round cell liposarcoma	FUS-DDIT3	t(12;16)(q13;p11)	>90%	TF
	EWSR1-DDIT3	t(12;22)(q13;q12)	>10%	TF
Dedifferentiated liposarcoma	CNOT2-ASTN2	t(9;12)(q33;q15)	NA	Putative TF
	CTDSP2-FAM19A2	?t(12)(q14q14)	NA	NA
	NR6A1-TRHDE	t(9;12)(q33;q21)	NA	NA
	NUP107-LGR5	?t(12)(q15q21)	NA	NA
	NUP107-PAPPA	t(9;12)(q33;q15)	NA	NA
	RCOR1-WDR70	t(5;14)(p13;q32)	NA	NA
Fibroblastic/myofibroblastic tumors				
Soft tissue angiofibroma	AHRR-NCOA2	t(5;8)(p15;q13)	NA	Putative TF
	GTF2I-NCOA2	t(7;8;14)(q11;q13;q31)	NA	Putative TF
Dermatofibrosarcoma protuberans	COL1A1-PDGFB	t(17;22)(q21;q13)	>90%	GF
Solitary fibrous tumor	NAB2-STAT6	inv(12)(q13q13)	>95%	TF
Infantile fibrosarcoma	ETV6-NTRK3	t(12;15)(p13;q25)	>95%	TK
Low-grade fibromyxoid sarcoma	FUS-CREB3L2	t(7;16)(q34;p11)	>95%	TF
	FUS-CREB3L1	t(11;16)(p11;p11)	< 5%	TF
	EWSR1-CREB3L1	t(11;22)(p11;q12)	NA	TF
Sclerosing epithelioid fibrosarcoma	FUS-CREB3L2	t(7;16)(q34;p11)	FUS fusions:10-25%	TF
	FUS-CREB3L1	t(11;16)(p13;p11)		TF
	EWSR1-CREB3L1	t(11;22)(p11;q12)	NA	TF
Inflammatory myofibroblastic tumor	CARS-ALK	t(2;11)(p23;p15)	ALK fusions: 75%	TK
	SEC31A-ALK	t(2;4)(p23;q21)		TK
	ATIC-ALK	inv(2)(p23;q35)		TK
	RANBP2-ALK	t(2;2)(p23;q13)		TK
	CLTC-ALK	t(2;17)(p23;q23)		TK
	TPM3-ALK	t(1;2)(q21;p23)		TK
	TPM4-ALK	t(2;19)(p23;p13)		TK
	PPFIBP1-ALK	t(2;12)(p23;p11)		TK
	RREB1-TFE3	t(X;6)(p11;p24)	NA	Putative TF
	MGEA5-TGFBR3	t(1;10)(p22;q24)	NA	GF
	ETV6-NTRK3	t(12;15)(p13;q25)	NA	TK
Myxofibrosarcoma	KIAA2026-NUDT11	t(9;X)(p24;p11)	NA	NA
	CCBL1-ARL1	t(9;12)(q34-q23)	NA	NA
	AFF3-PHF1	t(2;6)(q12;p21)	NA	NA
So-called fibrohistiocytic tumors				
Tenosynovial giant cell tumor	COL6A3-CSF1	t(1;2)(p13;q37)	NA	GF
Smooth muscle tumors				
Leiomyoma of the uterus	CUX1-AGR3	inv(7)(p21q22)	NA	Putative TF
	HMGA2-CCNB1IP1	t(12;14)(q14;q11)	HMGA2 fusions: 10%	Putative TF
	HMGA2-COG5	t(7;12)(q31;q14)		
	HMGA2-COX6C	t(8;12)(q22;q14)		
	HMGA2-RAD51L1	t(12;14)(q14;q24)		
Pericytic (perivascular) tumors				
Pericytoma with t(7;12)	ACTB-GLI1	t(7;12)(p22;q13)	NA	TF
Skeletal muscle tumors				
Alveolar rhabdomyosarcoma	PAX3-FOXO1	t(2;13)(q35;q14)	75%	TF
	PAX7-FOXO1	t(1;13)(p36;q14)	20%	TF
	PAX3-FOXO4	t(X;2)(q13;q36)	NA	TF
	PAX3-NCOA1	t(2;2)(p23;q36)	NA	TF
	PAX3-NCOA2	t(2;8)(q36;q13)	NA	TF
	FOXO1-FGFR1	t(8;13;9)(p11;q14;q32)	NA	GF
Spindle cell rhabdomyosarcoma	SRF-NCOA2	t(6;8)(p21;q13)	NA	Putative TF

	TEAD1-NCOA2	t(8;11)(q13;p15)	NA	
Vascular tumors				
Epithelioid hemangioendothelioma	WWTR1-CAMTA1	t(1;3)(p36;q25)	85%	Putative TF
	YAP1-TFE3	t(X;11)(p11;q22)	NA	Putative TF
Tumors of uncertain differentiation				
Angiomatoid fibrous histocytoma	EWSR1-CREB1	t(2;22) (q33;q12)	72%	TF
	FUS-ATF1	t(12;16) (q13;p11)	7%	TF
	EWSR1-ATF1	t(12;22) (q13;q12)	21%	TF
Ossifying fibromyxoid tumor	EP400-PHF1	t(6;12) (p21;q24)	40-50%	TF
	MEAF6-PHF1	t(1;6)(p34;p21)	NA	Putative TF
	ZC3H7B-BCOR	t(X;22)(p11;q13)	NA	Putative TF
Myoepithelial tumor	EWSR1-ATF1	t(12;22) (q13;q12)	NA	TF
	EWSR1-PBX1	t(1;22) (q23;q12)	NA	Putative TF
	EWSR1-POU5F1	t(6;22) (p21;q12)	NA	TF
	EWSR1-ZNF444	t(19;22) (q13;q12)	NA	Putative TF
	EWSR1-KLF17	t(1;22) (p34;q12)	NA	Putative TF
	EWSR1-PBX3	t(9;22) (q12;q33)	NA	Putative TF
	FUS-KLF17	t(1;16) (p34;p11)	NA	Putative TF
	FUS-POU5F1	t(6;16) (p21;p11)	NA	Putative TF
	PLAG1-LIFR	t(5;8) (p13;q12)	NA	Putative TF
Synovial sarcoma	SS18-SSX1	t(X;18) (p11;q11)	65%	TF
	SS18-SSX2	t(X;18) (p11;q11)	35%	TF
	SS18-SSX4	t(X;18) (p11;q11)	<1%	TF
	SS18L1-SSX1	t(X;20) (p11;q13)	NA	TF
Alveolar soft part sarcoma	ASPSCR1-TFE3	t(X;17) (p11;q25)	>95%	TF
Clear cell sarcoma	EWSR1-ATF1	t(12;22) (q13;q12)	90% soft tissue; 10% gastrointestinal tract	TF
	EWSR1-CREB1	t(2;22) (q33;q12)	90% gastrointestinal tract; 10% soft tissue	TF
	IRX2-TERT	del(5)(p15.33)	NA	NA
Extraskeletal myxoid chondrosarcoma	EWSR1-NR4A3	t(9;22) (q31;q12)	60-75%	TF
	TAF15-NR4A3	t(9;17) (q31;q12)	about 30%	TF
	TFG-NR4A3	t(3;9) (q12;q31)	<1%	TF
	TCF12-NR4A3	t(9;15) (q31;q21)	<1%	TF
	HSPA8-NR4A3	t(9;11)(q22;q24)	NA	TF
Desmoplastic small round cell tumor	EWSR1-EWT1	t(11;22) (p13;q12)	>95%	TF
	EWSR1-ERG	t(21;22) (q22;q12)	NA	TF
Ewing sarcoma and Ewing-like sarcomas	EWSR1-FLI1	t(11;22) (q24;q12)	90%	TF
	EWSR1-ERG	t(21;22) (q22;q12)	5%	TF
	FUS-ERG	der(21)t(16;21)	<1%	TF
	EWSR1-ETV1	t(7;22) (p21;q12)	<1%	TF
	EWSR1-ETV4	t(17;22) (q21;q12)		TF
	EWSR1-FEV	t(2;22) (q35;q12)		TF
	EWSR1-NFATC2	t(20;22) (q13;q12)	NA	TF
	EWSR1-PATZ1	inv(22) (q12q12)	NA	TF
	EWSR1-SMARCA5	t(4;22) (q31;q12)	NA	TF
	EWSR1-POU5F1	t(6;22)(p21;q12)	NA	TF
	EWSR1-SP3	t(2;22)(q31;q12)	NA	TF
	FUS-FEV	t(2;16)(q35;p11)	NA	TF
	CIC-DUX4	t(4;19)(q35;q13)	NA	TF
	CIC-FOXO4	t(X;19)(q13;q13.3)	NA	Putative TF
	BCOR-CCNB3	inv(X)(p11.4p11.22)	NA	TF
	FUS-NCATC2	t(16;20)(p11;q13)	NA	TF
	ETV6-NTRK3	t(12;15)(p13;q25)	NA	TK
Perivascular epithelioid cell tumors	SFPQ-TFE3	t(X;1)(p11;p34)	NA	NA
Undifferentiated/unclassified sarcomas				
Undifferentiated/unclassified sarcomas	BCOR-CCNB3	inv(X)(p11p11)	NA	TF
	CIC-DUX4	t(4;19)(q35;q13)	NA	TF
	EWSR1-POU5F1	t(6;22)(p21;q12)	NA	TF
	EWSR1-SP3	t(2;22)(q31;q12)	NA	TF
	MED12-PRDM10	t(X;11)(q13;q23)	NA	TF
	CITED2-PRDM10	t(6;11)(q24;q24)	NA	TF
Chondro-osseous tumors				
Soft tissue chondroma	HMGA2-LPP	t(3;12)(q28;q14)	NA	TF
Mesenchymal chondrosarcoma	HEY1-NCOA2	del(8)(q13;q21)	>90%	TF
	IRFBP2-CDX1	t(1;5)(q42;q32)	NA	TF
Miscellaneous tumors				
Endometrial sarcoma	EPC1-PHF1	t(6;10;10) (p21;q22;p1)	NA	TF
	JAZF1-PHF1	t(6;7)(p21;p15)	NA	TF

	JAZF1-SUZ12	t(7;17)(p15;q11)	NA	TF
	MEAF6-PHF1	t(1;6)(p34;p21)	NA	Putative TF
	YWHAE-FAM22A	t(10;17)(q23;p13)	NA	NA
	YWHAE-FAM22B	t(10;17)(q22;p13)	NA	NA
	ZC3H7B-BCOR	t(X;22)(p11;q13)	NA	Putative TF
	MBTD1-CXorf67	t(X;17)(p11;q21)	NA	NA
Epitheliod sarcoma of the ovary	CMKLR1-HNF1A	?t(12;12)(q23;q24)	NA	NA
	ERBB3-CRADD	?t(12;12)(q13;q22)	NA	NA
	SMARCB1-WASF2	t(1;22)(p36;q11)	NA	NA
Primary pulmonary myxoid sarcoma	EWSR1-CREB1	t(2;22)(q33;q12)	NA	TF

NA, not available; TF, transcription regulator; TK, kinase signaling regulator; GF, growth factor

Additional genetic changes may occur, in some cases, in sarcomas typified by a tumor-specific chromosomal translocation. Two most common such secondary changes (e.g. observed in myxoid liposarcoma, typified by the t(12;16) and t(12;22) that give rise, respectively, to *FUS-DDIT3* and *EWSR1-DDIT3* fusion genes) include chromosome 8 supernumerary copies and an unbalanced t(1;16) translocation, resulting in relative gain and loss of chromosome material on 1q and 16q, respectively (Miettinen, 2016).

The aberrant chimeric proteins generated following chromosome rearrangements in sarcomas can be functionally divided into three major groups: i) chimeric factors involved in transcriptional regulation that affect transcription profile ii) chimeric tyrosine kinases and iii) chimeric autocrine growth factors that both result in kinase signaling pathway deregulation (Miettinen, 2016).

For the first type, in most cases, the 5' partner gene provides a strong promoter as well as the N-terminal functional domain of the fusion protein (e.g. *EWSR1*, *FUS*) and so it determines the transactivation potential and expression level of the chimera (Antonescu, 2006); target specificity to the transcriptional activation function of the chimeric protein is conferred by the 3' partner gene, that contributes a DNA binding domain (e.g. *FLI1*, *ATF1*, *DDIT3*) (Antonescu, 2006; Rabbitts, 1994, 1999).

As regarding chimeric tyrosine kinases, they are commonly originated by the fusion of the catalytic domain of a tyrosine kinase receptor (e.g. NTRK3) with a ubiquitously expressed protein yielding a dimerization domain (e.g. ETV6): this event results in a constitutively activated, ligand independent, chimeric tyrosine kinase (Antonescu, 2006).

Lastly, the third type is a chimeric autocrine growth factor as seen with COL1A1-PDGFB in dermatofibrosarcoma protuberans: in this case, the fusion protein leads to autocrine growth stimulation through the PDGF receptor (Simon et al., 1997). Beyond translocations, also inversions, interstitial deletions (Miettinen, 2016) and, as we describe here, insertions are chromosomal structural rearrangements accounting for fusion gene formation.

In the context of fusion genes, molecular variants must be taken into consideration. They result, firstly, from the fusion of a gene with alternative partners. As an example, Extraskeletal Mixoid Chondrosarcoma (EMC, further described below) harbors specific reciprocal chromosomal rearrangements involving *NR4A3*. The most common is the t(9;22)(q22;q12) followed by the less frequent t(9;17)(q22;q11) which involves, respectively, *EWSR1* and *TAF15* genes. Occasional fusions with *TCF12* (15q21) or *TFG* (3q12) have been reported (Fletcher et al., 2013) and our laboratory has recently described a fusion of *NR4A3*

with *HSPA8* (11q24) (Urbini et al., 2017). Molecular variants are also the result of genomic breakpoint differences that lead to distinct exon combinations in fusion genes involving the same partners.
Finally, in some cases, fusion genes are associated with their amplification: *PAX7-FOXOA1* and *COL1A1-PDGFB* gain/amplification are secondary changes that increase the oncogenic potential of the chimera respectively in alveolar rhabdomyosarcoma and in dermatofibrosarcoma protuberans (Miettinen, 2016).

1.3 The role of fusion gene detection in sarcoma pathobiology

The introduction of genetic testing, primarily the detection of chromosomal rearrangements, refined STS classification which was previously based only on histological and clinical observations (Antonescu, 2006). In particular, the identification of the same chromosome rearrangement in previously distinct pathological diseases has led to their reclassification into a unique entity (Antonescu, 2006). Conversely, different translocation events were discovered in tumors harboring morphological similarities and previously considered as a unique entity (Antonescu, 2006).
Currently, sarcoma clinical practice guidelines highly recommend the complementation of the diagnosis, based on morphology and immunohistochemistry, with molecular investigations, especially when "the specific pathological diagnosis is doubtful, the clinical pathological presentation is unusual, and it may have prognostic and/or predictive relevance" (Casali et al., 2018a).
For instance, the detection of pathognomonic translocations is particularly helpful in the differential diagnosis of similar clinicopathological entities (Brenca and Maestro, 2015). An example is the identification of a t(X; 18) (*SS18* fused to *SSX1* or *SSX2*) instead of a t(11;22) (*EWSR1* fused to *FLI1*), which is crucial to differentiate poorly differentiated synovial sarcoma with a round cell pattern from extraskeletal Ewing sarcoma (Bridge et al., 1999; Fisher, 1998; Gu et al., 2000). Likewise detection of *NR4A3* rearrangement on chromosome 9 supports differential diagnosis of EMC as opposed to myoepithelial tumor (described in chapter 3).
Besides diagnostic value, the expression of a fusion gene may have a predictive impact. Stacchiotti et al. reported that the type of fusion gene may predict sensitivity to Sunitinib in EMC (Stacchiotti et al., 2014). In particular, in their series, *EWSR1-NR4A3* chimera was expressed in all cases responsive to Sunitinib whilst refractory cases harboured the *TAF15-NR4A3* fusion (Stacchiotti et al., 2014). Other examples include inflammatory myofibroblastic tumors and dermatofibrosarcoma protuberans for which genetic rearrangements (*ALK* rearrangement in the first case and *COL1A1-PDGFB* in the second case) could be predictive of the response to Crizotinib and Imatinib, respectively (Casali, 2012; Ugurel et al., 2014).
Finally, the expression of a fusion transcript has also a prognostic role in sarcoma pathobiology. For example, in EMC, translocations different from *EWSR1-NR4A3* are associated with rhabdoid phenotype, high-grade morphology and a more aggressive outcome compared with tumors harbouring a *EWSR1-NR4A3* rearrangement (Agaram et al., 2015). In infantile alveolar rhabdomyosarcoma the presence of a *PAX3-FKHR* or *PAX7-FKHR*

fusion correlates, respectively, with very high-risk or favourable outcome (Sorensen et al., 2002).

1.4 Genetic approaches for the detection of fusion genes: the massive parallel sequencing (MPS) revolution

In routine diagnostics, rearrangements leading to fusion gene formation are usually detected by interphase FISH analysis with break-apart, single gene probes (Miettinen, 2016). FISH with break-apart single gene probes is particularly useful in the case of rearranged sarcomas where one translocation partner is present in the majority of cases but the second partner varies (Lauer and Gardner, 2013). This strategy has the disadvantage of not identifying the second fusion partner. Instead FISH employing dual fusion probe sets enables the identification of both gene partners involved in the rearrangement. However, the use of dual fusion probes uncommonly enters the diagnostic routine, due to the frequent involvement of multiple partners and the rarity of commercially available probes (Mertens and Tayebwa, 2014).

While FISH allows for the detection of a chromosome translocation, the actual expression of the translocation-derived fusion transcript is determined by reverse transcriptase polymerase chain reaction (RT-PCR), often combined with sequencing of the PCR product. An appropriate primer designing, covering not only the variability among fusion gene partners but also the structural heterogeneity of translocation breakpoints, is necessary. Thus RT-PCR approach is usually used for gene fusion detection only when the number of alternative partners and/or possible breakpoint combinations is restricted. As a molecular technique, also rapid amplification of cDNA ends (RACE) should be mentioned as a successfully employed method to amplify chimeric transcripts with only one known partner (Yeku and Frohman, 2011).

Fusion proteins in translocation-associated sarcomas can be detected also by immunohistochemistry (IHC), exploiting the fact that only one portion of a given protein is overexpressed (Antonescu, 2006). To give an example, strong nuclear staining for TFE3 can be identified in tumors that harbour *TFE3* gene fusions, including alveolar soft part sarcoma and a subset of perivascular epithelioid cell tumors (PEComas) (Argani et al., 2003, 2010). Similarly MDM2 protein accumulation is a readout for chromosome 12q13-15 amplification that characterize well differentiated and dedifferentiated liposarcomas (Pauwels et al., 2006).

Although FISH, RT-PCR and IHC are easy to perform in clinical diagnostic routine, they are essentially hypothesis-driven approaches. That is to say that only a definite number of possible alternatives could be tested by using these techniques in order to sustain an anticipated histological diagnosis (Brenca and Maestro, 2015). Moreover, the presence of molecular variants (due to alternative partners and breakpoints) as well as genetic promiscuity between different sarcoma subtypes account for false-positive and false-negative results of these techniques (Brenca and Maestro, 2015). Array-based approaches have expanded sarcoma diagnostic tools, allowing molecular screening of a wide spectrum of relevant genetic abnormalities. However, if on one hand array-based comparative

genomic hybridization could provide information on gains and losses of chromosomal material, on the other hand balanced translocations or polyploidies cannot be detected with this technique (Miettinen, 2016).
Finally, the introduction of massive parallel sequencing (MPS) more than 10 years ago has redefined molecular testing approach in sarcoma diagnosis. In particular, RNA-sequencing may be used for detection and quantification of fusion transcripts, in the absence of a priori histological hypothesis. In the last years several novel chimeric transcripts involved in STS have been discovered by transcriptome sequencing and here we report only some examples: *EWSR1-PBX3* gene fusion was detected in myoepithelial tumors (Agaram et al., 2015); *NAB2-STAT6* rearrangement was found in solitary fibrous tumors (Robinson et al., 2013); *YAP1-TFE3* was identified in epithelioid hemangioendothelioma (Antonescu et al., 2013a); recurrent *NCOA2* gene rearrangements were uncovered in congenital/infantile spindle cell rhabdomyosarcoma (Mosquera et al., 2013); *ZC3H7B-BCOR* and *MEAF6-PHF1* fusions were identified in ossifying fibromyxoid tumors (Antonescu et al., 2014) and *PAX3-MAML3* fusion gene was uncovered to be involved in the t(2;4)(q35;q31.1) translocation in biphenotypic sinonasal sarcoma (Wang et al., 2014).

Here we report how the exploitation of an RNA sequencing approach allowed us to a) identify two fusions never associated before to the investigated entities, namely an *ETV6-NTRK*3 gene fusion in a GIST and a *PTCH1-GLI1* fusion in a case of myoepithelial tumor; b) to dissect the molecular diversity of two closely related simple karyotype sarcoma entities, myoepithelial tumors and EMC.

2. GASTROINTESTINAL STROMAL TUMORS (GIST)

Gastrointestinal Stromal Tumors (GIST) are the most common primary mesenchymal tumors of the gastrointestinal tract (Fletcher et al., 2013). They are thought to originate from the interstitial cells of Cajal (Corless et al., 2011), a population of gastrointestinal cells that function as pacemakers for peristaltic contractions.

2.1 Epidemiology

GIST are rare tumors with an estimated unadjusted incidence of around 1-2/100.000/year (Nilsson et al., 2005). Initially considered a rare sarcoma variant, they now account for about 1/3 of all STS. Indeed, GIST has been identified as a distinct pathological entity only in the nineties with the discovery of KIT as specific marker. Prior, GIST were variably classified as leiomyoma, leiomyosarcoma, leiomyoblastoma or even carcinoma of the gastrointestinal tract.

The incidence reported above covers clinically relevant GIST since small GIST-like lesions (about 1 cm in diameter) called micro GIST have been found at histopathological examination in over 20% of middle aged "healthy" individuals (Casali et al., 2018b). GIST typically occur in patients older than 50 years (Miettinen, 2016) with median age around 60-65 years (Casali et al., 2018b). There is a slight prevalence in males (Casali et al., 2018b). Occurrence in children is very rare with pediatric GIST representing a clinically and molecularly distinct subset (Casali et al., 2018b).

GIST occur most commonly in the stomach (54%), followed by the small intestine including duodenum (32%), rectum (4%), colon (1%) and esophagus (1%) (Fletcher et al., 2013; Miettinen, 2016). 9% of GIST are diagnosed as disseminated disease with an undefinable site of origin (Fletcher et al., 2013).

Most GIST are sporadic, but a fraction of them arise in patients affected by syndromic conditions (Fletcher et al., 2013). Most common syndromes include deficiencies in succinate dehydrogenase complex (SDH) that occur especially among young patients, sometimes in connection with the non-hereditary Carney triad (GIST, pulmonary chondroma, paraganglioma) or the autosomal dominant Carney-Stratakis syndrome (GIST plus paraganglioma) (Fletcher et al., 2013). Neurofibromatosis 1 (NF1) syndrome is associated to increased incidence of GIST (Miettinen, 2016), often multicentric (Casali et al., 2018b). Familial GIST syndrome is caused by heterozygous *KIT* or rarely *PDGFRA* activating germline mutations and is characterized by multiple or diffuse GIST that often become malignant (Fletcher et al., 2013; Miettinen, 2016). This syndrome is inherited in an autosomal dominant pattern (Miettinen, 2016).

2.2 Pathology

GIST are usually composed of spindle cells; epithelioid morphology, that may be associated with higher mitotic activity, or mixed histology is also observed in some cases (Fletcher et al., 2013). Immunohistochemically most GIST are positive for CD117 (KIT) which can be cytoplasmic, membrane associated or seen as perinuclear dots (Fletcher et al., 2013).

However 5% of GIST, especially those with gastric location and mutations in *PDGFRA*, feature a very limited CD117 staining (Fletcher et al., 2013). Positivity for DOG1 is often observed in CD117 negative GIST (Fletcher et al., 2013). Other GIST markers include CD34, h-caldesmon and SMA (smooth muscle actin); rare cases are positive for desmin, keratin 18 or S100 protein (Fletcher et al., 2013). Finally SDH-deficient GIST are identified by immunohistochemical loss of SDHB (succinate dehydrogenase complex subunit B) (Fletcher et al., 2013).

2.3 Clinical features and treatment

Clinical presentation of GIST ranges from small benign, incidentally detected tumors to malignant neoplasms that spread throughout the abdomen (Miettinen, 2016). Malignant GIST, that represent approximately 30% of all GIST (DeMatteo et al., 2000; Miettinen and Lasota, 2006), may diffuse into the peritoneal and retroperitoneal space and commonly metastasize (Fletcher et al., 2013; Miettinen, 2016).

The standard treatment of localized GIST is surgery associated with adjuvant therapy with Imatinib for 3 years in patients with a significant risk of relapse (Casali et al., 2018b). Imatinib is also the standard treatment for inoperable and metastatic disease and, in the latter case, the drug should be administered indefinitely. (Casali et al., 2018b). If progression of the disease or intolerance to Imatinib occur, Sunitinib and Regorafenib are used as standard second and third line of treatment, respectively (Casali et al., 2018b).

The benefit associated to Imatinib may vary according to the genetics of the tumor (see below). In particular, tumors with *KIT* exon 11 mutations respond better than those with *KIT* exon 9 mutations that require higher dosage of drug (Corless et al., 2014; Joensuu et al., 2017); GIST carrying the *PDGFRA* D842V (exon 18) mutation are typically resistant to Imatinib as they are those tumors devoid of canonical *KIT* or *PDGFRA* mutations (Casali et al., 2018b).

2.4 Genetics

About 85% of sporadic GIST harbor oncogenic mutations affecting the tyrosine kinase KIT (70-75%) or PDGFRA (10-15%) (Schaefer et al., 2017). KIT is a member of the type III receptor tyrosine kinase family that includes also the platelet-derived growth factor receptor-α (PDGFRA) (Hanks, Quinn, and Hunter 1988).

KIT mutations more frequently occur in exon 11 (67%) and exon 9 (10%), less commonly in exon 17, 13 and 8 (Fletcher et al., 2013; Ito et al., 2014). They result in constitutive, ligand-independent kinase activity, downstream RAS-RAF-MAPK signaling pathway activation and in longer receptor half-life (Bauer et al., 2006; Corless et al., 2011; Fumo et al., 2004). Most *KIT* mutations are heterozygous (Fletcher et al., 2013) but approximately 15% of tumors become hemizygous for the mutation, due to the loss of the wild type allele, an event that correlates with tumor progression (Antonescu et al., 2005; Chen et al., 2008; Heinrich et al., 2003; O'Riain et al., 2005).

PDGFRA mutated GIST are typically gastric GIST(Corless et al., 2011). Mutations usually affect exon 18, less commonly exon 14 or exon 12 (Fletcher et al., 2013). *KIT* and *PDGFRA*

mutations are usually mutually exclusive, consistent with the functional overlap of the two receptors (Hirota et al., 1998; Pauls et al., 2005; Wasag et al., 2004).

About 15% of GIST are devoid of *KIT* or *PDGFRA* mutations (Corless et al., 2011). About 1% of these *KIT*/*PDGFRA* wild-type cases carry *BRAF* mutations that sustain RAS-RAF-MAPK pathway activation (Corless, 2014; Rossi et al., 2016). Occasional *KRAS* or *PIK3CA* (phosphatidylinositol-4,5-bisphosphate 3-kinase catalytic subunit alpha) mutations have been reported (Mavroeidis et al. 2018; Daniels et al. 2011; Miranda et al. 2012;).

GIST devoid of canonical *KIT*/*PDGFRA*/*BRAF* mutations can be observed in patients affected by SDH protein complex-related syndromes (Doyle and Hornick, 2014) or neurofibromatosis type 1 (Gasparotto et al., 2017; Ratner and Miller, 2015). SDH inactivation, that accounts for about one third of *KIT*/*PDGFRA*/*BRAF* wild type GIST (Pantaleo et al., 2015) may arise as a consequence of promoter hypermethylation (Haller et al., 2014; Killian et al., 2014) or germline inactivating mutations in any of the four genes encoding the SDH complex (McWhinney et al., 2007; Pasini et al., 2008). Although it is still unclear how the loss of SDH expression promotes tumorigenesis, it has been hypothesizes that the accumulation of succinate, as a result of SDH inactivation, leads to reduced turnover of HIF1A (hypoxia-induced factor 1 alpha) which in turn activates VEGF (vascular endothelial growth factor) (Selak et al., 2005).

The remaining two third of *KIT*/*PDGFRA*/*BRAF* wild type GIST that retain SDH activity (10% of all GIST), hereafter referred to as ‘quadruple-negative’ GIST, overall respond poorly to standard treatments (Corless, 2014). In the attempt to shed light on the biology of ‘quadruple-negative’, we sought to explore the possibility that, similar to other simple karyotype sarcomas, also this fraction of tumors could express oncogenic fusion transcripts. This thesis reports the first oncogenic fusion event identified in a GIST (Brenca et al., 2016).

3. MYOEPITHELIAL TUMORS

Myoepithelial tumors (MyoT) are a very uncommon and heterogeneous group of tumors (estimated in less than 1% of all sarcomas) that may affect different sites, mostly soft tissues and salivary glands, less frequently bone, skin, and viscera (Fletcher et al., 2013).
MyoT are classified by the WHO system as tumors of uncertain differentiation (Fletcher et al., 2013). Indeed, despite the expression of features consistent with myoepithelial differentiation, the high degree of variability in terms of morphology and immunoprofile prevents a clear cut definition of the lineage of differentiation of these tumors.

3.1 Epidemiology

Although MyoT are rare tumors, their morphologic, immunohistochemical and genetic properties have been increasingly characterized over the past 15 years (Fletcher et al., 2013; Jo and Fletcher, 2015). Male and female are equally affected and age range is wide with a median of 40 years (Fletcher et al., 2013). Recent reports suggest that MyoT may be an under-recognized entity (Fletcher, 2015).

3.2 Clinical features and treatment

Based on morphological features, MyoT are classified as mixed tumor/chondroid syringoma, myoepithelioma and myoepithelial carcinoma. In general MyoT of soft tissues tend to feature a benign clinical course, with rare phenomena of tumor spreading (Fletcher et al., 2013; Hornick and Fletcher, 2003; Mentzel et al., 2003). However, myoepithelial carcinomas, including the MyoT located in the soft tissues, are considered a higher grade variant due to their more aggressive behavior and propensity to recurrence and distant metastasis (up to 50% of the cases) (Gleason and Fletcher, 2007; Hornick and Fletcher, 2003; Jo, 2015). The role of adjuvant chemotherapy or radiation therapy remains to be determined, although combination chemotherapy (carboplatin plus taxanes) seems to provide a certain control over metastatic disease (Hornick, 2013).
For the sake of simplicity, hereafter we will just refer to the general category of MyoT and we will focus primarily on the tumors of soft tissues.

3.3 Pathology

MyoT cell morphology is typically spindled, ovoid or epithelioid and a combination of reticular, trabecular and nested growth pattern is observed (Jo and Fletcher, 2015). The stroma appears variably myxoid and/or hyalinized or chondroid and most MyoT show a well-circumscribed and lobulated or nodular texture (Jo and Fletcher, 2015).
As regarding histology, epithelial, neuronal and mesenchymal traits coexist. MyoT often express epithelial antigens (e.g. cytokeratins and EMA, epithelial membrane antigen) together with S100 protein and GFAP (glial fibrillary acidic protein) (Jo and Fletcher, 2015). The expression of myogenic markers is variable (Jo, 2015) with smooth muscle actin (SMA) observed in up to 64% of cases (Jo and Fletcher, 2015). p63 expression, a typical epithelial marker, may be detected in up to 45% of the cases (Jo and Fletcher, 2015) and loss of

SMARCB1/INI1, likely related to the 22q11.2 chromosome loss, is also observed in a small subset of cases (Jo and Fletcher, 2015). Expression of PLAG1 is frequently observed in the mixed tumor variant of MyoT (58-100%) whilst is absent in the other two subtypes (Jo and Fletcher, 2015).
This variability in morphology and immunophenotype probably mirrors the intrinsic plasticity of myoepithelial cells (Flucke et al., 2012). Needless to say that this high degree of heterogeneity significantly impacts on the diagnosis, which remains challenging due to the overlap with a wide spectrum of different entities.

3.4 Genetics

From a genetic standpoint, up to 45% of MyoT harbor *EWSR1* (22q12) gene rearrangements (Fletcher et al., 2013). A plethora of possible *EWSR1* partners in MyoT has been identified, including *POU5F1* (6p21), *PBX1* (1q23), *ZNF444* (19q13), *PBX3* (9q33), *KLF17* (1p34), *ATF1* (12q13) and others (Fletcher et al., 2013; Jo, 2015). Rare *FUS* or *PLAG1* gene rearrangements have been reported namely *FUS-POU5F1* (Puls et al., 2014), *FUS-KLF17* (Huang et al., 2015) and *PLAG1-LIFR* (Antonescu et al., 2013b). A fraction of MyoT cases lacking *EWSR1* gene rearrangement feature homozygous deletion of the *SMARCB1* gene (Le Loarer et al., 2014).
A sizeable number of MyoT are "orphan" of genetic marker due to the absence of known fusions or the presence of rearrangements involving *EWSR1*, *FUS* or *PLAG1* but with unknown partners. A thorough characterization of these "orphan" tumors may help in better defining their pathobiology and may disclose novel tools to overcome diagnostic, prognostic and therapeutic challenges. In this context, the differential diagnosis with extraskeletal myxoid chondrosarcoma (EMC) represents an urgent need (see below).

3.5 Differential diagnosis with EMC

In the case of a MyoT of soft tissues the primary differentiation is vs EMC, although there may be an overlap also with other entities (e.g. metastatic chordoma, ossifying fibromyxoid tumor, epithelioid schwannoma and chondroid lipoma) (Hornick, 2013).
EMC is a rare tumor that represents less than 3% of all STS (Fletcher et al., 2013). Like MyoT, also EMC are classified by the WHO (Fletcher et al., 2013) as neoplasms of uncertain differentiation. In fact, despite the historical and misleading name, due to initial apparent cartilagineous features, EMC is definitively not a chondrosarcoma (Fletcher et al., 2013). EMC is considered an "indolent but capricious tumor" (Saleh et al., 1992) due to its high rates of local recurrence and distant metastasis irrespective of apparently curative surgery (Fletcher et al., 2013).
EMC shares with MyoT the major sites of development (limbs, limb girdles, head-and-neck). Although MyoT tend to display a higher degree of architectural and cytologic heterogeneity (Jo and Fletcher, 2015), both tumour types share a lobular/multinodular texture, variable amounts of myxoid stroma, reticular growth pattern and cell morphology (epithelioid, round and spindled) (Flucke et al., 2012; Hornick, 2013). Furthermore some EMC are characterized by diffuse hypercellularity, epithelioid morphology and elevated nuclear grade, a feature that may recall myoepithelial carcinoma (Jo, 2015).

Beside morphology, the two sarcoma subtypes share several immunophenotypic markers: S100 protein is positive in almost all MyoT and in up to 20% of EMC, where usually displays a focal staining pattern (Hornick, 2013). Most MyoT are positive for keratins (Fletcher et al., 2013) and variable fractions show EMA, GFAP and SMA positivity (Jo and Fletcher, 2015). EMC are usually negative for these markers, although scattered cells positive for EMA and keratin as well as for SMA or GFAP have been occasionally reported (Hornick, 2013). Other overlapping features are the loss of SMARCB1/INI1 (Fletcher et al., 2013) and the positivity for p63, although with different frequencies (Fletcher et al., 2013; Flucke et al., 2012; Jo and Fletcher, 2011, 2015).

From a genetic standpoint, both tumors may translocate the *EWSR1* gene. However, the rearrangement of *NR4A3*, which may fuse to *EWSR1* (over 60%), *TAF15* (about 30%), *TCF12*, *TFG* or *HSPA8* (rare), is considered a hallmark of EMC (Agaram et al., 2014; Fletcher et al., 2013; Urbini et al., 2017b). On these grounds, FISH for *EWSR1* should not be used to distinguish between EMC and MyoT whilst FISH for *NR4A3* may be more informative (Flucke et al., 2012). It is important to stress that this "genetic diagnostic bar" is arbitrary. Whether all EMC must rearrange *NR4A3* or whether EMC and MyoT are just two genetic variants of the same disease is still to be defined. In other words, it is questionable whether the genetics actually identifies two different entities or it just reflects alternative genetic flavors of the same tumor. This is not trivial in the light of the different clinical course and the possible alternative therapeutic options.

4. AIM OF THE STUDY

In this study we exploited RNA-sequencing to identify and characterize novel oncogenic fusion transcripts involved in the pathogenesis of two subsets of simple karyotype sarcoma devoid of known genetic alterations, namely GIST and MyoT.

In addition, we aimed at better defining MyoT pathobiology, by exploring the molecular diversity of MyoT and EMC. To this end RNA-sequencing profiling was extended on a series of EMC cases and MyoT and EMC transcriptomes were then compared.

RESULTS AND DISSCUSSION

5. PART I: TRANSCRIPTOME SEQUENCING IDENTIFIES ETV6-NTRK3 IN A CASE OF QUADRUPLE NEGATIVE GIST

5.1 RESULTS

5.1.1 Samples included in the study

In the attempt to shed light on the genetics of GIST devoid of canonical oncogenic mutations we speculated that, although never reported before, these tumors could be driven by oncogenic fusion genes, similarly to other simple karyotype sarcomas. To address this hypothesis, we retrieved 5 quadruple-negative GIST (*KIT*, *PDGFRA*, *BRAF* mutation negative; SDHB retained) from the pathological files of the Treviso General Hospital (table 2). Diagnosis was made according to the World Health Organization (WHO) classification.
Although the status of *KIT*, *PDGFRA*, *BRAF* and SDH had been assessed during the diagnostic routine, the actual condition of quadruple negativity was verified by NGS targeted profiling as described in (Gasparotto et al., 2017).

Table 2. Quadruple negative GIST cases investigated

Case #	Site	Age	Sex	Size (cm)	Mitotic Index
1	rectum	44	M	5	34
2	small intestine	86	F	8	8
3	small intestine	26	F	5	10
4	small intestine	71	F	10	>8
5	small intestine	31	F	9	20

5.1.2 Transcriptome analysis of a series of 'quadruple negative' GIST unveils an ETV6-NTRK3 positive tumor

RNA-sequencing was followed by detection of fusion genes using several bioinformatics tools, including FusionCatcher (Nicorici et al., 2014) ChimeraScan (Iyer et al., 2011) and an in-house algorithm. Different potential fusions, most of which involving neighboring genes, were identified in the 5 tested samples (Table 3). For instance, a sample expressed a *POLA2-CDC42EP2*, an intrachromosomal fusion transcript of uncertain significance recently described in other GIST cases (Kang et al., 2016). Surprisingly, we found that one GIST, GIST#1, expressed a fusion transcript that had been previously associated to infantile fibrosarcoma, namely *ETV6-NTRK3*.
Clinical history of GIST#1 case indicated that the patient was a 44 years-old man. An ulcerated mass in the posterior wall of the rectal ampulla was diagnosed as GIST based on pathological examination of the tumor biopsy. The tumor was 5 cm in size, nodular and provided of pseudocapsule. Microscopically it was characterized by hypercellularity, epithelioid morphology, moderate nuclear atypia, high mitotic index (fig. 1 C) and presence of necrosis. Positivity for DOG1 and CD117/KIT (fig. 1D) was strong and diffuse while S100,

synaptophysin, chromogranin and desmin were negative. The tumor was classified as a high-risk GIST according to NCCN criteria. The patient underwent surgery with no subsequent adjuvant therapy, based on the poor response of mutation-negative GIST to Imatinib. Since surgery, the patient has been disease-free and is currently followed with periodic examinations.

Table 3. Potential fusions, involving protein-coding genes, identified by RNA-sequencing in the 5 'quadruple-negative' GIST

Case #	Tool	Gene1	Chromosome Gene 1	Gene2	Chromosome Gene 2	Type of fusion
1	chimerascan	*ETV6*	12	*NTRK3*	15	interchromosomal
	fusioncatcher	*ETV6*	12	*NTRK3*	15	interchromosomal
	chimerascan	*PARG*	10	*TIMM23*	10	read-through
2	chimerascan	*YY1AP1*	1	*ASH1L*	1	read-through
	chimerascan	*HARS2*	5	*ZMAT2*	5	read-through
	chimerascan	*IGSF5*	21	*PCP4*	21	read-through
3	chimerascan	*NAIP*	5	*OCLN*	5	read-through
4	chimerascan	*AGAP*	10	*FRMPD2*	10	read-through
	chimerascan	*STAG3*	7	*GTF2IRD2*	7	read-through
	chimerascan	*GALNT8*	12	*KCNA6*	12	read-through
	chimerascan	*ZNF782*	9	*ZNF510*	9	read-through
	chimerascan	*AP5S1*	20	*MAVS*	20	read-through
	chimerascan	*CIRBP*	19	*C19orf24*	19	read-through
	chimerascan	*SLC4A7*	3	*NEK10*	3	read-through
	chimerascan	*HOXB6*	17	*HOXB3*	17	read-through
5	chimerascan	*PDCD6IP*	3	*HERC2*	15	interchromosomal
	chimerascan	*ZNF782*	9	*ZNF510*	9	read-through
	chimerascan	*CTSC*	11	*RAB38*	11	read-through
	chimerascan	*CUL5*	11	*ACAT1*	11	read-through
	chimerascan	*CLN8*	8	*ARHGEF10*	8	read-through
	chimerascan	*GKAP1*	9	*KIF27*	9	read-through
	chimerascan	*FEN1*	11	*FADS2*	11	read-through
	chimerascan	*TMEM219*	16	*TAOK2*	16	read-through
	chimerascan	*POLA2*	11	*CDC42EP2*	11	read-through
	chimerascan	*COL22A1*	8	*FAM135B*	8	read-through
	chimerascan	*CLDN12*	7	*PFTK1*	7	read-through
	chimerascan	*HOXC10*	12	*HOXC4*	12	read-through
	fusioncatcher	*SLC35G1*	10	*PLCE1*	10	read-through
	fusioncatcher	*C6orf47*	6	*BAG6*	6	read-through

5.1.3 Characterization of the ETV6-NTRK3 case

A thorough characterization of the fusion revealed that the chimeric transcript was the result of an in-frame fusion event between exon 4 of the ETS variant 6 transcription factor (*ETV6*) located on chromosome 12p13.2 and exon 14 of the neurotrophin tyrosine kinase receptor 3 (*NTRK3*) located on chromosome 15q25.3 (fig. 1A top). The fusion retained the open reading frame across the fused exons. The resulting chimeric protein appeared to retain the ETV6 sterile α-motif (SAM) interaction domain and the NTRK3 tyrosine kinase domain.

The actual presence of the chromosome translocation t(12;15), as the primary source of the fusion transcript, was verified by FISH analysis. Using an *ETV6* break-apart probe, we verified that the vast majority GIST#1 tumor cells showed split signals, indicating that the gene was actually broken (fig. 1B). By reverse transcriptase-PCR (RT-PCR) with primers flanking the breakpoint identified by the bioinformatic tools we verified the actual expression of the chimeric transcript (fig. 1A bottom). Moreover, the breakpoint sequence was confirmed by Sanger sequencing of the RT-PCR product (fig. 1A bottom).

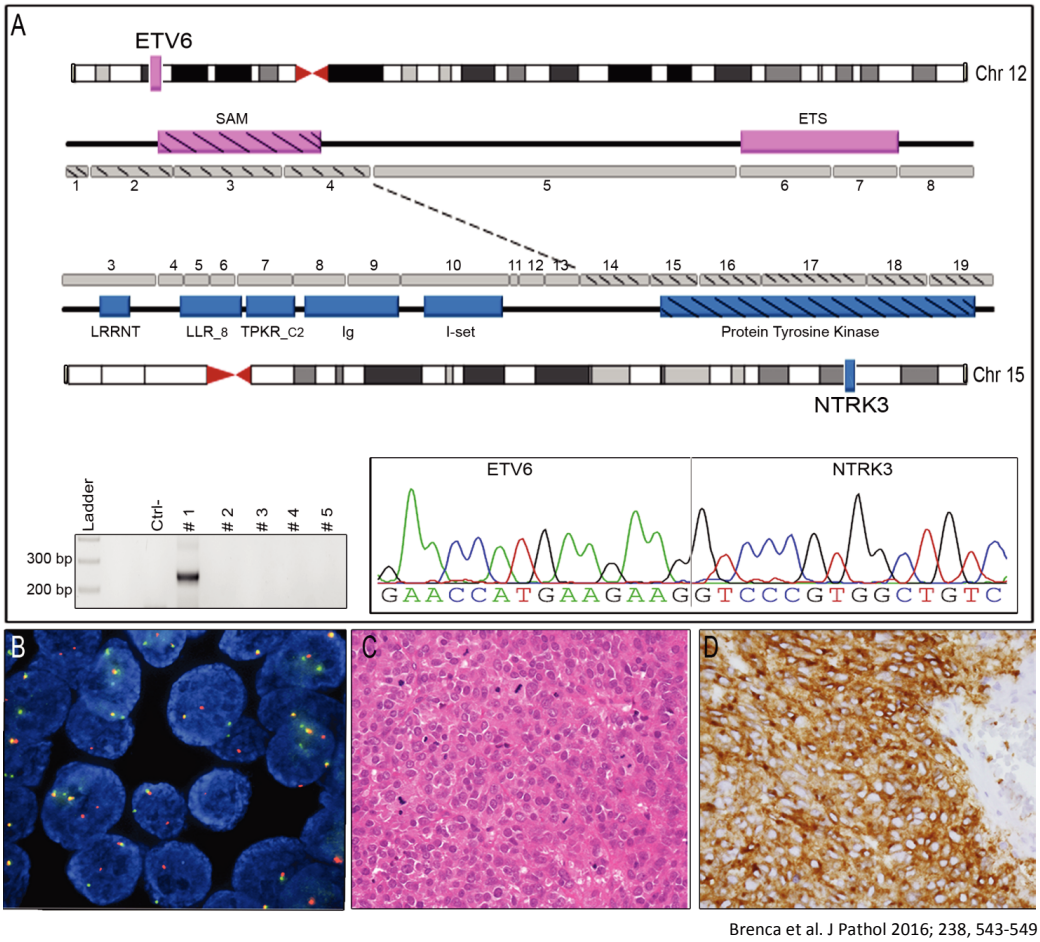

Brenca et al. J Pathol 2016; 238, 543-549

Figure 1. ETV6-NTRK3 fusion gene identified in a case of 'quadruple-negative' rectal GIST
(A) (Top) Schematic representation of the *ETV6-NTRK3* chimera reporting protein-coding exons and PFAM domains: the fusion involved exon 4 of *ETV6* and exon 14 of *NTRK3*; a diagonal pattern marks exons and domains retained in the chimera.
(Bottom) RT-PCR of the five 'quadruple-negative' GIST cases confirmed the actual expression of the fusion transcript only in the index case (#1). *Ctrl-, negative control*. Chromatogram, displaying the junction between *ETV6* and *NTRK3* genes, is reported. **(B)** FISH assay with *ETV6* break-apart probe showed split signals, proving the genomic rearrangement of the *ETV6* locus at 12p13 in the index case. **(C)** Hematoxylin eosin staining revealed that the tumor was hypercellular throughout with epithelioid morphology and remarkable mitotic activity. **(D)** Immunohistochemistry showed diffuse positivity for CD117.

In order to estimate the frequency of the *ETV6-NTRK3* fusion in GIST, a series of 26 additional primary tumors (enriched for mutation-negative and rectal GIST) was screened by FISH for *ETV6* rearrangement. Beside the index case, FISH failed to detect additional *ETV6* rearrangements, suggesting that *ETV6-NTRK3* is very likely an uncommon fusion that might characterize GIST with peculiar clinicopathological features.

5.1.4 ETV6-NTRK3 chimera sustains IGF1R signaling cascade and IRS1 nuclear localization

ETV6-NTRK3 chimeric transcript was first identified in infantile fibrosarcoma but with a different breakpoint (exon 5 of *ETV6*, exon 15 of *NTRK3*) yet involving the same previously described protein domains. The chimera has been subsequently identified in other tumors and breakpoints involve *ETV6* exon 4, 5 or 6 and *NTRK3* exon 14 and 15 (COSMIC Database, Catalogue of Somatic Mutations in Cancer).

The ETV6-NTRK3 fibrosarcoma variant (hereafter named as IF_EN) has been described to activate IRS-1 by direct NTRK3-IRS1 binding (Lannon et al., 2004; Morrison et al., 2002). On

these grounds, we asked whether also the variant identified in GIST#1 (hereafter named GIST_EN) retained this ability. To test this hypothesis we engineered HT1080 and U2OS cell lines to ectopically express the two variants of the EN chimeras (fig. 2A). GIST_EN, like the canonical IF_EN, was observed to induce phosphorylation of IRS1 both in basal and in serum-free conditions (fig. 2B top). Furthermore expression of GIST_EN (as well as IF_EN) was also associated to AKT activation, as revealed by increased Ser-473 phosphorylation (fig. 2B bottom).

IRS1 has been described to shuttle from the cytosol, where it works as adaptor of IGF1R, to the nucleus where it has been shown to activate c-myc, cyclin D1 and β-catenin (Reiss et al., 2012). Immunofluorescence analysis and subcellular fractionation (not shown) revealed that both ETV6-NTRK3 chimeras are able to induce IRS1 nuclear localization (fig. 2C).

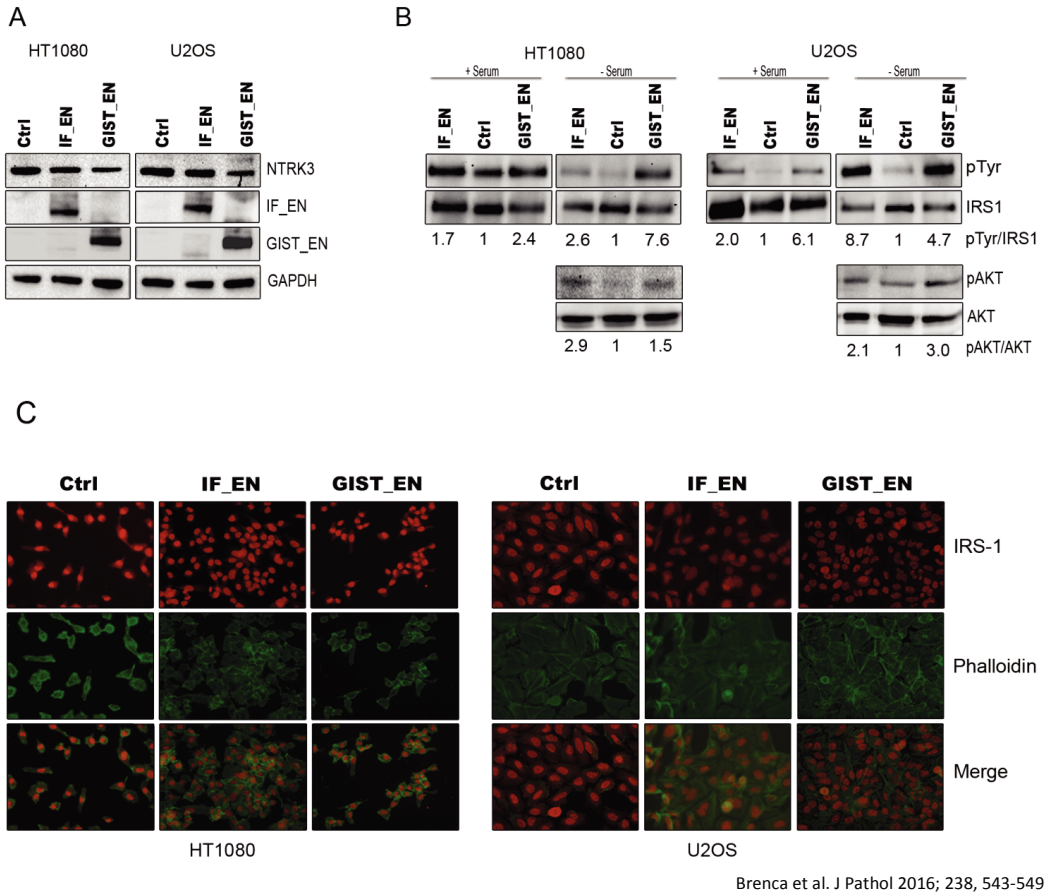

Brenca et al. J Pathol 2016; 238, 543-549

Figure 2. The GIST ETV6-NTRK3 chimera sustains canonical and nuclear IRS1 pathways

(A) Immunoblot shows ectopic expression of the two variants of the ETV6-NTRK3 chimera (IF_EN, infantile fibrosarcoma-variant and GIST_EN, GIST-variant) in HT1080 (left) and U2OS (right) engineered cells. Empty vector was used as a negative control (Ctrl). **(B) (Top)** HT1080 and U2OS protein lysates were immunoprecipitated for IRS1; immunoblot assays for phosphotyrosine and for IRS1 were performed; the amount of phosphorylated IRS1 was calculated as the pIRS1:total IRS1 ratio. Experiments were conducted both in the presence (+) and in the absence (16 hours) of serum (-). **(Bottom)** AKT phosphorylation (Ser 473) and total AKT were evaluated through immunoblotting under serum deprivation: the amount of activated AKT was calculated as the pAKT:total AKT ratio. **(C)** Immunofluorescence staining for IRS1 (red) and phalloidin (green).

5.1.5 ETV6-NTRK3 sensitizes cells to IGF1R inhibitors and to ALK inhibitors

To probe the role of ETV6-NTRK3 in IGF1R mediated pathway activation, we treated cells with two IGF1R inhibitors (AG1024 and PQ401). Cell viability assays revealed that expression of either EN chimeras sensitized cells to IGF1R inhibition (fig. 3A).

ETV6-NTRK3 has been recently reported as a target of the ALK inhibitor Crizotinib (Roberts et al., 2014; Taipale et al., 2013). We treated engineered cells with this compound and with another FDA (Food and Drug Administration) approved ALK inhibitor, Ceritinib, revealing that GIST_EN variant significantly sensitized cells to both drugs, at nanomolar potency (fig. 3B). These responses were associated with reduced IRS1 phosphorylation (fig. 3C).

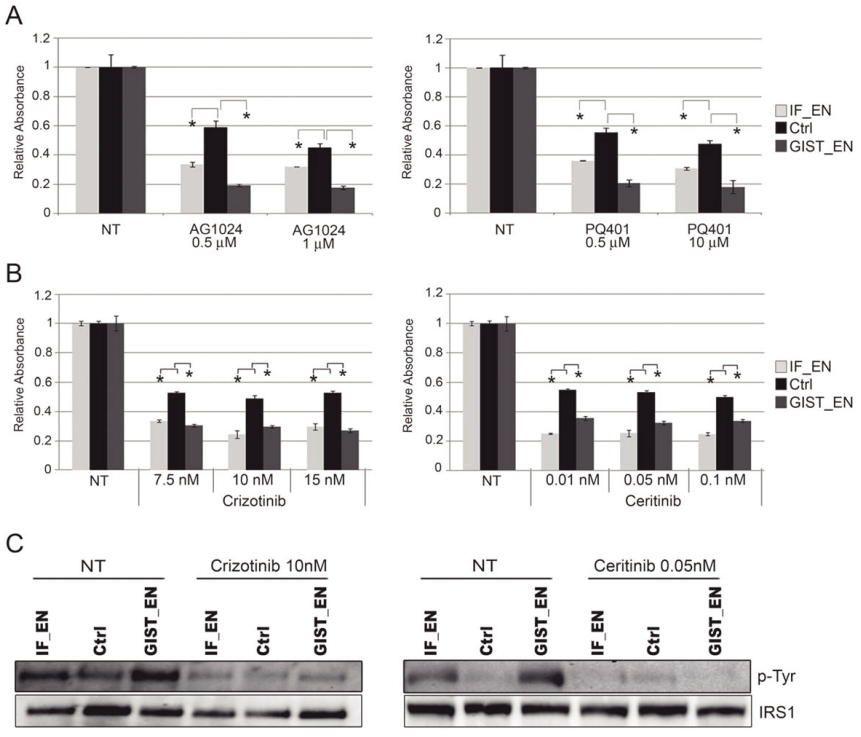

Brenca et al. J Pathol 2016; 238, 543-549

Figure 3. ETV6-NTRK3 expressing cells are sensitive to IGF1R and ALK inhibitors

Sulphorhodamine-B (SRB) cell viability/cytotoxicity assay was used to evaluate response to **(A)** IGF1R-inhibitors (AG1024 and PQ401) and to **(B)** ALK inhibitors (Crizotinib and Ceritinib) in U2OS ectopically expressing the EN chimeras (48 hours of treatment). Concentrations of the drugs are indicated below the graphs. Data shown are mean ratio of treated vs untreated (NT) samples±95% CI; *statistical significance (p<0.05). **(C)** IRS-1 immunoprecipitation on cells treated with Crizotinib (left) and Ceritinib (right) unveiled the inhibitory effect of both drugs on phospho-IRS1 activation.

5.2 DISCUSSION

GIST are the most common primary mesenchimal tumors of the gastrointestinal tract (Fletcher et al., 2013). They are characterized, for the vast majority, by mutations in either *KIT* or *PDGFRA* (Fletcher et al., 2013); infrequent molecular alterations include *BRAF*, *KRAS*, *PIK3CA* or *NF1* mutations and SDH inactivation (Corless, 2014; Daniels et al., 2011; Doyle and Hornick, 2014; Mavroeidis et al., 2018; Miranda et al., 2012; Ratner and Miller, 2015). About 10% of all GIST, defined as 'quadruple negative GIST', are devoid of distinct genetic alterations, a fact that accounts for their insensitivity to standard treatments (Corless, 2014).
In an attempt to provide insight into molecular pathogenesis of 'quadruple negative GIST' we performed RNA-sequencing followed by fusion gene analysis in a series of 5 such tumors. The working hypothesis was that, similar to other simple karyotype sarcomas, also quadruple negative GIST could be driven by oncogenic fusion genes. Intriguingly we detected an *ETV6-NTRK3* fusion transcript in one case of rectal GIST.
This chimera had been originally described in IF as a result of a t(12;15) chromosome translocation (Knezevich et al., 1998) and has been subsequently identified in other tumors including mesoblastic nephroma (Rubin et al., 1998), adult acute myeloid and chronic eosinophilic leukaemia (Eguchi et al., 1999; Forghieri et al., 2011; Setoyama et al., 1998), secretory breast carcinoma (Tognon et al., 2002), mammary analogue secretory carcinoma of the salivary glands (Skálová et al., 2010), radiation induced thyroid cancers (Leeman-Neill et al., 2014) and inflammatory myofibroblastic tumour (Alassiri et al., 2016). Although resulting from different breakpoints, chimeric proteins in all described cases retain the SAM interaction domain of the ETV6 protein and the NTRK3 tyrosine kinase domain.
The originally detected IF_EN has been described to bind directly to the phosphotyrosine binding domain of IRS-1 (the major substrate of the insulin-like growth factor 1 receptor, IGF1R) through a highly conserved C-terminal sequence of NTRK3 protein (Lannon et al., 2004) and to induce constitutive IRS-1 phosphorylation (Morrison et al., 2002). These events, leading to activation of RAS-ERK1/2 and PI3K/AKT pathways, trigger IGF1R signaling cascade thus sustaining cell proliferation and transformation (Tognon et al., 2001). Intriguingly, the IGF1R signaling is suggested to be involved in the pathogenesis of mutation-negative GIST, although with still unclear mechanisms (Beadling et al., 2013) and clinical trials evaluating IGF1R target therapies in these tumors are in progress (Arnaldez and Helman, 2012; Lasota et al., 2013).
In an attempt to investigate the clinicotherapeutic implications of the ETV6-NTRK3 fusion in GIST we generated sarcoma cell lines ectopically expressing the chimeric protein. In these models we show that the GIST_EN variant is able to phosphorylate IRS1 and activate AKT, thus triggering IGF1R downstream cascade. Furthermore IRS1 not only behaves as a cytosolic adaptor of the IGF1R transduction pathway but is also able to support malignant transformation through an alternative nuclear pathway. Active IRS1 can indeed shuttle to the nucleus where it modulates the expression of cyclin D1, c-myc and β-catenin and it affects DNA repair (Reiss et al., 2012). Accordingly we evaluate IRS1 nuclear pathway activation in engineered cells: GIST_EN, as well as the canonical IF_EN, enhance IRS1 nuclear

localization. Overall these data suggest that the role of ETV6-NTRK3 in promoting GIST development may involve the activation of IGF1R downstream signaling and the alternative nuclear IRS1 pathway. The observation that the GIST_EN chimeric protein sensitizes cells to IGF1R inhibition corroborates this notion.

We also report an ability of the GIST_EN chimera to sensitize cells to the ALK inhibitors Crizotinib and Ceritinib. Responses were associated with reduced IRS1 phosphorylation, supporting the notion that the drugs interfere with ETV6-NTRK3 mediated pathway activation.

Our has been the first report of the involvement of an oncogenic fusion protein, namely ETV6-NTRK3, in GIST; our original finding has been subsequently corroborated by other groups (Shi et al., 2016).

We published our result in Journal of Pathology in January 2016 (Brenca et al., 2016). At that time the company Loxo Oncology was working on a small molecule NTRK inhibitor, LOXO-101 (Larotrectinib). Stemming from our results, Loxo Oncology invited GIST patients with tumor negative for *KIT* and *PDGFRA* mutations to contact Loxo Oncology to be included in the ongoing clinical trial with LOXO-101. The results of the trial with Larotrectinib in diverse *NTRK* translocated tumors have been recently published and all 3 GIST cases included in the study demonstrated a good response (fig. 4) (Drilon et al., 2018; Shi et al., 2016).

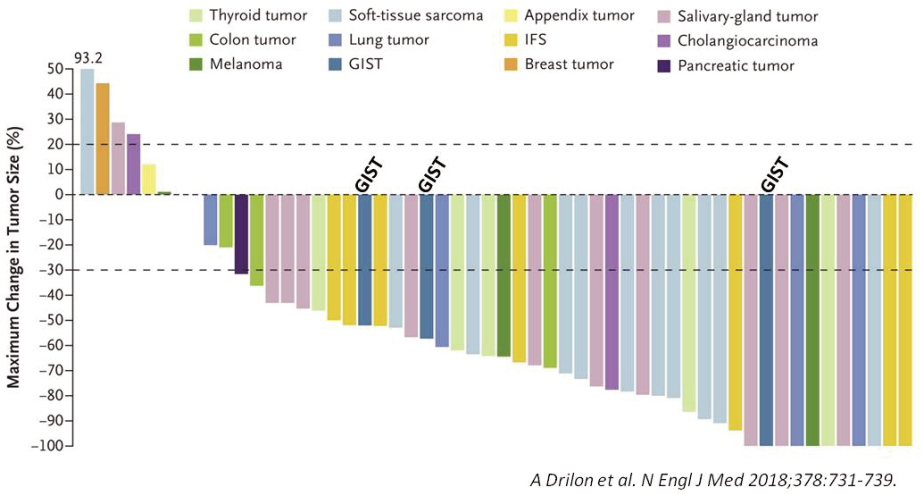

Figure 4. Efficacy of the NTRK inhibitor Larotrectinib in TRK fusion-positive cancers

The figure shows waterfall plot of the maximum change in tumor size, according to tumor type, after Larotrectinib treatment. The three GIST patients enrolled in the study are indicated. *Adapted from Drilon et al. 2018*

6. PART II: MOLECULAR PROFILING OF MYOEPITHELIAL TUMORS: PTCH1-GLI1 GENE FUSION DETECTION AND WHOLE TRANSCRIPTOME ANALYSIS

6.1 RESULTS

6.1.1 Samples included in the study

In the attempt to both investigate new molecular alterations involved in the pathogenesis of MyoT and to dissect the molecular diversity of this entity and the closely related EMC we conducted the study on a series of 7 MyoT of soft tissues and 12 EMC retrieved from the pathological files of the Fondazione Nazionale Tumori IRCCS (Milan) and the Treviso General Hospital (table 4 and 5). Diagnosis of MyoT and EMC was made according to the World Health Organization (WHO) classification by two expert sarcoma pathologists (SP and APDT). FISH or RT-PCR was performed to identify fusions that support histopathological diagnosis.

Among the 7 MyoT, FISH break-apart identified 1 *FUS* and 4 *EWSR1* translocated cases, with no indication of the partner involved. In the other two cases diagnosis was made only on histopathological features as no *FUS*, *EWSR1* or *PLAG1* rearrangement was detected (table 4). EMC were defined by *NR4A3* rearrangement: 7 were *EWSR1-NR4A3* and 5 *TAF15-NR4A3* (table 5).

FFPE tumor sections used in this study were previously confirmed to be highly representative of the tumor by hematoxylin-eosin staining (> 70% neoplastic cells).

RNA-sequencing of all 19 cases was performed and statistics for each sample is reported in table 6.

Table 4. MyoT cases used in this study

				FISH				
Case #	**Sex**	**Diagnosis**	**Site**	**NR4A3**	**EWSR1**	**FUS**	**PLAG1**	**Fusion detected by RNAseq in this study**
DR23	F	myoepithelial carc.	thoracic wall	-	-	-	-	no fusion detected
DR25	M	myoepithelial carc.	NA	ND	+	ND	ND	*EWSR1-ATF1*
DR26	F	mixed tumor	suprascapular	-	+	-	ND	no fusion detected
DR27	F	myoepithelioma	thigh	-	-	-	-	***PTCH1-GLI1***
DR28	F	myoepithelioma	thigh	-	-	+	ND	*FUS-KLF17*
DR29	M	myoepithelioma	forearm	-	+	-	ND	*EWSR1-ATF1*
DR30	F	myoepithelial carc.	NA	-*	+	ND	ND	*EWSR1-ATF1*

*NA, not available; ND, not done; *negative at RT-PCR*

Table 5. EMC cases used in this study

				FISH			
Case #	**Sex**	**Diagnosis**	**Site**	**NR4A3**	**EWSR1**	**TAF15**	**Fusion**
M118	F	EMC	upper leg	+	+	ND	*EWSR1-NR4A3*
M119	M	EMC	upper leg	+	+	ND	*EWSR1-NR4A3*
M120	M	EMC	groin	+	+	ND	*EWSR1-NR4A3*
M121	M	EMC	upper leg	+	+	ND	*EWSR1-NR4A3*
M227	F	EMC	upper leg	+	+	ND	*EWSR1-NR4A3*
M229	M	EMC	buttock	+	+	ND	*EWSR1-NR4A3*
M230	M	EMC	upper leg	+	+	ND	*EWSR1-NR4A3*
M231	M	EMC	buttock	+	-	+	*TAF15-NR4A3*
M314	M	EMC	lower leg	+	-	+	*TAF15-NR4A3*
M315	M	EMC	buttock	+	-	+	*TAF15-NR4A3*
M122	M	EMC	lower leg	+	-	+	*TAF15-NR4A3*
M117	M	EMC	lower leg	+	-	+	*TAF15-NR4A3*

ND, not done

Table 6. RNA-sequencing experiment statistics for EMC and MyoT samples

#Sample	Total Reads	Unmapped reads	Unique mapping reads
M117	66122978	1256902	55678584
M118	61443298	1478182	51582418
M119	62136658	1060364	53191222
M120	74521842	1288612	65095232
M121	82034158	959266	58042892
M122	62026434	1206310	52338048
M227	85796486	3556298	72458182
M229	80508972	3991358	66562476
M230	76596528	9739110	58262388
M231	73921252	11866040	53071548
M314	71487690	1571688	49207262
M315	100673398	518390	20566980
DR23	38349568	536660	32259462
DR25	38008260	626888	30096886
DR26	53106578	1058514	44727170
DR27	36605662	572480	30972456
DR28	37525650	842090	31183568
DR29	65031956	889538	54611444
DR30	69579204	718320	60087776

6.1.2 Transcriptome analysis of MyoT tumors: RNA-sequencing identified a PTCH1-GLI1 fusion transcript in a MyoT case

RNA-sequencing followed by fusion transcript analysis allowed us to identify the partner involved in the fusion in 4 cases: the *FUS* rearranged tumor (#DR28) turned out to express *FUS-KLF17* chimera whilst 3 of 4 *EWSR1* rearranged tumors (#DR25, #DR29 and #DR30) expressed the *EWSR1-ATF1* fusion transcript. No *EWSR1* fusion transcript was identified by RNAseq in the fouth case (#DR26), despite evidence of *EWSR1* chromosome rearrangement.
About the other 2 cases (#DR23 and #DR27) devoid of *FUS*, *EWSR1* or *PLAG1* rearrangement at the FISH break-apart analysis, several potential fusion transcripts were identified in case #DR23 by the different bioinformatic tools used but none of the predicted fusions has been previously reported in the literature and most of them appeared potential read-through. Instead, case #DR27 was predicted to express a *PTCH1-GLI1* fusion transcript. Although this fusion had never been reported in the literature prior our result, we sought to deepen its role, given the curious involvement of two components of the very same pathway. In fact the fusion involved the transmembrane receptor PTCH1 and the zinc finger transcription factor GLI1, the receptor and the nuclear effector of the Hedgehog (HH) pathway respectively.

6.1.3 Characterization of PTCH1-GLI1 fusion

An in depth characterization of the breakpoint sequence indicated that *PTCH1-GLI1* is the result of an in-frame fusion between exon 1 of *PTCH1* (NM_001083602) located on chromosome 9q22.32 and exon 7 of *GLI1* (NM_005269) located on chromosome 12q13.3 (fig. 5 A). In the resulting chimeric transcript, *PTCH1* provides the 5'UTR region and the ATG codon while *GLI1* contributes with exons coding for the leucine zipper DNA binding domains, the nuclear localization signal and the transcriptional activation domain (Graham et al., 2017; Zhu and Lo, 2010) (fig. 5 A).

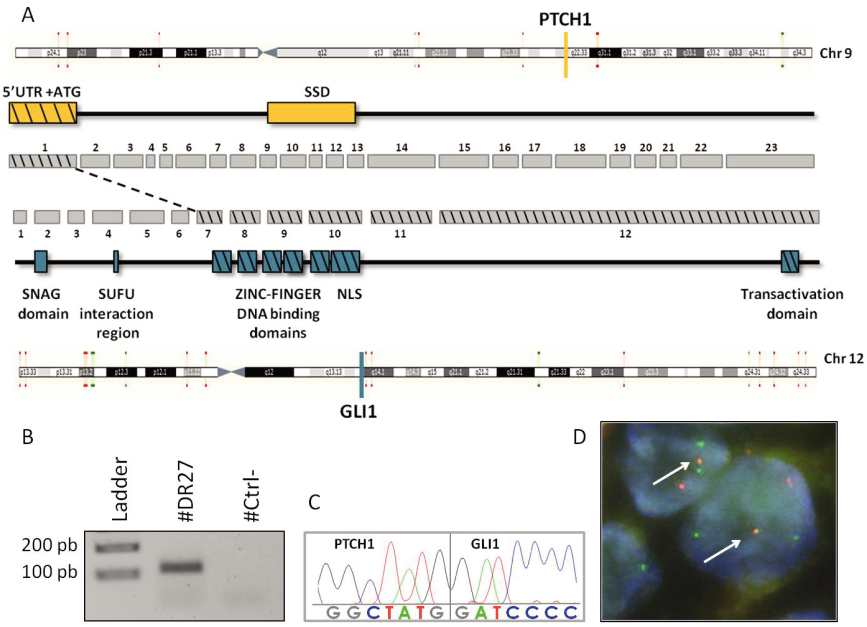

Figure 5. PTCH1-GLI1 fusion identified in a MyoT case. (A) Schematic representation of the *PTCH1-GLI1* fusion involving exon 1 of *PTCH1* and exon 7 of *GLI1*, identified in MyoT #DR27. Exons and domains are reported and those retained in the chimeric protein are marked with a diagonal pattern. **(B)** RT-PCR confirmed the expression of the fusion transcript in the index case (#DR27); *Ctrl-, negative control*. **(C)** Chromatogram shows the breakpoint sequence of the *PTCH1-GLI1* fusion transcript. **(D)** FISH on #DR27 FFPE section. BACs for *GLI1* (Spectrum Orange labeled RP11-181L23 and RP11-772J17) and *PTCH1* (Spectrum Green labeled RP11-691D16 and RP11-34J23) were labeled for dual color dual fusion FISH approach. Tumor cells show one single fusion signal (marked by the arrow) along with one normal signal for each *PTCH1* and *GLI1* and a diminished derivative *PTCH1* signal. FISH pattern is coherent with an insertion of *PTCH1* gene into the *GLI1* locus.

The actual expression of the fusion transcript in the #DR27 tumor was verified by RT-PCR (fig. 5 B) and the breakpoint sequence was confirmed by Sanger sequencing of the RT-PCR product (fig. 5 C).

To confirm the rearrangement at genomic level, FISH analysis was at first performed with break-apart probes. *PTCH1* break-apart showed a balanced translocation pattern i.e. one intact *PTCH1* gene copy and a translocated one (not shown) whilst *GLI1* break-apart FISH showed a normal disomic pattern with no evidence of *GLI1* gene rearrangement (not shown). Then a dual color dual fusion FISH approach demonstrated a single fusion of *GLI1* and *PTCH1* signals along with a one *GLI1* and two *PTCH1* signals in the vast majority of tumor cells (fig. 5 D). This FISH pattern unveiled that the fusion was the result of an insertion of a copy of the *PTCH1* gene within the *GLI1* locus.

Aside from the index case, no other *GLI1* rearrangement was detected in a series of 17 additional MyoT, including 8 of the soft tissues, 5 of the breast and 4 of the salivary glands. Immunohistochemistry with a GLI1 specific antibody indicated that only 2 of the 20 MyoT cases analyzed (3 cases of the original series plus the 17 additional cases) showed a strong nuclear GLI1 accumulation (not shown), but only the index case was rearranged. GLI1 protein accumulation in case #DR27 paralleled the elevated *GLI1* expression detected by RNAseq (fig. 6).

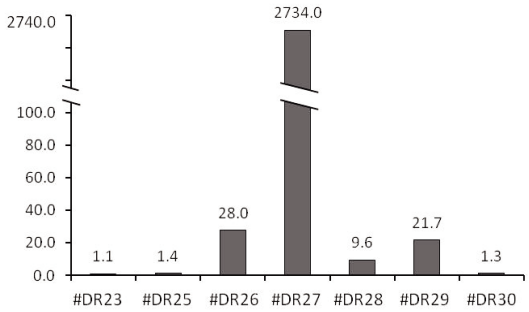

Figure 6. GLI1 expression in MyoT samples
GLI1 expression values in the 7 MyoT samples are expressed as TPM (transcripts per million).

6.1.4 PTCH1-GLI1 works as a hyperactive GLI1 allele and sustains GLI1 autoregolatory loop

Having verified that the *PTCH1-GLI1* chimera retains regions coding for the DNA binding, the nuclear localization signal and the transcriptional activation domain of GLI1, we hypothesized that the chimeric protein may work as a hyperactive GLI1 allele. To address this hypothesis we verified whether PTCH1-GLI1 conserved the GLI1 transcription regulation activity.

To this end, HT1080 cells were engineered to ectopically express the PTCH1-GLI1 chimera (fig. 7 A). GLI1 is known to activate its own expression through an autoregulatory loop (Ågren et al., 2004; Briscoe and Thérond, 2013; Dagklis et al., 2016; Zhu and Lo, 2010). Accordingly, PTCH1-GLI1 induced the expression of endogenous GLI1 in HT1080 cells both at protein and RNA level (fig. 7 A and 7 B). Also the expression of *PTCH1* is under GLI1 control (Ågren et al., 2004; Briscoe and Thérond, 2013) and, in agreement, *PTCH1* was upregulated in PTCH1-GLI1 engineered cells (fig. 8). Moreover, ectopic PTCH1-GLI1 expression elicited the induction of other canonical GLI1 target genes such as *FOXA2* (Sasaki et al., 1997; Zhu and Lo, 2010), *HHIP* (Chuang and McMahon, 1999; Vokes et al., 2007) and *CCND2* (Yoon et al., 2002) as demonstrated by quantitative RT-PCR (fig. 8).

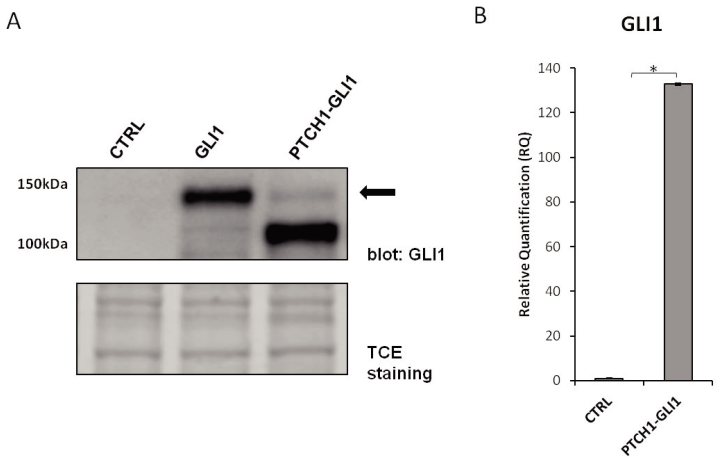

Figure 7. PTCH1-GLI sustains endogenous GLI1 expression in engineered cell lines

(A) Representative western blotting of HT1080 cells engineered to ectopically express the PTCH1-GLI1 chimera and the GLI1 full length protein (used as control). The arrow indicates expression of endogenous GLI1 in chimera positive cells. Endogenous GLI1 expression is not detectable in the control (CTRL, empty vector). Trichloroethylene (TCE) staining is used as loading control. **(B)** Expression of endogenous *GLI1* in PTCH1-GLI1 expressing cells is measured as relative quantification (RQ) assayed by q RT-PCR (a representative plot is shown). Empty vector was used as control. *statistical significance (p<0.05)

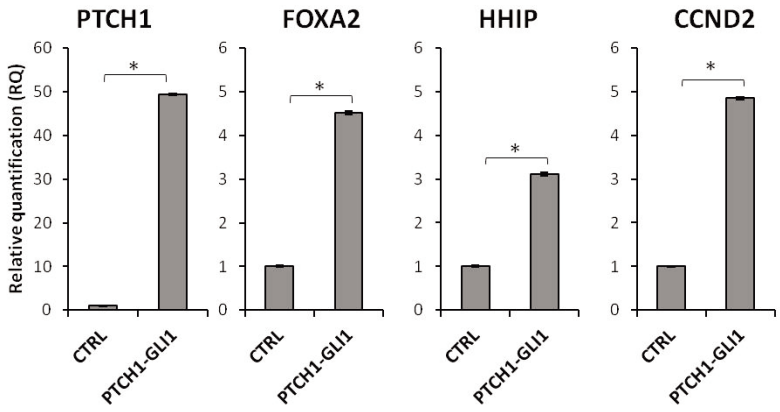

Figure 8. PTCH1-GLI elicits expression of GLI1 target genes in engineered cell lines

Representative plot showing expression of GLI1 target genes (endogenous *PTCH1*, *FOXA2*, *HHIP* and *CCND2*) in HT1080 ectopically expressing PTCH1-GLI1, measured as relative quantification (RQ) assayed by q RT-PCR. Empty vector was used as control. *statistical significance (p<0.05)

6.1.5 Transcriptome profiling of a series of MyoT and EMC: different transcriptome profiles characterize MyoT and EMC

In order to investigate molecular diversity of MyoT and the closely related entity EMC, we compared the transcriptome profile of MyoT with that of a series of 12 EMC (table 5). Principal component analysis (PCA) showed a separation of MyoT and EMC into two distinct groups along the principal component 1 (fig. 9 A). Similarly, unsupervised hierarchical clustering also indicates a trend of separation of MyoT from EMC according to their transcriptional profiles (fig. 9 B).

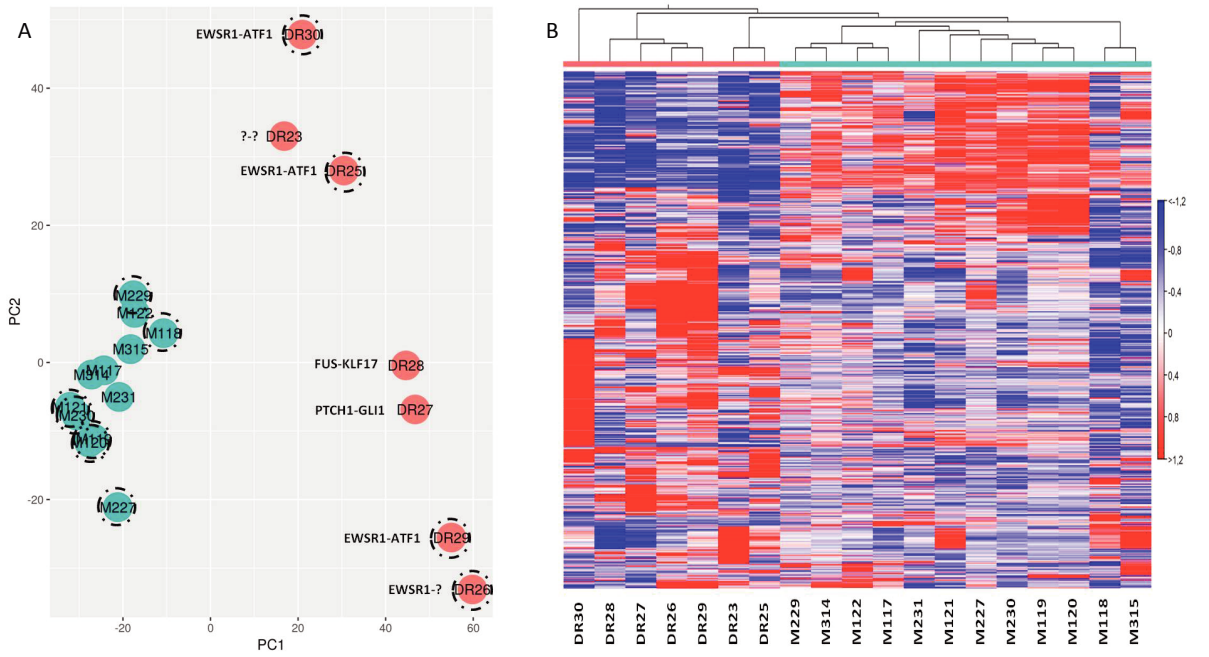

Figure 9. MyoT and EMC transcriptional profiling

(A) PCA shows a separation of MyoT (coral) and EMC (pale blue) samples, according to their transcriptional profiles, along the principal component 1 (PC1). Samples harboring EWSR1 rearrangement are dashed circled. Fusions identified through RNA-sequencing are indicated near the corresponding MyoT samples. **(B)** Unsupervised hierarchical clustering indicates a trend of separation of MyoT from EMC (represented on the horizontal axis dendogram with coral and pale blue bars, respectively) according to their transcriptional patterns. Red colors correspond to high gene expression levels while blue colors to low levels.

In an attempt to dissect pathobiology of these tumors we scrutinized genes differentially expressed in EMC vs. MyoT. Overall 5209 genes resulted to be significantly differentially expressed between the two tumors with an absolute fold change variation greater than 50% (abs.$\log_2$FoldChange ≥0.6; FDR ≤0.1).

Functional annotation of the genes differentially expressed was performed by using different tools (WebGestalt, Ingenuity Pathway Analysis, IPA and GSEA-Broad). Results of these analyses are summarized in tables 7 and 8. Briefly, GO terms related to epidermis and muscle development, actin and intermediate filament-based processes, WNT signaling, leukocyte differentiation and immune response were among the negative (enriched in MyoT in the comparison EMC vs. MyoT) significant related categories. Synaptic processes were among the positive related GO terms (enriched in EMC) (table 7).

IPA analysis predicted that, among others, pathways related to immune response as well as 'Basal Cell Carcinoma (BCC) signaling' and 'Sonic Hedgehog signaling' (HH) were activated in MyoT compared to EMC (i.e. have a negative z-score in the comparison EMC vs. MyoT) (table 8). Also when using the KEGG pathway database, HH, BCC and WNT signaling pathways emerged as significantly enriched in MyoT compared to EMC (FDR <0.05) (not shown).

Table 7. Gene Set Enrichment Analysis (GO terms): EMC vs. MyoT

Gene sets (GO terms)	NES	FDR
Epidermis development	-2.54	0.00
Skin development	-2.48	0.00
Actin filament-based movement	-2.22	0.00
Muscle cell differentiation	-2.09	0.01
Muscle system process	-2.09	0.01
Muscle tissue development	-2.04	0.01
Intermediate filament-based process	-2.03	0.01
Regulation of epithelial cell differentiation	-1.97	0.02
Leukocyte cell-cell adhesion	-1.96	0.02
Actomyosin structure organization	-1.93	0.03
Cell-cell signaling by WNT	-1.92	0.03
Activation of immune response	-1.85	0.04
Leukocyte differentiation	-1.85	0.04
Presynaptic process involved in chemical synaptic transmission	1.92	0.04
Neuron-neuron synaptic transmission	2.03	0.03
Vesicle-mediated transport in synapse	2.28	0.00

The table lists selected, non-redundant GO terms significantly enriched in MyoT (negative NES) and EMC (positive NES) identified by gene set enrichment analysis performed by WebGestalt and GSEA-Broad Institute (preranked analysis). NES and FDR values, according to Webgestalt, are reported. Terms are ordered by their NES. *NES, normalized enrichment score.*

Table 8. IPA canonical pathways: EMC vs. MyoT

INGENUITY CANONICAL PATHWAYS	-log(p-value)	Ratio	z-score
Dendritic Cell Maturation	4.91	0.28	-5.36
Th1 Pathway	5.64	0.32	-4.67
PI3K Signaling in B Lymphocytes	3.36	0.27	-4.12
PKC-Theta Signaling in T Lymphocytes	2.80	0.25	-4.02
Role of NFAT in Regulation of the Immune Response	1.82	0.22	-4.00
IL-8 Signaling	2.23	0.23	-3.81
Interferon Signaling	5.76	0.50	-3.64
Th2 Pathway	3.38	0.27	-3.14
Sonic Hedgehog Signaling	1.44	0.30	-2.83
Leukocyte Extravasation Signaling	6.77	0.30	-2.72
Basal Cell Carcinoma Signaling	3.33	0.32	-2.50
IL-6 Signaling	1.57	0.22	-2.41
IL-7 Signaling Pathway	1.90	0.25	-2.13
CD28 Signaling in T Helper Cells	1.89	0.24	-2.13

Core analysis was performed on IPA and the table displays a list of selected, non redundant significant (pval <0.05 and absolute z-score >2) enriched canonical pathways with negative z-score. The z-score is a prediction of pathway activation and negative z-score predicts activation of the pathway in MyoT (in the comparison EMC vs. MyoT). The significance value (calculated by Fisher's exact test right-tailed) is reported as -log(p-value). Ratio refers to the number of molecules of our dataset that map to the pathway divided by the total number of molecules that map to the canonical pathway.

On these grounds we scrutinized the expression, in MyoT and EMC, of genes known to be target of HH and WNT. Besides canonical GLI1 targets (*PTCH1*, *HHIP* and *GLI1* itself), also WNT targets including *CCND1* (Shtutman et al., 1999), *AXIN2* (Jho et al., 2002), *FOSL1* (Mann et al., 1999), *TCF4* (Kolligs et al., 2002) and *TCF7* (Roose et al., 1999) were overall significantly upregulated in MyoT tumors compared to EMC (abs.$\log_2$FoldChange >1; FDR <0.1) (fig. 10).

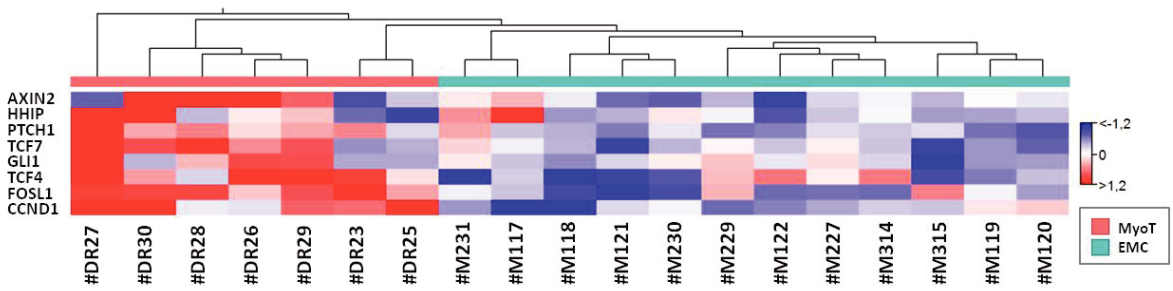

Figure 10. HH and WNT target genes are differentially expressed in MyoT compared to EMC

Heat map of HH and WNT target genes in MyoT and EMC was built by using Biomedical Genomic Workbench. Euclidean distance, average linkage and the specified features (*GLI1*, *HHIP*, *PTCH1*, *AXIN2*, *CCND1*, *FOSL1*, *TCF4 and TCF7*) were used as clustering settings. Red colors correspond to high gene expression levels while blue colors to low levels. Listed genes are significantly (abs.log2FoldChange >1; FDR <0.1) overexpressed in MyoT compared to EMC.

The upregulation of BCC and HH signalings in MyoT compared to EMC was true also when the *PTCH1-GLI1* positive case (#DR27) was excluded from the analysis.

6.2 DISCUSSION

Several fusion genes have been reported to be associated to MyoT. Yet a sizeable number of MyoT are “orphan” of genetic markers due to the absence of known fusions or the presence of rearrangements involving *EWSR1*, *FUS* or *PLAG1* but with unknown partners. We considered that a thorough characterization of these “orphan” tumors may help in better defining their pathobiology and may disclose novel tools to overcome diagnostic, prognostic and therapeutic challenges.

To make a step forward in this direction RNA-sequencing followed by fusion gene analysis was performed on a series of 7 soft tissue MyoT. *FUS-KLF17* and *EWSR1-ATF1*, two chimeras previously identified in MyoT, were detected in the one *FUS* and in three *EWSR1* rearranged tumors, respectively. No *EWSR1* fusion transcript was identified in the remaining *EWSR1* rearranged MyoT despite evidence of chromosome alterations at the *EWSR1* locus. Several potential fusions were identified by different bioinformatic tools in one case (#DR23) but none has been previously described and most of them are potential read-through.

Intriguingly, a *PTCH1-GLI1* in-frame fusion was detected in one tumor (#DR27). The fusion transcript retained exons coding for the DNA-binding zinc finger domains and the transactivation domain of GLI1 preceded by the 5’UTR and the ATG start codon of *PTCH1*. Notably, *PTCH1* and *GLI1* genes code for, respectively, the receptor and the nuclear effector of the canonical HH pathway.

Activation of the canonical HH pathway is initiated by the binding of the HH ligands Desert HH (DHH), Indian HH (IHH) or Sonic HH (SHH) to the 12 pass transmembrane Patched receptor (PTCH1 or PTCH2) (Ingham and McMahon, 2001). Upon binding of HH to PTCH, the G-protein receptor SMO is released from the inhibitory action of PTCH (Ingham and McMahon, 2001). In turn, activated SMO releases the GLI transcription factors (GLI1, GLI2 or GLI3) from the complex that they form with Suppressor of Fused (SUFU), thus allowing GLI nuclear translocation (Briscoe and Thérond, 2013; Monkkonen and Lewis, 2017). After entering the nucleus, GLI proteins bind the consensus sequence 5’-GACCACCCA-3’ through the DNA-binding domain and regulate expression of a number of genes involved in survival, cell proliferation and differentiation (Briscoe and Thérond, 2013; Hallikas et al., 2006) among which *CCND2* (Yoon et al., 2002) and *FOXA2* (Sasaki et al., 1997; Zhu and Lo, 2010). GLI dependent transcription also elicits expression of negative regulators of HH signaling, including PTCH1 (Ågren et al., 2004; Briscoe and Thérond, 2013) and HHIP (Briscoe and Thérond, 2013; Chuang and McMahon, 1999; Vokes et al., 2007) thus inducing an autoregulatory negative feedback. Positive autoregulatory feedback also occurs as GLI dependent transcription increases expression of GLI1 itself (Ågren et al., 2004; Briscoe and Thérond, 2013; Dagklis et al., 2016; Zhu and Lo, 2010) and GAS1 coreceptor (Briscoe and Thérond, 2013). Although this pathway is mainly active during embryogenesis, in some adult tissues participates to the control of homeostasis and stem-cell maintenance (Bellusci et al., 1997; Hebrok et al., 2000; Lai et al., 2003; Machold et al., 2003; Petrova and Joyner, 2014).

A *PTCH1-GLI1* fusion has been very recently reported by Antonescu and coll. in a series of soft tissue neoplasms. Based on immunoprofile and clinical pattern, the authors seem to rule

out the possibility that these neoplasms are MyoT but rather suggest that they represent a novel and distinct pathological entity (Antonescu et al., 2018). The histopathological features of our *PTCH1-GLI1* translocated tumor are definitively coherent with the diagnosis of MyoT. Also its transcriptional profile, according to PCA and hierarchical clustering, was in line with that of the other MyoT included in the series; moreover it shares with the other MyoT analyzed the activation of the HH and BCC pathways since, even when we excluded the *PTCH1-GLI1* positive case from the analysis, these pathways emerged as upregulated. Thus, we conclude that the *PTCH1-GLI1* translocation is to be included in the genetic variants of classical MyoT.

Furthermore, from a genetic standpoint, the chromosomal rearrangements leading to the generation of the *PTCH1-GLI1* fusion in ours and in the case reported by Antonescu and coll. were different. In the case described by Antonescu and coll. the *GLI1* locus was broken, as highlighted by the break-apart FISH pattern. In our case, the pattern observed was consistent with an insertion of the *PTCH1* gene into the *GLI1* locus, which then maintained a normal disomic pattern of *GLI1*-specific break-apart signals. Considering that *PTCH1* and *GLI1* genes have opposite orientations, fusions involving the two genes are unlikely be due to a classical balanced translocation but must be sustained by more complex chromosomal events such as three way translocations or insertions. In the light of these observations we consider that a dual color/dual fusion FISH approach could better identify *PTCH1-GLI1* fusion events, compared to the classical *GLI1* break-apart approach.

GLI1 gene rearrangements have been identified in different types of tumor so far. In particular, *GLI1*, located on 12q13.3, has been described to be fused with *MALAT1* (Antonescu et al., 2018; Graham et al., 2017; Spans et al., 2016) located on 11q13.1, *ACTB* (Antonescu et al., 2018; Bridge et al., 2012; Castro et al., 2016; Dahlén et al., 2004a, 2004b; Koh et al., 2018) located on 7p22.1, or rearranged with *INHBE* as a consequence of focal intrachromosomal deletions or inversions (Nault et al., 2017).

The pathogenetic consequence of these fusions is the overexpression of *GLI1*. The expression of *GLI1*, being under the control of the HH signaling, is often used as a readout of such pathway activation (Dagklis et al., 2016; Gupta et al., 2010; Yauch et al., 2008). Also in our case carrying *PTCH1-GLI1*, GLI1 was overexpressed both at RNA and protein level. Furthermore in vitro experiments proved that the chimera conserved the ability to induce canonical HH targets. Aberrant activation of HH pathway is a feature of a variety of human tumours that include basal cell carcinoma, glioma, osteosarcoma, rhabdomyosarcoma, medulloblastoma, lymphoma and pericytoma (Dahlén et al., 2004a; Dierks et al., 2007; Ferretti et al., 2008; Hahn et al., 1996; Katoh and Katoh, 2009; Khatib et al., 1993; Kinzler et al., 1987; Raffel et al., 1997; Reifenberger et al., 2005; Werner et al., 1997). Other than *GLI1* fusion genes, alternative mechanisms of HH activation include *GLI1* overexpression and/or amplification, *PTCH* or *SUFU* loss of function mutations, *SMO* gain of function mutations, *SHH* or *IHH* transcriptional upregulation, *HHIP* transcriptional downregulation and *SMO* and *GLI1* miRNA dysregulation (Dahlén et al., 2004a; Dierks et al., 2007; Ferretti et al., 2008; Hahn et al., 1996; Katoh and Katoh, 2009; Khatib et al., 1993; Kinzler et al., 1987; Raffel et al., 1997; Reifenberger et al., 2005; Werner et al., 1997). The identification of a tumor with

PTCH1-GLI1 fusion extends the series of aberrant HH signaling neoplasms also to MyoT. This notion has been corroborated by the detection of an *ACTB-GLI1* fusion in a tumor belonging to an additional series of MyoT analyzed by collaborators of ours.
Intriguingly, inhibition of the HH signaling is a strategy that is currently being evaluated for treatment of different malignancies (Xin et al., 2018). In particular, inhibitors of GLI mediated transcription include different compounds, among which Arsenic Trioxide (ATO) which has been approved by the FDA for the treatment of acute promyelocytic leukemia (Xin et al., 2018).

Besides extending the subset of genetic alterations involved in MyoT pathogenesis, we sought to better explore pathobiology of this very uncommon tumor. Indeed the high degree of variability, in terms of morphology and immunoprofile, not only prevents a clear cut definition of the MyoT lineage of differentiation, but also impacts on the diagnosis, which remains challenging due to the overlap with a wide spectrum of different entities, primarily EMC. Conventionally, EMC are considered to be marked by the rearrangement of the *NR4A3* gene (Fletcher et al., 2013). However, whether this marker actually identifies a distinct entity or whether instead EMC and MyoT are just two genetic variants of the same disease is still unclear. To shed light on this issue we sought to compare the transcriptional profiles of the two entities.
PCA and unsupervised hierarchical clustering showed that EMC and MyoT formed a two separated cluster. In particular, EMC formed a compact cluster, irrespective of whether *NR4A3* was fused to *TAF15* or *EWSR1*. A higher heterogeneity was instead evident for the transcriptional profiles of MyoT, which tended to separate one to the other even in the presence of the same genetic alteration (compare cases #DR30, #DR25 and #DR29 which bear the same *EWSR1-ATF1* gene fusion). Molecular heterogeneity of MyoT probably mirrors the engagement of different routes of neoplastic progression exploited by these tumors. Overall, our results support the notion that EMC, as defined by *NR4A3* rearrangement, does represent a distinct entity compared to MyoT, which instead appear as a quite heterogeneous group of tumors.
In the attempt to make a step ahead in the direction of a better definition of the biology of MyoT, we asked whether these tumors, considered as a whole, relied on common pathways compared to EMC. To this end we performed functional annotation of the genes differentially expressed between MyoT and EMC. This analysis highlighted an overrepresentation of the immune system in MyoT compared to EMC, in line with the hypothesis that EMC may be poorly infiltrated tumors. GO terms related to epidermis development, epithelial and muscle cell differentiation emerged as common features of MyoT, in line with their myoepithelial differentiation lineage (Hornick, 2013). Pathway analysis indicated HH, BCC and WNT signaling as significantly enriched in MyoT compared to EMC.
Intriguingly, as described above, the identification of a rearrangement, in a MyoT tumor, involving two components of the HH pathway (*PTCH1-GLI1*) strongly supports the involvement of this signaling in a fraction of MyoT. Indeed, the *PTCH1-GLI1* fusion likely

represents one of possible mechanisms of activation of the HH downstream pathway in MyoT and even when the *PTCH1-GLI1* rearranged case was excluded from the analysis, still the HH and BCC signaling appeared to be enriched in MyoT. In this regard, HH targets including *PTCH1*, *HHIP* and *GLI1* itself were overall upregulated in MyoT cases compared to EMC. HH signaling has been reported to affect myogenic differentiation processes (Drummond et al., 2018; Elia et al., 2007; Hettmer et al., 2016; Koleva et al., 2005) and to be involved in normal muscle regeneration (Straface et al., 2009). The fact that MyoT feature myogenic traits, as highlighted also by the comparison EMC vs. MyoT, is in line with the involvement of HH pathway in these tumors.

Also the WNT pathway appeared to be hyperactive in MyoT compared to EMC and WNT targets (e.g. *CCND1* (Shtutman et al., 1999), *AXIN2* (Jho et al., 2002), *FOSL1* (Mann et al., 1999), *TCF4* (Kolligs et al., 2002) and *TCF7* (Roose et al., 1999)) were upregulated in the first category. The WNT/β-catenin signaling is activated through interaction of WNT ligands with Frizzled receptors (FZD) and low-density lipoprotein (LRP5/LRP6) coreceptors at the cell surface (Katoh and Katoh, 2007; Nakamura and Hoppler, 2017). Upon this binding, β-catenin phosphorylation and degradation is inhibited allowing its un-phosphorylated form to accumulate in the cytosol and then to migrate to the nucleus where it functions as transcriptional coactivator (Pala et al., 2017). Here β-catenin interacts with T-cell specific factor (TCF), lymphoid enhancer-binding factor (LEF) and co-activators to activate transcription of WNT target genes (Gordon and Nusse, 2006; Katoh and Katoh, 2007; Krishnamurthy and Kurzrock, 2018). WNT pathway is known to cross-regulate and interact at multiple levels with HH signaling (Li et al., 2007; Noubissi et al., 2009), although the mechanisms of this bi-directional interplay are not fully elucidated yet. Moreover, the intersection of the two pathways identifies a distinct pathway, the BCC signaling, that is also upregulated in MyoT compared to EMC. Our data suggest that the interaction of HH and WNT networks may be a common feature of MyoT.

CONCLUSIONS

Our study allowed the identification, through RNA-sequencing, of *ETV6-NTRK3* and *PTCH1-GLI1* fusion transcripts respectively in a case of GIST and MyoT. The study unveiled also that MyoT are a quite heterogenous group of tumors that clearly segregate a part from EMC. Although heterogeneous, MyoT seem to feature a peculiar activation of HH and WNT pathways according to functional analysis.

MATERIALS AND METHODS

Patients and tumor samples

The study was conducted on a series of GIST, MyoT and EMC samples retrieved from the pathological files of Treviso General Hospital (Treviso) and Fondazione Nazionale Tumori IRCCS (Milan). The study was approved by the institutional review board.

DNA extraction and NGS targeted profiling

Targeted sequencing of GIST samples was performed as described in (Gasparotto et al., 2017). Briefly, DNA was extracted from Formalin Fixed, Paraffin-Embedded (FFPE) samples and matched normal samples using the QIAamp DNA FFPE Tissue Kit (Qiagen) and the EZ1 biorobot (Qiagen). MPS libraries were prepared by using a TruSeq Custom Amplicon panel (Illumina) targeting the following genes: KIT, PDGFRA, BRAF, SDHA, SDHB, SDHC, SDHD, HRAS, KRAS, NRAS, NF1, NF2, HIF1A, PTEN, RAF1, RUNX1, SMARCB1, VHL, CDKN2A, PIK3CA, RB1, SPRED1 and TP53. Sequencing was performed on the MiSeq platform (Illumina) and data were analyzed by using the Miseq Reporter software.

RNA extraction, whole-transcriptome sequencing, fusion gene detection and functional annotation analysis

Total RNA was isolated from FFPE samples using the Ambion Recover All^{TM} Total Nucleic Acid Isolation Kit (Life Technology) and from cell cultures using TRIzol reagent (Ambion).

RNA-sequencing libraries were prepared according to Illumina's TruSeq RNA protocol and sequenced on a Illumina HiSeq 1000 apparatus (Illumina, San Diego, USA) to a depth of 50-80 million paired-end reads/sample. The quality of the raw sequence data was assessed using FastQC software. Reads mapping, quantification, and differential expression analysis were performed by using respectively STAR, HTseqcount and DEseq2. FusionCatcher (Nicorici et al., 2014), ChimeraScan (Iyer et al., 2011), PyPRADA (Torres-García et al., 2014), STAR fusion (Dobin et al., 2013), JAFFA (Davidson et al., 2015), MANTA (Chen et al., 2016) and an in-house algorithm were used for fusion gene detection. We consider fusion transcripts confirmed by at least two different bioinformatic tools or supported by at least 1 spanning and 2 encompassing reads.

Principal component analysis (PCA), based on the top 500 genes with higher variance, was performed by using DeSeq2. Biomedical Genomics Workbench (QIAGEN Bioinformatics) was exploited to perform TPM (transcripts per million) estimation and hierarchical clustering. More in detail, the 1000 genes with the highest coefficient of variation (the ratio of the standard deviation to the mean) and with more than 10 counts in at least one sample were considered for unsupervised hierarchical clustering, according to QIAGEN user manual. Gene set enrichment, functional annotation and pathway analysis were performed by using the following suites: WebGestalt 2017 (Wang et al., 2017), GSEA-Broad Institute 3.0 (Subramanian et al., 2005) and Ingenuity Pathway Analysis (IPA) (Krämer et al., 2014).

The WebGestalt suite was used for gene set enrichment analysis with geneontology_Biological_Process_noRedundant as enrichment categories. The analysis was

performed on the list of differentially expressed genes in EMC vs. MyoT filtered for abs.log_2(FoldChange) ≥0.6 and p.val ≤0.05. Other parameters settings were: minimum number of genes in the category: 5; maximum number of genes in the category: 2000; significance level: FDR <0.05; number of permutations: 1000.
GSEA-Broad Institute was exploited to run a preranked analysis on the list of differentially expressed genes in EMC vs. MyoT by using predefined c5.all.v6.2 and c2.cp.kegg.v6.2 gene set databases. For basic and advanced fields were used default settings.
IPA core analysis was performed on the list of differentially expressed genes in EMC vs MyoT. In order to obtain a list suitable for IPA analysis, cutoff values were 1 and 0.1 respectively for absolute.log_2(FoldChange) and FDR.

FISH analysis, RT-PCR and quantitative RT-PCR (qRT-PCR)
Vysis ETV6 and EWSR1 (Abbott Molecular), Zito Light FUS (Zyto Vision), NR4A3 RP11-30N20 and RP11-30L7, TAF15 RP11-646F19 and RP11-616N20 and PLAG1 RP11-246A9 and RP11-1130K23 probes were used to investigate respective gene rearrangements. GLI1 gene status was investigated by dual color break-apart FISH using both in house labeled BAC (Spectrum Orange labeled RP11-181L23; Spectrum Green labeled RP11-772J17) as well as a commercially available DDIT3 break-apart probe kit (Abbott Molecular). PTCH1 gene status was assessed by break-apart FISH with in house labeled BAC clones (Spectrum Orange labeled RP11-691D16, Spectrum Green labeled RP11-34J23). BACs for GLI1 and PTCH1 were then labeled for dual color dual fusion FISH approach (Spectrum Orange and Spectrum Green, respectively).
Total RNA (1 μg) was retro-transcribed into cDNA using the SuperScript III Reverse Transcriptase (Life Technologies) and random examers, according to supplier protocol. RT-PCR for ETV6-NTRK3 and PTCH1-GLI1 rearrangements were carried out using the following forward and reverse primers (mapping respectively, on the 5' and 3' of the breakpoint region predicted by RNA-seq):
ETV6 F1 5' GCTGCTGACCAAAGAGGACTTTC 3'; *ETV6* F2 5' GCAGAGGAAACCTCGGATTC 3';
NTRK3 R 5' ATGCCGTGGTTGATGTGGTGCAGTGG 3'; PTCH1 F 5' GAATTGATGTGAAATCCAAG 3'; GLI1 R 5' GTCCTCCCGCCCATCCAG 3'.
qRT-PCR reactions were prepared by using Sso Fast EvaGreen Supermix (Bio-Rad) and carried out on a CFX96 Real-Time System (Bio-Rad). Bio-Rad CFX manager software was used. Normalized expression levels were relative to control by using the comparative Ct method (DDCt). The geometric average of a set of three housekeeping genes (SF3A1, PPIA, B2M) was used. Three independent experiments were performed in duplicate.
Primers are indicated below:
CCND2 F 5' GAGAAGCTGTCTCTGATCCGCA 3'; CCND2 R 5' CTTCCAGTTGCGATCATCGACG 3'; HHIP F 5' GCCATTCAGTAATGGTCCTTTGG 3'; HHIP R 5' GCCACTGCTTTGTCACAGGAC 3'; FOXA2 F 5' GGAGCGGTGAAGATGGAAGG3 3'; FOXA2 R 5' CGTGTTCATGCCGTTCATCC 3'; PTCH1 F 5' GTGGCCCTCACGTCCATCAGC 3'; PTCH1 R 5' CCATGGCAAAATTGAACACCAC 3'; GLI1 F 5' GGATGATCCCACATCCTCAGTC 3'; GLI1 R 5' GTGGATGTGCTCGCTGTTGATG 3'; SF3A1 F 5' ACCTTCTAAGCCAGTTGTGGG 3'; SF3A1 R 5' TAGCTTCAAATTCAGGCCCGT 3'; PPIA F 5'

TCTGCACTGCCAAGACTGAG 3'; PPIA R 5' TGGTCTTGCCATTCCTGGAC 3'; B2M F 5' GAGTATGCCTGCCGTGTG 3'; B2M R 5' AATCCAAATGCGGCATCT 3'.

Cells and constructs

U2OS and HT1080 were maintained in Dulbecco's Modified Eagle's Medium-high glucose (Sigma-Aldirich) supplemented with 10% heat inactivated fetal bovine serum (FBS) (Sigma-Aldrich).

For IRS1 immunoprecipitation experiments, cells were grown both in basal conditions (DMEM supplemented with 10% FBS) or in serum starvation for 16 hours. For AKT immunoblotting, cells were serum starved for 16 hours. In q RT-PCR evaluation of CCND2, cells were grown in basal conditions, then starved for 2 hours before RNA extraction.

As regarding retroviral infection, viral supernatants were prepared according to standard calcium-phosphate transfection method in Linx-A cells (Hannon et al., 1999). Infection was performed with polybrene 4 μg/ml by centrifugation at 1600 rpm for 1 hour and overnight incubation at 32°C. Medium was then replaced and 48 hours later, puromycin selection was started for 4 days. After 24 hour of recovery from antibiotic selection, cells were used for experiments. Two different biological replicates were obtained by using independently produced virus to infect target cells. The following plasmid constructs were used: pMSCV-IF EN, pMSCV-GIST EN and pMSCV Empty for GIST study; pLPCX-PTCH1-GLI1, pLPCX-GLI1 and pLPCX Empty for MyoT study. pMSCV-IF EN (exons 1-5 ETV6_exons 15-19 NTRK3) was a kind gift of PH Sorensen; the cDNA coding for GIST EN (exons 1-4 ETV6_exons 14-19 NTRK3) chimera and PTCH1-GLI1 (exon 1 PTCH1_exons 7-12 GLI1) were cloned, respectively, in pMSCV and pLPCX vectors (Clontech). PTCH1 exon1 sequence was amplified from the BAC clone RP11-691D16 (Invitrogen) and GLI1 sequence was cloned from pBluescript KS-GLI1 (GLI K12 16419, Addgene).

Cell viability/cytotoxicity assay was performed through Sulforhodamine B colorimetric assay (SRB) (Vichai and Kirtikara, 2006) as follows. Cells were plated in 96-well plates and after overnight cell adhesion were treated for 48 hours with the drug; then were fixed using cold 50% trichloroacetic acid for 1 hour at 4°C and stained using Sulphorhodamine B (Sigma) 0.4% in 1% acetic acid. Tris-base 10 mM was used for solubilization. The absorbance of protein biomass, which is proportional to the cell number, was read at 550 nm by using Tecan infinite M1000Pro apparatus and Tecan i-control software. Time zero plates were used for background subtraction and calculation of relative absorbance values was performed as previously described (Vichai and Kirtikara, 2006). The experiment was performed in eight technical replicates. Drugs used were the follows: Crizotinib (S1068; SelleckChem), Ceritinib (S7083; SelleckChem), AG1024 (Calbiochem), and PQ401 (Calbiochem).

Western blot, immunoprecipitation and immunofluorescence analysis

Protein cell lysates were prepared by using RIPA buffer (Santa Cruz Biotechnology) supplemented with protease and phosphatase inhibitors. Protein lysates (35 ug) were separated by SDS-page on 4%-15% gradient TGX Stain-Free™ gel (Bio-Rad) and electroblotted onto 0.45 μm nitrocellulose blotting membrane (Sartorius). TRK, GAPDH,

Phospho-Tyrosine (pTyr), IRS1, pAKT, AKT and GLI1 immunostainings were performed with antibodies described below. Secondary antibodies were HRP (HorseRadish peroxidase) coniugated (PerkinElmer) and chemiluminescence signal was revealed by ChemiDOC XRS+ apparatus and ImageLab Software (Bio-Rad). GAPDH or Trichloroethylene (TCE) staining were used to normalize protein loading.

IRS1 immunoprecipitation was carried out overnight at 4°C with mixing in 20 mM TRIS-HCl/150 mM NaCl/1 mM EDTA/0.5% IGEPAL containing buffer with protein G-conjugated Sepharose beads (GE Healthcare) and IRS1 polyclonal antibody. Immunoprecipitated lysates were analyzed through SDS-PAGE. Immunoblot was performed first for phosphotyrosine and then for IRS1; the amount of phosphorylated IRS1 was calculated as the phospho-IRS1:total-IRS1 ratio.

For AKT immunoblotting, after SDS-PAGE, blots were first probed with anti-phospho-AKT (Ser 473) followed by anti total-AKT. The amount of activated AKT was calculated as the phospho-AKT:total-AKT ratio.

In subcellular fractionation, cytosolic- and nuclear-fraction enriched protein lysates were obtained, respectively, with buffer A (10 mM Hepes/10 mM KCl/0.1 mM EDTA/0.1 mM EGTA/0.1% NP40) and buffer B (20 mM HEPES/400 mM NaCl/1 mM EDTA/1% NP40) supplemented with protease and phosphatase inhibitors.

IRS1-immunofluorescence was carried out by fixing and permeabilizing the cells with, respectively, 4% paraformaldehyde (10 min) and 0.2% Triton/0.1 % BSA (15 min) solutions. IRS1 immunostaining and phalloidin cytoplasmic counterstainig were performed according to the manufacturer's instructions.

Antibodies used were: TRK: SC-139 (Santa Cruz Biotechnology) dilution 1:1000; GAPDH: SC-32233 (Santa Cruz Biotechnology) dilution 1:10000; pTyr: P11230 (Transduction Laboratories) dilution 1:1000; IRS-1 (western blot and immunoprecipitation): 06-248 (Millipore Merk) dilution 1:1000; IRS-1 (immunofluorescence): ab52167 (Millipore Merk) dilution 1:500; Phalloidin: A12379 (Alexa Fluor) dilution 1:200; GL1: 2553 (Cell Signaling) dilution 1:1000. For immunohistochemistry antibodies used were: CD117/KIT: A4502 (DakoCytomation) dilution 1:700; DOG1: clone K9 (Novocastra) dilution 1:100; SDHB: 21A11 (Abcam) dilution 1:750; GLI1 sc-20687 (Santa Cruz Biotechnology).

Statistics

Statistical significance in cell viability/cytotoxicity assays and q RT-PCR analysis was assessed by two-tailed unpaired t-test and one sample t-test, respectively.

REFERENCES

Abeshouse, A., Adebamowo, C., Adebamowo, S.N., Akbani, R., Akeredolu, T., Ally, A., Anderson, M.L., Anur, P., Appelbaum, E.L., Armenia, J., et al. (2017). Comprehensive and Integrated Genomic Characterization of Adult Soft Tissue Sarcomas. Cell *171*, 950-965.e28.

Agaram, N.P., Zhang, L., Sung, Y.-S., Singer, S., and Antonescu, C.R. (2014). Extraskeletal myxoid chondrosarcoma with non-EWSR1-NR4A3 variant fusions correlate with rhabdoid phenotype and high-grade morphology. Hum. Pathol. *45*, 1084–1091.

Agaram, N.P., Chen, H.-W., Zhang, L., Sung, Y.-S., Panicek, D., Healey, J.H., Nielsen, G.P., Fletcher, C.D.M., and Antonescu, C.R. (2015). EWSR1-PBX3: a novel gene fusion in myoepithelial tumors. Genes. Chromosomes Cancer *54*, 63–71.

Ågren, M., Kogerman, P., Kleman, M.I., Wessling, M., and Toftgård, R. (2004). Expression of the PTCH1 tumor suppressor gene is regulated by alternative promoters and a single functional Gli-binding site. Gene *330*, 101–114.

Alassiri, A.H., Ali, R.H., Shen, Y., Lum, A., Strahlendorf, C., Deyell, R., Rassekh, R., Sorensen, P.H., Laskin, J., Marra, M., et al. (2016). ETV6-NTRK3 Is Expressed in a Subset of ALK-Negative Inflammatory Myofibroblastic Tumors. Am. J. Surg. Pathol. *40*, 1051–1061.

Antonescu, C.R. (2006). The role of genetic testing in soft tissue sarcoma. Histopathology *48*, 13–21.

Antonescu, C.R., Besmer, P., Guo, T., Arkun, K., Hom, G., Koryotowski, B., Leversha, M.A., Jeffrey, P.D., Desantis, D., Singer, S., et al. (2005). Acquired resistance to imatinib in gastrointestinal stromal tumor occurs through secondary gene mutation. Clin. Cancer Res. Off. J. Am. Assoc. Cancer Res. *11*, 4182–4190.

Antonescu, C.R., Le Loarer, F., Mosquera, J.-M., Sboner, A., Zhang, L., Chen, C.-L., Chen, H.-W., Pathan, N., Krausz, T., Dickson, B.C., et al. (2013a). Novel YAP1-TFE3 fusion defines a distinct subset of epithelioid hemangioendothelioma. Genes. Chromosomes Cancer *52*, 775–784.

Antonescu, C.R., Zhang, L., Shao, S.Y., Mosquera, J.-M., Weinreb, I., Katabi, N., and Fletcher, C.D.M. (2013b). Frequent PLAG1 gene rearrangements in skin and soft tissue myoepithelioma with ductal differentiation. Genes. Chromosomes Cancer *52*, 675–682.

Antonescu, C.R., Sung, Y.-S., Chen, C.-L., Zhang, L., Chen, H.-W., Singer, S., Agaram, N.P., Sboner, A., and Fletcher, C.D. (2014). Novel ZC3H7B-BCOR, MEAF6-PHF1, and EPC1-PHF1 fusions in ossifying fibromyxoid tumors--molecular characterization shows genetic overlap with endometrial stromal sarcoma. Genes. Chromosomes Cancer *53*, 183–193.

Antonescu, C.R., Agaram, N.P., Sung, Y.-S., Zhang, L., Swanson, D., and Dickson, B.C. (2018). A Distinct Malignant Epithelioid Neoplasm With GLI1 Gene Rearrangements, Frequent S100 Protein Expression, and Metastatic Potential: Expanding the Spectrum of Pathologic Entities With ACTB/MALAT1/PTCH1-GLI1 Fusions. Am. J. Surg. Pathol. *42*, 553–560.

Argani, P., Lal, P., Hutchinson, B., Lui, M.Y., Reuter, V.E., and Ladanyi, M. (2003). Aberrant nuclear immunoreactivity for TFE3 in neoplasms with TFE3 gene fusions: a sensitive and specific immunohistochemical assay. Am. J. Surg. Pathol. *27*, 750–761.

Argani, P., Aulmann, S., Illei, P.B., Netto, G.J., Ro, J., Cho, H., Dogan, S., Ladanyi, M., Martignoni, G., Goldblum, J.R., et al. (2010). A distinctive subset of PEComas harbors TFE3 gene fusions. Am. J. Surg. Pathol. *34*, 1395–1406.

Arnaldez, F.I., and Helman, L.J. (2012). Targeting the insulin growth factor receptor 1. Hematol. Oncol. Clin. North Am. *26*, 527–542, vii–viii.

Aurias, A., Rimbaut, C., Buffe, D., Dubousset, J., and Mazabraud, A. (1983). [Translocation of chromosome 22 in Ewing's sarcoma]. Comptes Rendus Seances Acad. Sci. Ser. III Sci. Vie *296*, 1105–1107.

Bauer, S., Yu, L.K., Demetri, G.D., and Fletcher, J.A. (2006). Heat shock protein 90 inhibition in imatinib-resistant gastrointestinal stromal tumor. Cancer Res. *66*, 9153–9161.

Beadling, C., Patterson, J., Justusson, E., Nelson, D., Pantaleo, M.A., Hornick, J.L., Chacón, M., Corless, C.L., and Heinrich, M.C. (2013). Gene expression of the IGF pathway family distinguishes subsets of gastrointestinal stromal tumors wild type for KIT and PDGFRA. Cancer Med. *2*, 21–31.

Bellusci, S., Furuta, Y., Rush, M.G., Henderson, R., Winnier, G., and Hogan, B.L. (1997). Involvement of Sonic hedgehog (Shh) in mouse embryonic lung growth and morphogenesis. Dev. Camb. Engl. *124*, 53–63.

Borden, E.C., Baker, L.H., Bell, R.S., Bramwell, V., Demetri, G.D., Eisenberg, B.L., Fletcher, C.D.M., Fletcher, J.A., Ladanyi, M., Meltzer, P., et al. (2003). Soft tissue sarcomas of adults: state of the translational science. Clin. Cancer Res. Off. J. Am. Assoc. Cancer Res. *9*, 1941–1956.

Brenca, M., and Maestro, R. (2015). Massive parallel sequencing in sarcoma pathobiology: state of the art and perspectives. Expert Rev. Anticancer Ther. *15*, 1473–1488.

Brenca, M., Rossi, S., Polano, M., Gasparotto, D., Zanatta, L., Racanelli, D., Valori, L., Lamon, S., Tos, A.P.D., and Maestro, R. (2016). Transcriptome sequencing identifies ETV6–NTRK3 as a gene fusion involved in GIST. J. Pathol. *238*, 543–549.

Bridge, J.A. (2008). Contribution of cytogenetics to the management of poorly differentiated sarcomas. Ultrastruct. Pathol. *32*, 63–71.

Bridge, J.A. (2014). The role of cytogenetics and molecular diagnostics in the diagnosis of soft-tissue tumors. Mod. Pathol. Off. J. U. S. Can. Acad. Pathol. Inc *27 Suppl 1*, S80-97.

Bridge, J.A., and Cushman-Vokoun, A.M. (2011). Molecular Diagnostics of Soft Tissue Tumors. Arch. Pathol. Lab. Med. *135*, 588–601.

Bridge, J.A., Fidler, M.E., Neff, J.R., Degenhardt, J., Wang, M., Walker, C., Dorfman, H.D., Baker, K.S., and Seemayer, T.A. (1999). Adamantinoma-like Ewing's sarcoma: genomic confirmation, phenotypic drift. Am. J. Surg. Pathol. *23*, 159–165.

Bridge, J.A., Sanders, K., Huang, D., Nelson, M., Neff, J.R., Muirhead, D., Walker, C., Seemayer, T.A., and Sumegi, J. (2012). Pericytoma with t(7;12) and ACTB-GLI1 fusion arising in bone. Hum. Pathol. *43*, 1524–1529.

Briscoe, J., and Thérond, P.P. (2013). The mechanisms of Hedgehog signalling and its roles in development and disease. Nat. Rev. Mol. Cell Biol. *14*, 416–429.

Casali, P.G. (2012). Histology- and non-histology-driven therapy for treatment of soft tissue sarcomas. Ann. Oncol. Off. J. Eur. Soc. Med. Oncol. *23 Suppl 10*, x167-169.

Casali, P.G., Abecassis, N., Bauer, S., Biagini, R., Bielack, S., Bonvalot, S., Boukovinas, I., Bovee, J.V.M.G., Brodowicz, T., Broto, J.M., et al. (2018a). Soft tissue and visceral sarcomas: ESMO–EURACAN Clinical Practice Guidelines for diagnosis, treatment and follow-up. Ann. Oncol. *29*, iv51–iv67.

Casali, P.G., Abecassis, N., Bauer, S., Biagini, R., Bielack, S., Bonvalot, S., Boukovinas, I., Bovee, J.V.M.G., Brodowicz, T., Broto, J.M., et al. (2018b). Gastrointestinal stromal tumours: ESMO–EURACAN Clinical Practice Guidelines for diagnosis, treatment and follow-up. Ann. Oncol. *29*, iv68–iv78.

Castro, E., Cortes-Santiago, N., Ferguson, L.M.S., Rao, P.H., Venkatramani, R., and López-Terrada, D. (2016). Translocation t(7;12) as the sole chromosomal abnormality resulting in ACTB-GLI1 fusion in pediatric gastric pericytoma. Hum. Pathol. *53*, 137–141.

Chen, L.L., Holden, J.A., Choi, H., Zhu, J., Wu, E.F., Jones, K.A., Ward, J.H., Andtbacka, R.H., Randall, R.L., Scaife, C.L., et al. (2008). Evolution from heterozygous to homozygous KIT mutation in gastrointestinal stromal tumor correlates with the mechanism of mitotic nondisjunction and significant tumor progression. Mod. Pathol. Off. J. U. S. Can. Acad. Pathol. Inc *21*, 826–836.

Chen, X., Schulz-Trieglaff, O., Shaw, R., Barnes, B., Schlesinger, F., Källberg, M., Cox, A.J., Kruglyak, S., and Saunders, C.T. (2016). Manta: rapid detection of structural variants and indels for germline and cancer sequencing applications. Bioinforma. Oxf. Engl. *32*, 1220–1222.

Chuang, P.-T., and McMahon, A.P. (1999). Vertebrate Hedgehog signalling modulated by induction of a Hedgehog-binding protein. Nature *397*, 617–621.

Corless, C.L. (2014). Gastrointestinal stromal tumors: what do we know now? Mod. Pathol. Off. J. U. S. Can. Acad. Pathol. Inc *27 Suppl 1*, S1-16.

Corless, C.L., Barnett, C.M., and Heinrich, M.C. (2011). Gastrointestinal stromal tumours: origin and molecular oncology. Nat. Rev. Cancer *11*, 865–878.

Corless, C.L., Ballman, K.V., Antonescu, C.R., Kolesnikova, V., Maki, R.G., Pisters, P.W.T., Blackstein, M.E., Blanke, C.D., Demetri, G.D., Heinrich, M.C., et al. (2014). Pathologic and molecular features correlate with long-term outcome after adjuvant therapy of resected primary GI stromal tumor: the ACOSOG Z9001 trial. J. Clin. Oncol. Off. J. Am. Soc. Clin. Oncol. *32*, 1563–1570.

Dagklis, A., Demeyer, S., De Bie, J., Radaelli, E., Pauwels, D., Degryse, S., Gielen, O., Vicente, C., Vandepoel, R., Geerdens, E., et al. (2016). Hedgehog pathway activation in T-cell acute lymphoblastic leukemia predicts response to SMO and GLI1 inhibitors. Blood *128*, 2642–2654.

Dahlén, A., Fletcher, C.D.M., Mertens, F., Fletcher, J.A., Perez-Atayde, A.R., Hicks, M.J., Debiec-Rychter, M., Sciot, R., Wejde, J., Wedin, R., et al. (2004a). Activation of the GLI Oncogene through Fusion with the β-Actin Gene (ACTB) in a Group of Distinctive Pericytic Neoplasms: Pericytoma with t(7;12). Am. J. Pathol. *164*, 1645–1653.

Dahlén, A., Mertens, F., Mandahl, N., and Panagopoulos, I. (2004b). Molecular genetic characterization of the genomic ACTB-GLI fusion in pericytoma with t(7;12). Biochem. Biophys. Res. Commun. *325*, 1318–1323.

Daniels, M., Lurkin, I., Pauli, R., Erbstößer, E., Hildebrandt, U., Hellwig, K., Zschille, U., Lüders, P., Krüger, G., Knolle, J., et al. (2011). Spectrum of KIT/PDGFRA/BRAF mutations and Phosphatidylinositol-3-Kinase pathway gene alterations in gastrointestinal stromal tumors (GIST). Cancer Lett. *312*, 43–54.

Davidson, N.M., Majewski, I.J., and Oshlack, A. (2015). JAFFA: High sensitivity transcriptome-focused fusion gene detection. Genome Med. *7*, 43.

DeMatteo, R.P., Lewis, J.J., Leung, D., Mudan, S.S., Woodruff, J.M., and Brennan, M.F. (2000). Two hundred gastrointestinal stromal tumors: recurrence patterns and prognostic factors for survival. Ann. Surg. *231*, 51–58.

Dierks, C., Grbic, J., Zirlik, K., Beigi, R., Englund, N.P., Guo, G.-R., Veelken, H., Engelhardt, M., Mertelsmann, R., Kelleher, J.F., et al. (2007). Essential role of stromally induced hedgehog signaling in B-cell malignancies. Nat. Med. *13*, 944–951.

Dobin, A., Davis, C.A., Schlesinger, F., Drenkow, J., Zaleski, C., Jha, S., Batut, P., Chaisson, M., and Gingeras, T.R. (2013). STAR: ultrafast universal RNA-seq aligner. Bioinforma. Oxf. Engl. *29*, 15–21.

Doyle, L.A., and Hornick, J.L. (2014). Gastrointestinal stromal tumours: from KIT to succinate dehydrogenase. Histopathology *64*, 53–67.

Drilon, A., Laetsch, T.W., Kummar, S., DuBois, S.G., Lassen, U.N., Demetri, G.D., Nathenson, M., Doebele, R.C., Farago, A.F., Pappo, A.S., et al. (2018). Efficacy of Larotrectinib in TRK Fusion-Positive Cancers in Adults and Children. N. Engl. J. Med. *378*, 731–739.

Drummond, C.J., Hanna, J.A., Garcia, M.R., Devine, D.J., Heyrana, A.J., Finkelstein, D., Rehg, J.E., and Hatley, M.E. (2018). Hedgehog Pathway Drives Fusion-Negative Rhabdomyosarcoma Initiated From Non-myogenic Endothelial Progenitors. Cancer Cell *33*, 108-124.e5.

Eguchi, M., Eguchi-Ishimae, M., Tojo, A., Morishita, K., Suzuki, K., Sato, Y., Kudoh, S., Tanaka, K., Setoyama, M., Nagamura, F., et al. (1999). Fusion of ETV6 to neurotrophin-3 receptor TRKC in acute myeloid leukemia with t(12;15)(p13;q25). Blood *93*, 1355–1363.

Elia, D., Madhala, D., Ardon, E., Reshef, R., and Halevy, O. (2007). Sonic hedgehog promotes proliferation and differentiation of adult muscle cells: Involvement of MAPK/ERK and PI3K/Akt pathways. Biochim. Biophys. Acta *1773*, 1438–1446.

Ferretti, E., Smaele, E.D., Miele, E., Laneve, P., Po, A., Pelloni, M., Paganelli, A., Marcotullio, L.D., Caffarelli, E., Screpanti, I., et al. (2008). Concerted microRNA control of Hedgehog signalling in cerebellar neuronal progenitor and tumour cells. EMBO J. *27*, 2616–2627.

Fisher, C. (1998). Synovial sarcoma. Ann. Diagn. Pathol. *2*, 401–421.

Fletcher, C.D.M. (2015). Myoepithelial tumors of soft tissue: an overview. North American Society of Head and Neck Pathology, USCAP, 2015 Annual Meeting. https://handouts.uscap.org/AN2015/Companion%20Meeting%20(CM)/CM20-15/USCAP-Head%20and%20Neck%20Society%20Final%202015%20Fletcher.pdf.

Fletcher, C.D.M., Bridge, J.A., Hogendoorn, P.C.W., and Mertens, F. (2013). WHO Classification of Tumors of Soft Tissue and bone. *International Agency for Research on Cancer*.

Flucke, U., Tops, B.B.J., Verdijk, M.A.J., van Cleef, P.J.H., van Zwam, P.H., Slootweg, P.J., Bovée, J.V.M.G., Riedl, R.G., Creytens, D.H., Suurmeijer, A.J.H., et al. (2012). NR4A3 rearrangement reliably

distinguishes between the clinicopathologically overlapping entities myoepithelial carcinoma of soft tissue and cellular extraskeletal myxoid chondrosarcoma. Virchows Arch. *460*, 621–628.

Forghieri, F., Morselli, M., Potenza, L., Maccaferri, M., Pedrazzi, L., Paolini, A., Bonacorsi, G., Artusi, T., Giacobbi, F., Corradini, G., et al. (2011). Chronic eosinophilic leukaemia with ETV6-NTRK3 fusion transcript in an elderly patient affected with pancreatic carcinoma. Eur. J. Haematol. *86*, 352–355.

Fumo, G., Akin, C., Metcalfe, D.D., and Neckers, L. (2004). 17-Allylamino-17-demethoxygeldanamycin (17-AAG) is effective in down-regulating mutated, constitutively activated KIT protein in human mast cells. Blood *103*, 1078–1084.

Gasparotto, D., Rossi, S., Polano, M., Tamborini, E., Lorenzetto, E., Sbaraglia, M., Mondello, A., Massani, M., Lamon, S., Bracci, R., et al. (2017). Quadruple-Negative GIST Is a Sentinel for Unrecognized Neurofibromatosis Type 1 Syndrome. Clin. Cancer Res. *23*, 273–282.

Gleason, B.C., and Fletcher, C.D.M. (2007). Myoepithelial carcinoma of soft tissue in children: an aggressive neoplasm analyzed in a series of 29 cases. Am. J. Surg. Pathol. *31*, 1813–1824.

Gordon, M.D., and Nusse, R. (2006). Wnt Signaling: Multiple Pathways, Multiple Receptors, and Multiple Transcription Factors. J. Biol. Chem. *281*, 22429–22433.

Graham, R.P., Nair, A.A., Davila, J.I., Jin, L., Jen, J., Sukov, W.R., Wu, T.-T., Appelman, H.D., Torres-Mora, J., Perry, K.D., et al. (2017). Gastroblastoma harbors a recurrent somatic MALAT1–GLI1 fusion gene. Mod. Pathol. *30*, 1443–1452.

Gu, M., Antonescu, C.R., Guiter, G., Huvos, A.G., Ladanyi, M., and Zakowski, M.F. (2000). Cytokeratin immunoreactivity in Ewing's sarcoma: prevalence in 50 cases confirmed by molecular diagnostic studies. Am. J. Surg. Pathol. *24*, 410–416.

Gupta, S., Takebe, N., and LoRusso, P. (2010). Targeting the Hedgehog pathway in cancer. Ther. Adv. Med. Oncol. *2*, 237–250.

Hahn, H., Wicking, C., Zaphiropoulous, P.G., Gailani, M.R., Shanley, S., Chidambaram, A., Vorechovsky, I., Holmberg, E., Unden, A.B., Gillies, S., et al. (1996). Mutations of the human homolog of Drosophila patched in the nevoid basal cell carcinoma syndrome. Cell *85*, 841–851.

Haller, F., Moskalev, E.A., Faucz, F.R., Barthelmeß, S., Wiemann, S., Bieg, M., Assie, G., Bertherat, J., Schaefer, I.-M., Otto, C., et al. (2014). Aberrant DNA hypermethylation of SDHC: a novel mechanism of tumor development in Carney triad. Endocr. Relat. Cancer *21*, 567–577.

Hallikas, O., Palin, K., Sinjushina, N., Rautiainen, R., Partanen, J., Ukkonen, E., and Taipale, J. (2006). Genome-wide Prediction of Mammalian Enhancers Based on Analysis of Transcription-Factor Binding Affinity. Cell *124*, 47–59.

Hannon, G.J., Sun, P., Carnero, A., Xie, L.Y., Maestro, R., Conklin, D.S., and Beach, D. (1999). MaRX: an approach to genetics in mammalian cells. Science *283*, 1129–1130.

Hebrok, M., Kim, S.K., St Jacques, B., McMahon, A.P., and Melton, D.A. (2000). Regulation of pancreas development by hedgehog signaling. Dev. Camb. Engl. *127*, 4905–4913.

Heinrich, M.C., Corless, C.L., Demetri, G.D., Blanke, C.D., von Mehren, M., Joensuu, H., McGreevey, L.S., Chen, C.-J., Van den Abbeele, A.D., Druker, B.J., et al. (2003). Kinase mutations and imatinib response in patients with metastatic gastrointestinal stromal tumor. J. Clin. Oncol. Off. J. Am. Soc. Clin. Oncol. *21*, 4342–4349.

Hettmer, S., Lin, M.M., Tchessalova, D., Tortorici, S.J., Castiglioni, A., Desai, T., Mao, J., McMahon, A.P., and Wagers, A.J. (2016). Hedgehog-driven myogenic tumors recapitulate skeletal muscle cellular heterogeneity. Exp. Cell Res. *340*, 43–52.

Hirota, S., Isozaki, K., Moriyama, Y., Hashimoto, K., Nishida, T., Ishiguro, S., Kawano, K., Hanada, M., Kurata, A., Takeda, M., et al. (1998). Gain-of-function mutations of c-kit in human gastrointestinal stromal tumors. Science *279*, 577–580.

Hornick, J.L. (2013). Practical Soft Tissue Pathology A diagnostic approach.

Hornick, J.L., and Fletcher, C.D.M. (2003). Myoepithelial Tumors of Soft Tissue: A Clinicopathologic and Immunohistochemical Study of 101 Cases With Evaluation of Prognostic Parameters. Am. J. Surg. Pathol. *27*, 1183–1196.

Huang, S.-C., Chen, H.-W., Zhang, L., Sung, Y.-S., Agaram, N.P., Davis, M., Edelman, M., Fletcher, C.D.M., and Antonescu, C.R. (2015). Novel FUS-KLF17 and EWSR1-KLF17 fusions in myoepithelial tumors. Genes. Chromosomes Cancer *54*, 267–275.

Hui, J.Y.C. (2016). Epidemiology and Etiology of Sarcomas. Surg. Clin. North Am. *96*, 901–914.

Ingham, P.W., and McMahon, A.P. (2001). Hedgehog signaling in animal development: paradigms and principles. Genes Dev. *15*, 3059–3087.

Ito, T., Yamamura, M., Hirai, T., Ishikawa, T., Kanda, T., Nakai, T., Ohkouchi, M., Hashikura, Y., Isozaki, K., and Hirota, S. (2014). Gastrointestinal stromal tumors with exon 8 c-kit gene mutation might occur at extragastric sites and have metastasis-prone nature. Int. J. Clin. Exp. Pathol. *7*, 8024–8031.

Iyer, M.K., Chinnaiyan, A.M., and Maher, C.A. (2011). ChimeraScan: a tool for identifying chimeric transcription in sequencing data. Bioinforma. Oxf. Engl. *27*, 2903–2904.

Jho, E., Zhang, T., Domon, C., Joo, C.-K., Freund, J.-N., and Costantini, F. (2002). Wnt/beta-catenin/Tcf signaling induces the transcription of Axin2, a negative regulator of the signaling pathway. Mol. Cell. Biol. *22*, 1172–1183.

Jo, V.Y. (2015). Myoepithelial Tumors. Surg. Pathol. Clin. *8*, 445–466.

Jo, V.Y., and Fletcher, C.D.M. (2011). p63 immunohistochemical staining is limited in soft tissue tumors. Am. J. Clin. Pathol. *136*, 762–766.

Jo, V.Y., and Fletcher, C.D.M. (2015). Myoepithelial neoplasms of soft tissue: an updated review of the clinicopathologic, immunophenotypic, and genetic features. Head Neck Pathol. *9*, 32–38.

Joensuu, H., Wardelmann, E., Sihto, H., Eriksson, M., Sundby Hall, K., Reichardt, A., Hartmann, J.T., Pink, D., Cameron, S., Hohenberger, P., et al. (2017). Effect of KIT and PDGFRA Mutations on Survival in Patients With Gastrointestinal Stromal Tumors Treated With Adjuvant Imatinib: An Exploratory Analysis of a Randomized Clinical Trial. JAMA Oncol. *3*, 602–609.

Kang, G., Yun, H., Sun, C.-H., Park, I., Lee, S., Kwon, J., Do, I., Hong, M.E., Van Vrancken, M., Lee, J., et al. (2016). Integrated genomic analyses identify frequent gene fusion events and VHL inactivation in gastrointestinal stromal tumors. Oncotarget *7*, 6538–6551.

Katoh, M., and Katoh, M. (2007). WNT Signaling Pathway and Stem Cell Signaling Network. Clin. Cancer Res. *13*, 4042–4045.

Katoh, Y., and Katoh, M. (2009). Hedgehog target genes: mechanisms of carcinogenesis induced by aberrant hedgehog signaling activation. Curr. Mol. Med. *9*, 873–886.

Khatib, Z.A., Matsushime, H., Valentine, M., Shapiro, D.N., Sherr, C.J., and Look, A.T. (1993). Coamplification of the CDK4 gene with MDM2 and GLI in human sarcomas. Cancer Res. *53*, 5535–5541.

Killian, J.K., Miettinen, M., Walker, R.L., Wang, Y., Zhu, Y.J., Waterfall, J.J., Noyes, N., Retnakumar, P., Yang, Z., Smith, W.I., et al. (2014). Recurrent epimutation of SDHC in gastrointestinal stromal tumors. Sci. Transl. Med. *6*, 268ra177.

Kinzler, K.W., Bigner, S.H., Bigner, D.D., Trent, J.M., Law, M.L., O'Brien, S.J., Wong, A.J., and Vogelstein, B. (1987). Identification of an amplified, highly expressed gene in a human glioma. Science *236*, 70–73.

Knezevich, S.R., McFadden, D.E., Tao, W., Lim, J.F., and Sorensen, P.H. (1998). A novel ETV6-NTRK3 gene fusion in congenital fibrosarcoma. Nat. Genet. *18*, 184–187.

Koh, N.W.C., Seow, W.Y., Lee, Y.T., Lam, J.C.M., and Lian, D.W.Q. (2018). Pericytoma With t(7;12): The First Ovarian Case Reported and a Review of the Literature. Int. J. Gynecol. Pathol. Off. J. Int. Soc. Gynecol. Pathol.

Koleva, M., Kappler, R., Vogler, M., Herwig, A., Fulda, S., and Hahn, H. (2005). Pleiotropic effects of sonic hedgehog on muscle satellite cells. Cell. Mol. Life Sci. CMLS *62*, 1863–1870.

Kolligs, F.T., Nieman, M.T., Winer, I., Hu, G., Van Mater, D., Feng, Y., Smith, I.M., Wu, R., Zhai, Y., Cho, K.R., et al. (2002). ITF-2, a downstream target of the Wnt/TCF pathway, is activated in human cancers with beta-catenin defects and promotes neoplastic transformation. Cancer Cell *1*, 145–155.

Krämer, A., Green, J., Pollard, J., and Tugendreich, S. (2014). Causal analysis approaches in Ingenuity Pathway Analysis. Bioinforma. Oxf. Engl. *30*, 523–530.

Krishnamurthy, N., and Kurzrock, R. (2018). Targeting the Wnt/beta-catenin pathway in cancer: Update on effectors and inhibitors. Cancer Treat. Rev. *62*, 50–60.

Lai, K., Kaspar, B.K., Gage, F.H., and Schaffer, D.V. (2003). Sonic hedgehog regulates adult neural progenitor proliferation in vitro and in vivo. Nat. Neurosci. *6*, 21–27.

Lannon, C.L., Martin, M.J., Tognon, C.E., Jin, W., Kim, S.-J., and Sorensen, P.H.B. (2004). A highly conserved NTRK3 C-terminal sequence in the ETV6-NTRK3 oncoprotein binds the phosphotyrosine binding domain of insulin receptor substrate-1: an essential interaction for transformation. J. Biol. Chem. *279*, 6225–6234.

Lasota, J., Wang, Z., Kim, S.Y., Helman, L., and Miettinen, M. (2013). Expression of the receptor for type i insulin-like growth factor (IGF1R) in gastrointestinal stromal tumors: an immunohistochemical study of 1078 cases with diagnostic and therapeutic implications. Am. J. Surg. Pathol. *37*, 114–119.

Lauer, S., and Gardner, J.M. (2013). Soft tissue sarcomas—New approaches to diagnosis and classification. Curr. Probl. Cancer *37*, 45–61.

Le Loarer, F., Zhang, L., Fletcher, C.D., Ribeiro, A., Singer, S., Italiano, A., Neuville, A., Houlier, A., Chibon, F., Coindre, J.-M., et al. (2014). Consistent SMARCB1 homozygous deletions in epithelioid sarcoma and in a subset of myoepithelial carcinomas can be reliably detected by FISH in archival material. Genes. Chromosomes Cancer *53*, 475–486.

Lee, R.S., Stewart, C., Carter, S.L., Ambrogio, L., Cibulskis, K., Sougnez, C., Lawrence, M.S., Auclair, D., Mora, J., Golub, T.R., et al. (2012). A remarkably simple genome underlies highly malignant pediatric rhabdoid cancers. J. Clin. Invest. *122*, 2983–2988.

Leeman-Neill, R.J., Kelly, L.M., Liu, P., Brenner, A.V., Little, M.P., Bogdanova, T.I., Evdokimova, V.N., Hatch, M., Zurnadzy, L.Y., Nikiforova, M.N., et al. (2014). ETV6-NTRK3 is a common chromosomal rearrangement in radiation-associated thyroid cancer. Cancer *120*, 799–807.

Li, X., Deng, W., Lobo-Ruppert, S.M., and Ruppert, J.M. (2007). Gli1 acts through Snail and E-cadherin to promote nuclear signaling by beta-catenin. Oncogene *26*, 4489–4498.

Machold, R., Hayashi, S., Rutlin, M., Muzumdar, M.D., Nery, S., Corbin, J.G., Gritli-Linde, A., Dellovade, T., Porter, J.A., Rubin, L.L., et al. (2003). Sonic Hedgehog Is Required for Progenitor Cell Maintenance in Telencephalic Stem Cell Niches. Neuron *39*, 937–950.

Mackall, C.L., Meltzer, P.S., and Helman, L.J. (2002). Focus on sarcomas. Cancer Cell *2*, 175–178.

Mann, B., Gelos, M., Siedow, A., Hanski, M.L., Gratchev, A., Ilyas, M., Bodmer, W.F., Moyer, M.P., Riecken, E.O., Buhr, H.J., et al. (1999). Target genes of beta-catenin-T cell-factor/lymphoid-enhancer-factor signaling in human colorectal carcinomas. Proc. Natl. Acad. Sci. U. S. A. *96*, 1603–1608.

Mavroeidis, L., Metaxa-Mariatou, V., Papoudou-Bai, A., Lampraki, A.M., Kostadima, L., Tsinokou, I., Zarkavelis, G., Papadaki, A., Petrakis, D., Gκoura, S., et al. (2018). Comprehensive molecular screening by next generation sequencing reveals a distinctive mutational profile of KIT/PDGFRA genes and novel genomic alterations: results from a 20-year cohort of patients with GIST from north-western Greece. ESMO Open *3*, e000335.

McWhinney, S.R., Pasini, B., Stratakis, C.A., and International Carney Triad and Carney-Stratakis Syndrome Consortium (2007). Familial gastrointestinal stromal tumors and germ-line mutations. N. Engl. J. Med. *357*, 1054–1056.

Mentzel, T., Requena, L., Kaddu, S., Soares de Aleida, L.M., Sangueza, O.P., and Kutzner, H. (2003). Cutaneous myoepithelial neoplasms: clinicopathologic and immunohistochemical study of 20 cases suggesting a continuous spectrum ranging from benign mixed tumor of the skin to cutaneous myoepithelioma and myoepithelial carcinoma. J. Cutan. Pathol. *30*, 294–302.

Mertens, F., and Tayebwa, J. (2014). Evolving techniques for gene fusion detection in soft tissue tumours. Histopathology *64*, 151–162.

Miettinen, M. (2016). Modern Soft Tissue Pathology Tumors and Non-Neoplastic Conditions. *Cambridge University Press*.

Miettinen, M., and Lasota, J. (2006). Gastrointestinal stromal tumors: pathology and prognosis at different sites. Semin. Diagn. Pathol. *23*, 70–83.

Miranda, C., Nucifora, M., Molinari, F., Conca, E., Anania, M.C., Bordoni, A., Saletti, P., Mazzucchelli, L., Pilotti, S., Pierotti, M.A., et al. (2012). KRAS and BRAF mutations predict primary resistance to imatinib in gastrointestinal stromal tumors. Clin. Cancer Res. Off. J. Am. Assoc. Cancer Res. *18*, 1769–1776.

Modena, P., Lualdi, E., Facchinetti, F., Galli, L., Teixeira, M.R., Pilotti, S., and Sozzi, G. (2005). SMARCB1/INI1 tumor suppressor gene is frequently inactivated in epithelioid sarcomas. Cancer Res. *65*, 4012–4019.

Monkkonen, T., and Lewis, M.T. (2017). New paradigms for the Hedgehog signaling network in mammary gland development and breast Cancer. Biochim. Biophys. Acta *1868*, 315–332.

Morrison, K.B., Tognon, C.E., Garnett, M.J., Deal, C., and Sorensen, P.H.B. (2002). ETV6-NTRK3 transformation requires insulin-like growth factor 1 receptor signaling and is associated with constitutive IRS-1 tyrosine phosphorylation. Oncogene *21*, 5684–5695.

Mosquera, J.M., Sboner, A., Zhang, L., Kitabayashi, N., Chen, C.-L., Sung, Y.S., Wexler, L.H., LaQuaglia, M.P., Edelman, M., Sreekantaiah, C., et al. (2013). Recurrent NCOA2 gene rearrangements in congenital/infantile spindle cell rhabdomyosarcoma. Genes. Chromosomes Cancer *52*, 538–550.

Nakamura, Y., and Hoppler, S. (2017). Genome-wide analysis of canonical Wnt target gene regulation in Xenopus tropicalis challenges β-catenin paradigm. Genes. N. Y. N 2000 *55*.

Nault, J.-C., Couchy, G., Balabaud, C., Morcrette, G., Caruso, S., Blanc, J.-F., Bacq, Y., Calderaro, J., Paradis, V., Ramos, J., et al. (2017). Molecular Classification of Hepatocellular Adenoma Associates With Risk Factors, Bleeding, and Malignant Transformation. Gastroenterology *152*, 880-894.e6.

Nicorici, D., Satalan, M., Edgren, H., Kangaspeska, S., Murumagi, A., Kallioniemi, O., Virtanen, S., and Kilkku, O. (2014). FusionCatcher - a tool for finding somatic fusion genes in paired-end RNA-sequencing data. BioRxiv 011650.

Nilsson, B., Bümming, P., Meis-Kindblom, J.M., Odén, A., Dortok, A., Gustavsson, B., Sablinska, K., and Kindblom, L.-G. (2005). Gastrointestinal stromal tumors: the incidence, prevalence, clinical course, and prognostication in the preimatinib mesylate era--a population-based study in western Sweden. Cancer *103*, 821–829.

Noubissi, F.K., Goswami, S., Sanek, N.A., Kawakami, K., Minamoto, T., Moser, A., Grinblat, Y., and Spiegelman, V.S. (2009). Wnt signaling stimulates transcriptional outcome of the Hedgehog pathway by stabilizing GLI1 mRNA. Cancer Res. *69*, 8572–8578.

O'Riain, C., Corless, C.L., Heinrich, M.C., Keegan, D., Vioreanu, M., Maguire, D., and Sheahan, K. (2005). Gastrointestinal stromal tumors: insights from a new familial GIST kindred with unusual genetic and pathologic features. Am. J. Surg. Pathol. *29*, 1680–1683.

Pala, R., Alomari, N., and Nauli, S.M. (2017). Primary Cilium-Dependent Signaling Mechanisms. Int. J. Mol. Sci. *18*.

Pantaleo, M.A., Nannini, M., Corless, C.L., and Heinrich, M.C. (2015). Quadruple wild-type (WT) GIST: defining the subset of GIST that lacks abnormalities of KIT, PDGFRA, SDH, or RAS signaling pathways. Cancer Med. *4*, 101–103.

Pasini, B., McWhinney, S.R., Bei, T., Matyakhina, L., Stergiopoulos, S., Muchow, M., Boikos, S.A., Ferrando, B., Pacak, K., Assie, G., et al. (2008). Clinical and molecular genetics of patients with the Carney-Stratakis syndrome and germline mutations of the genes coding for the succinate dehydrogenase subunits SDHB, SDHC, and SDHD. Eur. J. Hum. Genet. EJHG *16*, 79–88.

Pauls, K., Merkelbach-Bruse, S., Thal, D., Büttner, R., and Wardelmann, E. (2005). PDGFRalpha- and c-kit-mutated gastrointestinal stromal tumours (GISTs) are characterized by distinctive histological and immunohistochemical features. Histopathology *46*, 166–175.

Pauwels, P., Meulemans, E.V., Ruland, A.M., Debiec-Rychter, M., Sciot, R., and Speel, E.-J.M. (2006). Evaluation of MDM2 and CDK4 gene amplification and expression as potential tools for the diagnosis

of atypical lipomatous tumors/well-differentiated liposarcomas in paraffin-embedded material. Cancer Res. *66*, 272–272.

Petrova, R., and Joyner, A.L. (2014). Roles for Hedgehog signaling in adult organ homeostasis and repair. Dev. Camb. Engl. *141*, 3445–3457.

Puls, F., Arbajian, E., Magnusson, L., Douis, H., Kindblom, L.-G., and Mertens, F. (2014). Myoepithelioma of bone with a novel FUS-POU5F1 fusion gene. Histopathology *65*, 917–922.

Rabbitts, T.H. (1994). Chromosomal translocations in human cancer. Nature *372*, 143–149.

Rabbitts, T.H. (1999). Perspective: chromosomal translocations can affect genes controlling gene expression and differentiation--why are these functions targeted? J. Pathol. *187*, 39–42.

Raffel, C., Jenkins, R.B., Frederick, L., Hebrink, D., Alderete, B., Fults, D.W., and James, C.D. (1997). Sporadic medulloblastomas contain PTCH mutations. Cancer Res. *57*, 842–845.

Ratner, N., and Miller, S.J. (2015). A RASopathy gene commonly mutated in cancer: the neurofibromatosis type 1 tumour suppressor. Nat. Rev. Cancer *15*, 290–301.

Reifenberger, J., Wolter, M., Knobbe, C.B., Köhler, B., Schönicke, A., Scharwächter, C., Kumar, K., Blaschke, B., Ruzicka, T., and Reifenberger, G. (2005). Somatic mutations in the PTCH, SMOH, SUFUH and TP53 genes in sporadic basal cell carcinomas. Br. J. Dermatol. *152*, 43–51.

Reiss, K., Del Valle, L., Lassak, A., and Trojanek, J. (2012). Nuclear IRS-1 and cancer. J. Cell. Physiol. *227*, 2992–3000.

Roberts, K.G., Li, Y., Payne-Turner, D., Harvey, R.C., Yang, Y.-L., Pei, D., McCastlain, K., Ding, L., Lu, C., Song, G., et al. (2014). Targetable kinase-activating lesions in Ph-like acute lymphoblastic leukemia. N. Engl. J. Med. *371*, 1005–1015.

Robinson, D.R., Wu, Y.-M., Kalyana-Sundaram, S., Cao, X., Lonigro, R.J., Sung, Y.-S., Chen, C.-L., Zhang, L., Wang, R., Su, F., et al. (2013). Identification of recurrent NAB2-STAT6 gene fusions in solitary fibrous tumor by integrative sequencing. Nat. Genet. *45*, 180–185.

Roose, J., Huls, G., Beest, M. van, Moerer, P., Horn, K. van der, Goldschmeding, R., Logtenberg, T., and Clevers, H. (1999). Synergy Between Tumor Suppressor APC and the β-Catenin-Tcf4 Target Tcf1. Science *285*, 1923–1926.

Rossi, S., Sbaraglia, M., Dell'Orto, M.C., Gasparotto, D., Cacciatore, M., Boscato, E., Carraro, V., Toffolatti, L., Gallina, G., Niero, M., et al. (2016). Concomitant KIT/BRAF and PDGFRA/BRAF mutations are rare events in gastrointestinal stromal tumors. Oncotarget *7*, 30109–30118.

Rubin, B.P., Chen, C.J., Morgan, T.W., Xiao, S., Grier, H.E., Kozakewich, H.P., Perez-Atayde, A.R., and Fletcher, J.A. (1998). Congenital mesoblastic nephroma t(12;15) is associated with ETV6-NTRK3 gene fusion: cytogenetic and molecular relationship to congenital (infantile) fibrosarcoma. Am. J. Pathol. *153*, 1451–1458.

Saleh, G., Evans, H.L., Ro, J.Y., and Ayala, A.G. (1992). Extraskeletal myxoid chondrosarcoma. A clinicopathologic study of ten patients with long-term follow-up. Cancer *70*, 2827–2830.

Sasaki, H., Hui, C., Nakafuku, M., and Kondoh, H. (1997). A binding site for Gli proteins is essential for HNF-3beta floor plate enhancer activity in transgenics and can respond to Shh in vitro. Dev. Camb. Engl. *124*, 1313–1322.

Schaefer, I.-M., Mariño-Enríquez, A., and Fletcher, J.A. (2017). What is New in Gastrointestinal Stromal Tumor? Adv. Anat. Pathol. *24*, 259–267.

Selak, M.A., Armour, S.M., MacKenzie, E.D., Boulahbel, H., Watson, D.G., Mansfield, K.D., Pan, Y., Simon, M.C., Thompson, C.B., and Gottlieb, E. (2005). Succinate links TCA cycle dysfunction to oncogenesis by inhibiting HIF-α prolyl hydroxylase. Cancer Cell *7*, 77–85.

Setoyama, M., Tojo, A., Nagamura, F., Asano, S., Ishimae, M., Eguchi, M., and Kamada, N. (1998). A unique translocation of the TEL gene in a case of acute myelogenous leukemia with inv(12)(p13q15). Blood *92*, 1454–1455.

Shi, E., Chmielecki, J., Tang, C.-M., Wang, K., Heinrich, M.C., Kang, G., Corless, C.L., Hong, D., Fero, K.E., Murphy, J.D., et al. (2016). FGFR1 and NTRK3 actionable alterations in “Wild-Type” gastrointestinal stromal tumors. J. Transl. Med. *14*.

Shtutman, M., Zhurinsky, J., Simcha, I., Albanese, C., D’Amico, M., Pestell, R., and Ben-Ze’ev, A. (1999). The cyclin D1 gene is a target of the beta-catenin/LEF-1 pathway. Proc. Natl. Acad. Sci. U. S. A. *96*, 5522–5527.

Simon, M.P., Pedeutour, F., Sirvent, N., Grosgeorge, J., Minoletti, F., Coindre, J.M., Terrier-Lacombe, M.J., Mandahl, N., Craver, R.D., Blin, N., et al. (1997). Deregulation of the platelet-derived growth factor B-chain gene via fusion with collagen gene COL1A1 in dermatofibrosarcoma protuberans and giant-cell fibroblastoma. Nat. Genet. *15*, 95–98.

Skálová, A., Vanecek, T., Sima, R., Laco, J., Weinreb, I., Perez-Ordonez, B., Starek, I., Geierova, M., Simpson, R.H.W., Passador-Santos, F., et al. (2010). Mammary analogue secretory carcinoma of salivary glands, containing the ETV6-NTRK3 fusion gene: a hitherto undescribed salivary gland tumor entity. Am. J. Surg. Pathol. *34*, 599–608.

Sorensen, P.H.B., Lynch, J.C., Qualman, S.J., Tirabosco, R., Lim, J.F., Maurer, H.M., Bridge, J.A., Crist, W.M., Triche, T.J., and Barr, F.G. (2002). PAX3-FKHR and PAX7-FKHR gene fusions are prognostic indicators in alveolar rhabdomyosarcoma: a report from the children’s oncology group. J. Clin. Oncol. Off. J. Am. Soc. Clin. Oncol. *20*, 2672–2679.

Spans, L., Fletcher, C.D., Antonescu, C.R., Rouquette, A., Coindre, J.-M., Sciot, R., and Debiec-Rychter, M. (2016). Recurrent MALAT1–GLI1 oncogenic fusion and GLI1 up-regulation define a subset of plexiform fibromyxoma. J. Pathol. *239*, 335–343.

Stacchiotti, S., Pantaleo, M.A., Astolfi, A., Dagrada, G.P., Negri, T., Dei Tos, A.P., Indio, V., Morosi, C., Gronchi, A., Colombo, C., et al. (2014). Activity of sunitinib in extraskeletal myxoid chondrosarcoma. Eur. J. Cancer *50*, 1657–1664.

Straface, G., Aprahamian, T., Flex, A., Gaetani, E., Biscetti, F., Smith, R.C., Pecorini, G., Pola, E., Angelini, F., Stigliano, E., et al. (2009). Sonic hedgehog regulates angiogenesis and myogenesis during post-natal skeletal muscle regeneration. J. Cell. Mol. Med. *13*, 2424–2435.

Subramanian, A., Tamayo, P., Mootha, V.K., Mukherjee, S., Ebert, B.L., Gillette, M.A., Paulovich, A., Pomeroy, S.L., Golub, T.R., Lander, E.S., et al. (2005). Gene set enrichment analysis: A knowledge-based approach for interpreting genome-wide expression profiles. Proc. Natl. Acad. Sci. *102*, 15545–15550.

Taipale, M., Krykbaeva, I., Whitesell, L., Santagata, S., Zhang, J., Liu, Q., Gray, N.S., and Lindquist, S. (2013). Chaperones as thermodynamic sensors of drug-target interactions reveal kinase inhibitor specificities in living cells. Nat. Biotechnol. *31*, 630–637.

Tognon, C., Garnett, M., Kenward, E., Kay, R., Morrison, K., and Sorensen, P.H.B. (2001). The Chimeric Protein Tyrosine Kinase ETV6-NTRK3 Requires both Ras-Erk1/2 and PI3-Kinase-Akt Signaling for Fibroblast Transformation. Cancer Res. *61*, 8909–8916.

Tognon, C., Knezevich, S.R., Huntsman, D., Roskelley, C.D., Melnyk, N., Mathers, J.A., Becker, L., Carneiro, F., MacPherson, N., Horsman, D., et al. (2002). Expression of the ETV6-NTRK3 gene fusion as a primary event in human secretory breast carcinoma. Cancer Cell *2*, 367–376.

Torres-García, W., Zheng, S., Sivachenko, A., Vegesna, R., Wang, Q., Yao, R., Berger, M.F., Weinstein, J.N., Getz, G., and Verhaak, R.G.W. (2014). PRADA: pipeline for RNA sequencing data analysis. Bioinforma. Oxf. Engl. *30*, 2224–2226.

Ugurel, S., Mentzel, T., Utikal, J., Helmbold, P., Mohr, P., Pföhler, C., Schiller, M., Hauschild, A., Hein, R., Kämpgen, E., et al. (2014). Neoadjuvant imatinib in advanced primary or locally recurrent dermatofibrosarcoma protuberans: a multicenter phase II DeCOG trial with long-term follow-up. Clin. Cancer Res. Off. J. Am. Assoc. Cancer Res. *20*, 499–510.

Urbini, M., Astolfi, A., Indio, V., Tarantino, G., Serravalle, S., Saponara, M., Nannini, M., Gronchi, A., Fiore, M., Maestro, R., et al. (2017a). Identification of SRF-E2F1 fusion transcript in EWSR-negative myoepithelioma of the soft tissue. Oncotarget *8*, 60036–60045.

Urbini, M., Astolfi, A., Pantaleo, M.A., Serravalle, S., Tos, A.P.D., Picci, P., Indio, V., Sbaraglia, M., Benini, S., Righi, A., et al. (2017b). HSPA8 as a novel fusion partner of NR4A3 in extraskeletal myxoid chondrosarcoma. Genes. Chromosomes Cancer *56*, 582–586.

Vichai, V., and Kirtikara, K. (2006). Sulforhodamine B colorimetric assay for cytotoxicity screening. Nat. Protoc. *1*, 1112–1116.

Vokes, S.A., Ji, H., McCuine, S., Tenzen, T., Giles, S., Zhong, S., Longabaugh, W.J.R., Davidson, E.H., Wong, W.H., and McMahon, A.P. (2007). Genomic characterization of Gli-activator targets in sonic hedgehog-mediated neural patterning. Development *134*, 1977–1989.

Wang, J., Vasaikar, S., Shi, Z., Greer, M., and Zhang, B. (2017). WebGestalt 2017: a more comprehensive, powerful, flexible and interactive gene set enrichment analysis toolkit. Nucleic Acids Res. *45*, W130–W137.

Wang, X., Bledsoe, K.L., Graham, R.P., Asmann, Y.W., Viswanatha, D.S., Lewis, J.E., Lewis, J.T., Chou, M.M., Yaszemski, M.J., Jen, J., et al. (2014). Recurrent PAX3-MAML3 fusion in biphenotypic sinonasal sarcoma. Nat. Genet. *46*, 666–668.

Wasag, B., Debiec-Rychter, M., Pauwels, P., Stul, M., Vranckx, H., Oosterom, A.V., Hagemeijer, A., and Sciot, R. (2004). Differential expression of KIT/PDGFRA mutant isoforms in epithelioid and mixed variants of gastrointestinal stromal tumors depends predominantly on the tumor site. Mod. Pathol. Off. J. U. S. Can. Acad. Pathol. Inc *17*, 889–894.

Werner, C.A., Döhner, H., Joos, S., Trümper, L.H., Baudis, M., Barth, T.F., Ott, G., Möller, P., Lichter, P., and Bentz, M. (1997). High-level DNA amplifications are common genetic aberrations in B-cell neoplasms. Am. J. Pathol. *151*, 335–342.

Xin, M., Ji, X., Cruz, L.K.D.L., Thareja, S., and Wang, B. (2018). Strategies to target the Hedgehog signaling pathway for cancer therapy. Med. Res. Rev. *38*, 870–913.

Yauch, R.L., Gould, S.E., Scales, S.J., Tang, T., Tian, H., Ahn, C.P., Marshall, D., Fu, L., Januario, T., Kallop, D., et al. (2008). A paracrine requirement for hedgehog signalling in cancer. Nature *455*, 406–410.

Yeku, O., and Frohman, M.A. (2011). Rapid amplification of cDNA ends (RACE). Methods Mol. Biol. Clifton NJ *703*, 107–122.

Yoon, J.W., Kita, Y., Frank, D.J., Majewski, R.R., Konicek, B.A., Nobrega, M.A., Jacob, H., Walterhouse, D., and Iannaccone, P. (2002). Gene Expression Profiling Leads to Identification of GLI1-binding Elements in Target Genes and a Role for Multiple Downstream Pathways in GLI1-induced Cell Transformation. J. Biol. Chem. *277*, 5548–5555.

Zhu, H., and Lo, H.-W. (2010). The Human Glioma-Associated Oncogene Homolog 1 (GLI1) Family of Transcription Factors in Gene Regulation and Diseases. Curr. Genomics *11*, 238–245.

ACKNOWLEDGEMENTS

This study was supported by Associazione Italiana Ricerca sul Cancro (AIRC), the Italian Ministry of Health and a CRO 5 × 1000 intramural grant.

This work was possible thank to the valuable contribution of Dr. Silvana Pilotti, Dr. Silvia Stacchiotti, Dr. Gianpaolo Dagrada (Fondazione Nazionale Tumori IRCCS, Milan), Prof. Angelo P. Dei Tos (University of Padova), Dr. Sabrina Rossi, Dr. Marta Sbaraglia, Dr. Lucia Zanatta, Dr. Laura Valori, Dr. Stefano Lamon (Treviso General Hospital, Treviso) and Dr. Daniela Gasparotto (Centro di Riferimento Oncologico di Aviano, CRO, IRCCS, Aviano).

I would like to thank my supervisor Dr. Roberta Maestro for her support and scientific advices and all members of my research group Dr. Monica Brenca, Dr. Maurizio Polano and Dr. Kelly Fassetta for their experimental contribution.

Journal of Pathology
J Pathol 2016; **238:** 543–549
Published online 25 January 2016 in Wiley Online Library (wileyonlinelibrary.com) DOI: 10.1002/path.4677

ORIGINAL PAPER

Transcriptome sequencing identifies *ETV6–NTRK3* as a gene fusion involved in GIST

Monica Brenca,[1#] Sabrina Rossi,[2#] Maurizio Polano,[1] Daniela Gasparotto,[1] Lucia Zanatta,[2] Dominga Racanelli,[1] Laura Valori,[2] Stefano Lamon,[3] Angelo Paolo Dei Tos[2##] and Roberta Maestro[1##*]

[1] *Experimental Oncology 1, CRO Aviano National Cancer Institute, Aviano, Italy*
[2] *Department of Pathology, Treviso General Hospital, Italy*
[3] *Department of Oncology, Treviso General Hospital, Italy*

**Correspondence to: R Maestro, Experimental Oncology 1, CRO Aviano National Cancer Institute, Via Gallini 2, 33081 Aviano (PN,) Italy. E-mail: maestro@cro.it*

[#]Co-first authors.
[##]Co-last authors.

Abstract

Gastrointestinal stromal tumours (GISTs) are the most common mesenchymal neoplasms of the gastrointestinal tract. The vast majority of GISTs are driven by oncogenic activation of KIT, PDGFRA or, less commonly, BRAF. Loss of succinate dehydrogenase complex activity has been identified in subsets of *KIT/PDGFRA/BRAF*-mutation negative tumours, yet a significant fraction of GISTs are devoid of any of such alterations. To address the pathobiology of these 'quadruple-negative' GISTs, we sought to explore the possible involvement of fusion genes. To this end we performed transcriptome sequencing on five *KIT/PDGFRA/BRAF*-mutation negative, SDH-proficient tumours. Intriguingly, the analysis unveiled the presence of an *ETV6–NTRK3* gene fusion. The screening by FISH of 26 additional cases, including *KIT/PDGFRA*-mutated GISTs, failed to detect other *ETV6* rearrangements beside the index case. This was a 'quadruple-negative' GIST located in the rectum, an uncommon primary site for GIST development (~4% of all GISTs). The fusion transcript identified encompasses exon 4 of *ETV6* and exon 14 of *NTRK3* and therefore differs from the canonical *ETV6–NTRK3* chimera of infantile fibrosarcomas. However, it retains the ability to induce IRS1 phosphorylation, activate the IGF1R downstream signalling pathway and to be targeted by IGF1R and ALK inhibitors. Thus, the *ETV6–NTRK3* fusion might identify a subset of GISTs with peculiar clinicopathological characteristics which could be eligible for such therapies.

Keywords: GIST; transcriptome sequencing; fusion genes; *ETV6–NTRK3* chimera

Received 31 August 2015; Revised 6 October 2015; Accepted 18 November 2015

No conflicts of interest were declared.

Introduction

Gastrointestinal stromal tumours (GISTs) are the most common mesenchymal neoplasm of the gastrointestinal tract, arising from the interstitial Cajal cells [1]. The majority of GISTs carry activating mutations in either KIT or PDGFRA receptor tyrosine kinases (RTK), a fact that accounts for their sensitivity to the kinase inhibitor Imatinib. Infrequent mutations in other components of the RTK pathway, viz. *BRAF*, or *NF1* gene alterations have been reported. About 10–15% of sporadic GISTs are devoid of *KIT/PDGFRA/BRAF* mutations and about one-third of these mutation-negative GISTs feature loss of expression of the succinate dehydrogenase protein complex (SDH) [1,2]. In the remaining fraction of tumours, hereafter defined as 'quadruple-negative' GISTs (*KIT/PDGFRA/BRAF* mutation-negative, SDH proficient), no distinct oncogenic driver alteration has been identified so far. Mutation-negative GISTs tend to respond poorly to standard treatments [1] and a better molecular characterization of these tumours might disclose novel therapeutic avenues.

In an attempt to shed light on the molecular bases of 'quadruple-negative' GIST development, we performed RNA sequencing on five such tumours to assess the possible involvement of fusion proteins in the pathogenesis of this subset of GISTs (see supplementary material, Table S1). Intriguingly, one case, a rectal GIST, turned out to express an *ETV6–NTRK3* fusion transcript. The *ETV6–NTRK3* chimera, originally described in infantile fibrosarcoma (IF) as a result of a t(12;15) chromosome translocation [3], has been subsequently reported also in mesoblastic nephroma [4], adult acute myeloid and chronic eosinophilic leukaemia [5–7], secretory breast carcinoma [8], mammary analogue secretory carcinoma of the salivary gland [9], radiation-induced thyroid cancers [10] and, recently, in inflammatory myofibroblastic tumour [11]. All these fusions, which may result

from different breakpoints (see supplementary material, Table S2), yield a chimeric protein that retains the ETV6 sterile α-motif (SAM) interaction domain and the NTRK3 tyrosine kinase domain. This is the first report of *ETV6–NTRK3* involvement in GIST.

Materials and methods

Patients

The study was conducted on a series of GISTs retrieved from the pathological files of Treviso General Hospital (see supplementary material, Table S1). The study was approved by the institutional review board.

Paired-end RNA-sequencing and identification of fusion genes

Total RNA was extracted from formalin-fixed, paraffin-embedded (FFPE) sections of five 'quadruple-negative' GISTs using the Ambion RecoverAll™ Total Nucleic Acid Isolation Kit (Life Technology, Carlsbad, CA, USA). RNA-sequencing libraries were prepared following Illumina's TruSeq RNA protocol and sequenced on a Illumina HiSeq 1000 apparatus (Illumina, San Diego, CA, USA) to a depth of 50–80 million paired-end reads/sample. The quality of the raw sequence data was assessed using FastQC software. FusionCatcher v. 0.99.3c [12] ChimeraScan [13] and an in-house algorithm were used to identify fusion transcripts.

RT–PCR, Sanger sequencing and FISH analyses

Total RNA (1 μg) was retro-transcribed using SuperScript III (Life Technology). RT–PCR and Sanger sequencing were as previously described [14]. *ETV6–NTRK3* was amplified using the following forward (F) and reverse (R) primers: *ETV6* F1, GCTGCTG ACCAAAGAGGACTTTC; *ETV6* F2, GCAGAGGAA ACCTCGGATTC; *NTRK3* R, ATGCCGTGGTTGATG TGGTGCAGTGG.

GISTs were screened for *ETV6* rearrangement by fluorescence *in situ* hybridization (FISH), using the Vysis ETV6 Break Apart FISH Probe (Abbott Molecular, Abbott Park, IL, USA).

Cells and constructs

HT1080 and U2OS cell lines were maintained as described [14]. The GIST_EN variant was cloned in the pMSCV vector (Clontech, Mountain View, CA, USA). Retroviral infection and subcellular fractionation were as previously described [16,18].

Cell viability/cytotoxiciy was assessed by the Sulphorhodamine B (SRB) assay, as described [15]. Drugs used were: Crizotinib (S1068; SelleckChem, Huissen, The Netherlands), Ceritinib (S7083; SelleckChem), IGF1R inhibitor I (AG1024; Calbiochem, Darmstadt, Germany); and IGF1R Inhibitor II (PQ401, Calbiochem).

Protein expression analysis

Immunostaining, western blots and immunoprecipitation were as previously described [15–17]. For immunofluorescence, cells were fixed with 4% paraformaldehyde (10 min) and permeabilized with 0.2% Triton/0.1% BSA (15 min). IRS1 immunostaining was performed with anti-IRS1, according to the manufacturer's instructions, and phalloidin for cytoplasmic counterstaining. Information about the antibodies employed in this study is provided in Table S3 (see supplementary material).

Statistics

Statistical significance was evaluated in eight technical replicates by two-tailed unpaired *t*-test. The results were confirmed in three independent experiments.

Results and discussion

Transcriptome analysis of 'quadruple-negative' GISTs

RNA-sequencing was performed on five 'quadruple-negative' GISTs to investigate the role of fusion genes in the development of this oncogene-driver orphan group of tumours. Different potential fusions were identified, most involving neighbouring genes, and also reported in non-pathological samples [12] (see supplementary material, Table S4). Among these was *POLA2–CDC42EP2*, a read-through of uncertain significance recently described in GISTs [18]. Intriguingly, an *ETV6–NTRK3* fusion transcript was detected in one case of rectal GIST.

Characterization of *ETV6–NTRK3*-positive GIST

RNA-sequencing data analysis revealed an in-frame fusion event between exon 4 of the ETS variant gene 6 (*ETV6*) and exon 14 of the neurotrophin tyrosine kinase receptor 3 (*NTRK3*) gene (Figure 1A). The rearrangement was verified at genomic level by FISH, with the vast majority of GIST tumour cells displaying *ETV6* split signals (Figure 1B). The expression of the *ETV6–NTRK3* chimeric transcript was validated by RT–PCR on total RNA. Sanger sequencing of the RT–PCR product confirmed the breakpoint indentified by RNA sequencing (Figure 1A). The *ETV6–NTRK3* fusion transcript identified in the 'quadruple-negative' rectal GIST (GIST_EN) retains an open-reading frame across the fused exons. The GIST_EN chimera, which has also been reported recently in radiation-induced thyroid cancers [10], differs from the canonical *ETV6* exon 5–*NTRK3* exon 15 fusion transcript that typifies infantile fibrosarcoma (IF_EN). However, it involves the same protein domains, viz. the SAM interaction motif of ETV6 and the tyrosine kinase domain of NTRK3 (Figure 1A).

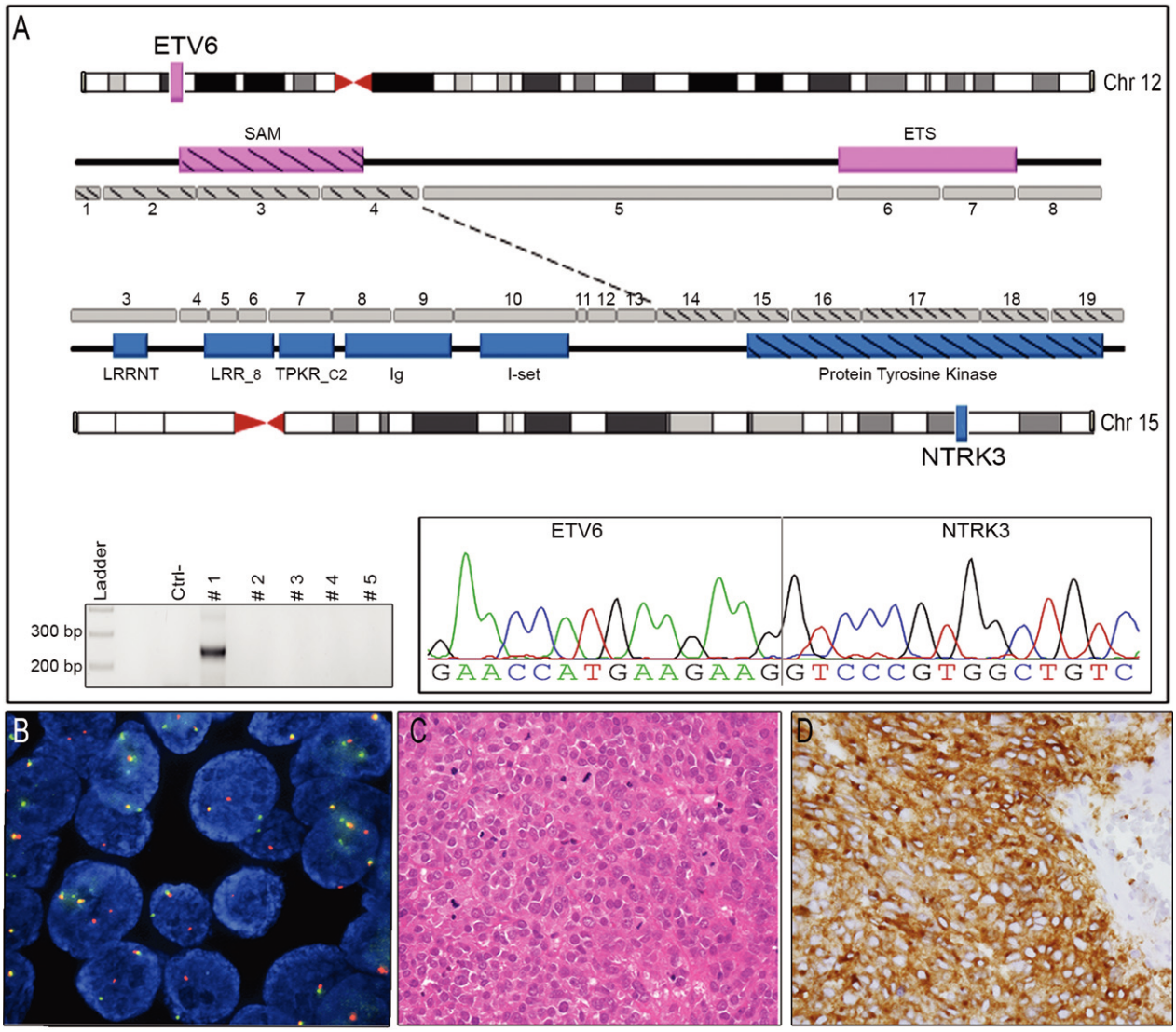

Figure 1. *ETV6–NTRK3* positive GIST. (A) (Top) Schematic representation of the *ETV6–NTRK3* fusion, involving exon 4 of *ETV6* (chromosome 12) and exon 14 of *NTRK3* (chromosome 15), identified in a 'quadruple-negative' rectal GIST: protein-coding exons and PFAM domains retained in the chimera are marked with a diagonal pattern; (bottom) RT–PCR of the five GISTs profiled by RNA sequencing confirmed the presence of the fusion transcript in the index case (#1); Ctrl-, negative control; chromatogram displays the junction between *ETV6* and *NTRK3*. (B) FISH assay with break-apart probe demonstrated rearrangement of the *ETV6* locus at 12p13 in the index case. (C) The 'quadruple-negative' rectal GIST was hypercellular throughout and featured epithelioid morphology and remarkable mitotic activity. (D) Tumour cells diffusely expressed CD117

The index case was a 44 year-old man who was admitted to the surgical department of Treviso General Hospital in autumn 2011 for perineal pain and rectal bleeding. The patient had a history of idiopathic pulmonary embolism (6 years earlier) and chronic thyroiditis. Rectal examination and colonoscopy revealed the presence of an ulcerated mass located in the posterior wall of the rectal ampulla (8 cm from the anal margin), which, according to MRI, involved the submucosa. Diagnosis of GIST was made based on pathological examination of the tumour biopsy. Analysis of the surgical specimen revealed a 5 cm nodular tumour of the rectal wall, with well-defined pushing margins and no interruption of the pseudocapsule. Microscopically, the tumour was hypercellular throughout, with an epithelioid morphology and a moderate degree of nuclear atypia. The mitotic index was high, with up to 34 mitoses/5 mm^2 (Figure 1C). Foci of neoplastic necrosis were present. The tumour showed strong and diffuse expression of DOG1 and CD117 (Figure 1D) but was negative for S100, synaptophysin, chromogranin and desmin. The tumour was then classified as a high-risk GIST according to AFIP criteria. Molecular analysis failed to detect mutations in *KIT*, *PDGFRA* or *BRAF*. Moreover, the tumour retained SDHB expression, ruling out SDH complex inactivation. Based on the poor response of mutation-negative GISTs to Imatinib, no adjuvant therapy was prescribed after surgery. The patient has been disease-free since surgery (44 months) and is currently followed with periodic colonoscopy examinations and abdominal–pelvic MRI scans.

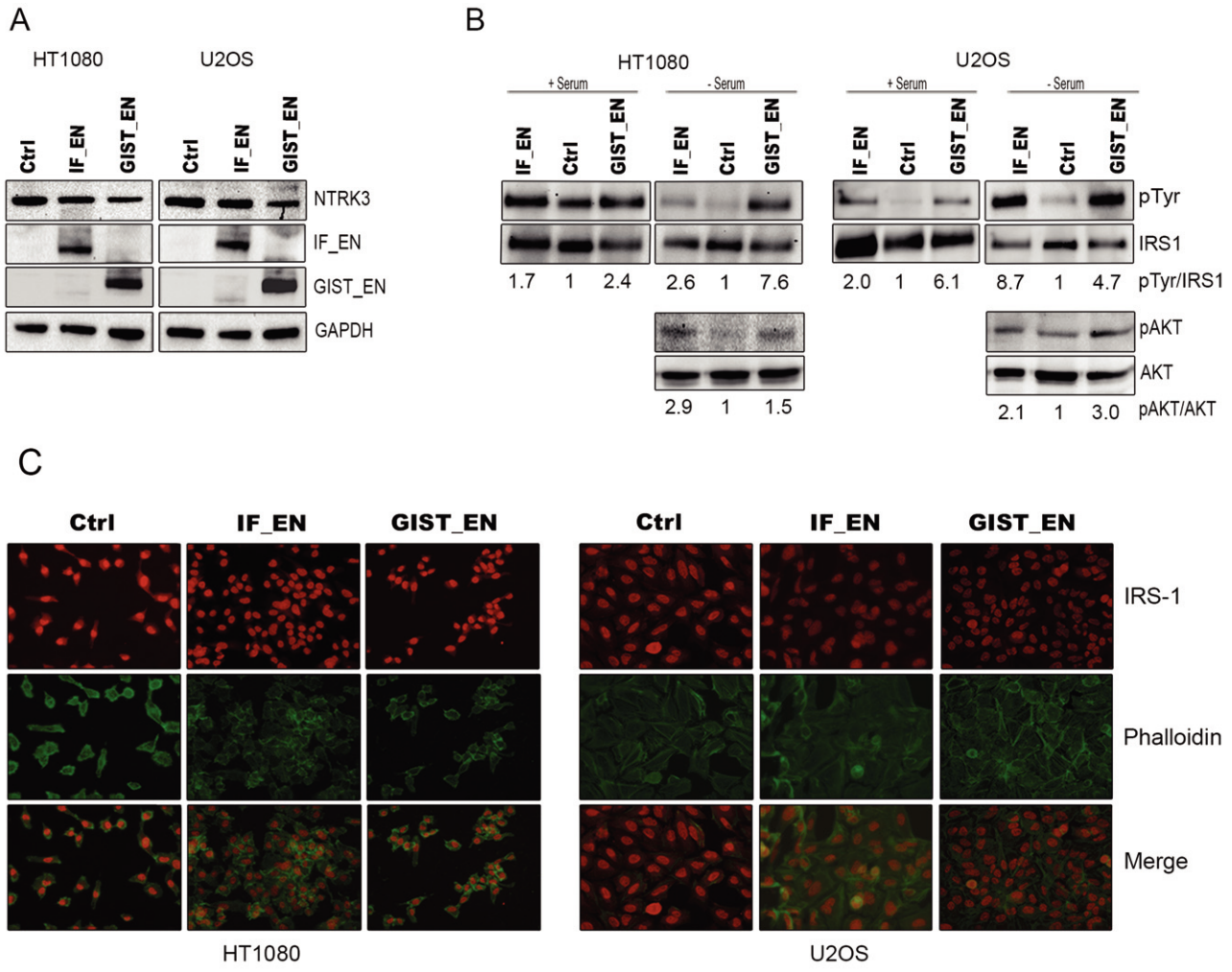

Figure 2. The GIST *ETV6–NTRK3* chimera impinges on the IRS1 pathway. (A) Immunoblot of (left) HT1080 and (right) U2OS cells engineered to ectopically express the infantile fibrosarcoma-associated *ETV6–NTRK3* chimera (IF_EN) or the *ETV6–NTRK3* variant detected in GIST (GIST_EN): empty vector was used as a negative control (Ctrl). (B) (Top) Cells were grown in the presence (+) or absence (–) of serum for 16 h, lysed and then immunoprecipitated with IRS1 polyclonal antibody; after SDS–PAGE, blots were first probed with anti-phosphotyrosine, followed by anti-IRS1; the amount of phosphorylated IRS1 was calculated as the pIRS1:total IRS1 ratio; (bottom) immunoblot for AKT phosphorylation at Ser 473 under serum deprivation: the amount of activated AKT was calculated as the pAKT:total AKT ratio. (C) Immunofluorescence staining for IRS1 (red) and phalloidin (green)

To determine the frequency of *ETV6–NTRK3* fusion in GIST, 26 additional primary tumours were screened for *ETV6* chromosome rearrangement by FISH analysis. In the light of clinicopathological characteristics of our index case, this series was tentatively enriched for mutation-negative GISTs and GISTs located in the rectum (see supplementary material, Table S1). Beside the index case, FISH failed to highlight additional *ETV6* rearrangements, indicating that the *ETV6–NTRK3* translocation is very likely an uncommon event that might identify a rare group of GISTs featuring peculiar clinicopathological characteristics.

Biological and pharmacological implications of the *ETV6–NTRK3* chimera

We then sought to explore the possible clinicotherapeutic implications of *ETV6–NTRK3* translocation in GIST. The infantile fibrosarcoma EN chimera has been shown to bind directly to and phosphorylate IRS1, the major substrate of the insulin-like growth factor 1 receptor (IGF1R) [17,19], thus sustaining cell survival and neoplastic transformation via the Ras–Erk1/2 and PI3K–Akt pathways [20]. Intriguingly, IGF1R signalling has been implicated in the transformation of mutation-negative GISTs, although the mechanism is still unclear [21], and IGF1R-targeted therapy for these tumours is being evaluated in clinical trials [22,23]. We hypothesized that the expression of *ETV6–NTRK3* may trigger the IGF1R signalling cascade in a fraction of GISTs. To test this hypothesis, we assessed whether the GIST_EN variant was capable of activating IRS1. To this end, HT1080 and U20S cell lines were engineered to ectopically express the EN chimeras (Figure 2A). Like the canonical IF_EN, GIST_EN also induced IRS1 phosphorylation (in both the presence and absence of serum) and, in turn, activated Akt, as revealed by increased Ser-473 phosphorylation (Figure 2B).

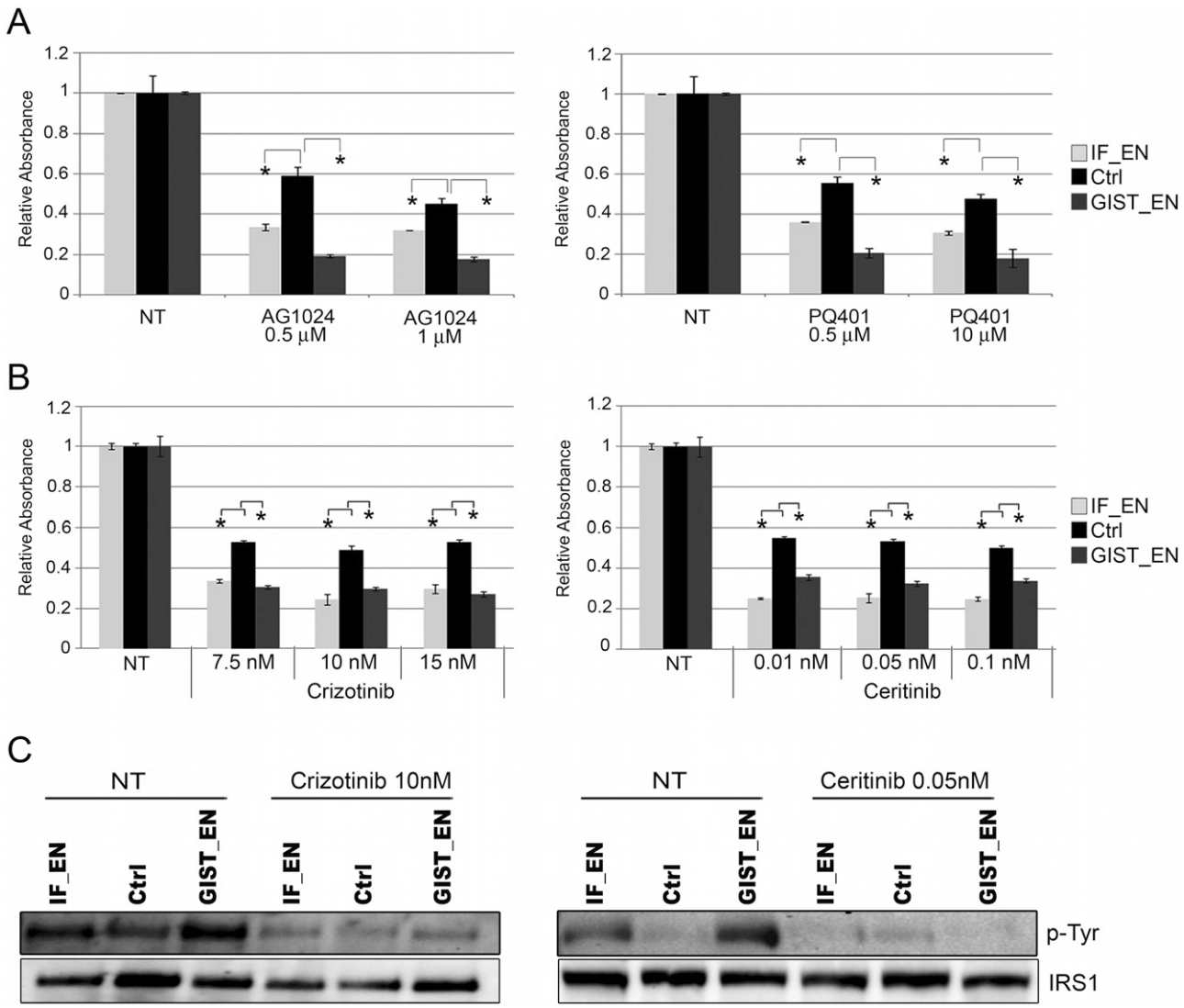

Figure 3. *ETV6–NTRK3* chimeras sensitize cells to IGF1R and ALK inhibitors. Sulphorhodamine-B (SRB) cell viability/citotoxicity assay, showing dose–response plots to chemical inhibitors in U2OS cells ectopically expressing EN chimeras (48 h treatment); data shown are mean ratio of treated vs untreated (NT) samples ± 95% CI; *statistical significance ($p < 0.05$). (A) Efficacy of (left) AG1024 and (right) PQ401 IGF1R-inhibitors. (B) Efficacy of (left) Crizotinib and (right) Ceritinib ALK inhibitors; EN-positive cells showed increased sensitivity to both IGF1R and ALK inhibitors. (C) Western blot of IRS1 immunoprecipitates in U2OS cells highlights the inhibitory effect of ALK inhibitors on phospho-IRS1 activation

In addition to its function as cytosolic adaptor of the IGF1R signal transduction pathway, IRS1 has been shown to shuttle to the nucleus where it contributes to malignant transformation by inducing cyclin D1, c-myc and beta-catenin expression and affecting DNA repair [24]. Subcellular fractionation (not shown) and immunofluorescence analyses in HT1080 and U20S cells indicated that *ETV6–NTRK3* chimeras enhance IRS1 nuclear localization (Figure 2C).

Overall these data support the notion that the *ETV6–NTRK3* gene fusion may play a role in the development of a fraction of GISTs by both promoting activation of the IGF1R downstream cascade and the alternative nuclear IRS1 pathway.

To probe the role of *ETV6–NTRK3* in IGF1R-mediated pathway activation, cells were treated with IGF1R inhibitors (AG1024 and PQ401). As reported in Figure 3A, expression of either EN chimera sensitized cells to IGF1R inhibition, as revealed by SRB assay. In addition, recent reports pointed to the *ETV6–NTRK3* fusion product as a target of the ALK inhibitor Crizotinib [25,26], which acts by halting NTRK3 autophosphorylation. Indeed the GIST_EN variant also significantly sensitized cells to Crizotinib (Figure 3B left) as well as to Ceritinib (Figure 3B right), another FDA-approved ALK inhibitor, at nanomolar potency. These responses were associated with reduced IRS1 phosphorylation (Figure 3C), corroborating the notion that these compounds hamper *ETV6–NTRK3*-mediated pathway activation.

In summary, we here provide evidence of involvement of *ETV6–NTRK3* fusion in a GIST case. To the best of our knowledge, this is the first study describing an oncogenic fusion transcript in GISTs. Our report expands the

spectrum of neoplasms associated with *ETV6–NTRK3*, unveils a possible mechanism of activation of IGF1R downstream signalling in mutation-negative GISTs and discloses novel therapeutic avenues for EN-positive GISTs.

The fusion was identified in a single case belonging to a rare subset of 'quadruple-negative' (<10% of all GISTs) rectal GISTs (~4% of all GISTs), and rectal GISTs are typically characterized by an aggressive clinical course [27]. Thus, the *ETV6–NTRK3* fusion might mark a subgroup of GISTs with peculiar clinicopathological features. The analysis of a larger tumour series, with a sizable number of cases with these characteristics, will allow more definitive conclusions to be drawn on the actual role of *ETV6–NTRK3* translocation in GISTs.

Acknowledgements

This study was supported by Associazione Italiana Ricerca sul Cancro (AIRC), the Italian Ministry of Health and a Centro di Riferimento Oncologico di Aviano (CRO) 5 × 1000 intramural grant; MB is the recipient of a Fondazione Italiana Ricerca sul Cancro (FIRC) fellowship. We are grateful to PH Sorensen for the kind gift of pMSCV IF_EN.

Author contributions

RM and APDT conceived and supervised the study; MB and SR designed experiments and drafted the article; DG carried out RNA-seq library generation and RT–PCR analyses; MP carried out bioinformatic analyses; MB and DR carried out cloning and *in vitro* experiments; SR and APDT did sample selection and histopathological analyses; LZ and LV performed FISH; and SL carried out clinical data analysis. All authors were involved in writing the paper and had final approval of the submitted and published versions.

Abbreviations

GIST_EN, GIST-associated *ETV6–NTRK3* chimera; IF_EN, infantile fibrosarcoma-associated *ETV6–NTRK3* chimera; quadruple-negative GIST, GIST wild-type for KIT/PDGFRA/BRAF, SDHB-proficient.

References

1. Corless CL. Gastrointestinal stromal tumors: what do we know now? *Mod Pathol Off J US Can Acad Pathol Inc* 2014; **27**(suppl 1): S1–16.
2. Rossi S, Gasparotto D, Miceli R, *et al. KIT*, *PDGFRA*, and *BRAF* mutational spectrum impacts on the natural history of imatinib-naive localized GIST: a population-based study. *Am J Surg Pathol* 2015; **39**: 922–930.
3. Knezevich SR, McFadden DE, Tao W, *et al.* A novel *ETV6–NTRK3* gene fusion in congenital fibrosarcoma. *Nat Genet* 1998; **18:** 184–187.
4. Rubin BP, Chen CJ, Morgan TW, *et al.* Congenital mesoblastic nephroma t(12;15) is associated with *ETV6–NTRK3* gene fusion: cytogenetic and molecular relationship to congenital (infantile) fibrosarcoma. *Am J Pathol* 1998; **153:** 1451–1458.
5. Eguchi M, Eguchi-Ishimae M, Tojo A, *et al.* Fusion of *ETV6* to neurotrophin-3 receptor *TRKC* in acute myeloid leukemia with t(12;15)(p13;q25). *Blood* 1999; **93:** 1355–1363.
6. Setoyama M, Tojo A, Nagamura F, *et al.* A unique translocation of the *TEL* gene in a case of acute myelogenous leukemia with inv(12)(p13q15). *Blood* 1998; **92:** 1454–1455.
7. Forghieri F, Morselli M, Potenza L, *et al.* Chronic eosinophilic leukaemia with *ETV6–NTRK3* fusion transcript in an elderly patient affected with pancreatic carcinoma. *Eur J Haematol* 2011; **86:** 352–355.
8. Tognon C, Knezevich SR, Huntsman D, *et al.* Expression of the *ETV6–NTRK3* gene fusion as a primary event in human secretory breast carcinoma. *Cancer Cell* 2002; **2:** 367–376.
9. Skálová A, Vanecek T, Sima R, *et al.* Mammary analogue secretory carcinoma of salivary glands, containing the *ETV6–NTRK3* fusion gene: a hitherto undescribed salivary gland tumor entity. *Am J Surg Pathol* 2010; **34:** 599–608.
10. Leeman-Neill RJ, Kelly LM, Liu P, *et al. ETV6–NTRK3* is a common chromosomal rearrangement in radiation-associated thyroid cancer. *Cancer* 2014; **120:** 799–807.
11. Alassiri A, Rola A, Lum A, *et al. ETV6–NTRK3* is expressed in a subset of ALK-negative inflammatory myofibroblastic tumors: case series of 20 patients. *Bone Soft Tissue Pathol Lab Invest* 2015; **95:** 12–30.
12. Nicorici D, Satalan M, Edgren H, *et al.* FusionCatcher – a tool for finding somatic fusion genes in paired-end RNA-sequencing data. Report No. 011650, 2014 [cited 6 August 2015]: http://biorxiv.org/lookup/doi/10.1101/011650
13. Iyer MK, Chinnaiyan AM, Maher CA. ChimeraScan: a tool for identifying chimeric transcription in sequencing data. *Bioinforma (Oxf Engl)* 2011; **27:** 2903–2904.
14. Piccinin S, Tonin E, Sessa S, *et al.* A 'twist box' code of *p53* inactivation: twist box–p53 interaction promotes *p53* degradation. *Cancer Cell* 2012; **22:** 404–415.
15. Brenca M, Rossi S, Lorenzetto E, *et al. SMARCB1–INI1* genetic inactivation is responsible for tumorigenic properties of epithelioid sarcoma cell line VAESBJ. *Mol Cancer Ther* 2013; **12:** 1060–1072.
16. Gasparotto D, Rossi S, Bearzi I, *et al.* Multiple primary sporadic gastrointestinal stromal tumors in the adult: an underestimated entity. *Clin Cancer Res Off J Am Assoc Cancer Res* 2008; **14:** 5715–5721.
17. Morrison KB, Tognon CE, Garnett MJ, *et al. ETV6–NTRK3* transformation requires insulin-like growth factor 1 receptor signaling and is associated with constitutive IRS-1 tyrosine phosphorylation. *Oncogene* 2002; **21:** 5684–5695.
18. Kang G, Yun H, Sun C-H, *et al.* Integrated genomic analyses identify frequent gene fusion events and VHL inactivation in gastrointestinal stromal tumors. *Oncotarget* 2015; PMID: 25987131 [Epub ahead of print].
19. Lannon CL, Martin MJ, Tognon CE, *et al.* A highly conserved NTRK3 C-terminal sequence in the *ETV6–NTRK3* oncoprotein binds the phosphotyrosine binding domain of insulin receptor substrate-1: an essential interaction for transformation. *J Biol Chem* 2004; **279:** 6225–6234.
20. Tognon C, Garnett M, Kenward E, *et al.* The chimeric protein tyrosine kinase *ETV6–NTRK3* requires both Ras–Erk1/2 and PI3–kinase–Akt signaling for fibroblast transformation. *Cancer Res* 2001; **61:** 8909–8916.

21. Beadling C, Patterson J, Justusson E, *et al.* Gene expression of the IGF pathway family distinguishes subsets of gastrointestinal stromal tumors wild-type for *KIT* and *PDGFRA*. *Cancer Med* 2013; **2:** 21–31.
22. Arnaldez FI, Helman LJ. Targeting the insulin growth factor receptor 1. *Hematol Oncol Clin North Am* 2012; **26:** 527–542.
23. Lasota J, Wang Z, Kim SY, *et al.* Expression of the receptor for type 1 insulin-like growth factor (IGF1R) in gastrointestinal stromal tumors: an immunohistochemical study of 1078 cases with diagnostic and therapeutic implications. *Am J Surg Pathol* 2013; **37:** 114–119.
24. Reiss K, Del Valle L, Lassak A, *et al.* Nuclear IRS-1 and cancer. *J Cell Physiol* 2012; **227:** 2992–3000.
25. Taipale M, Krykbaeva I, Whitesell L, *et al.* Chaperones as thermodynamic sensors of drug–target interactions reveal kinase inhibitor specificities in living cells. *Nat Biotechnol* 2013; **31:** 630–637.
26. Roberts KG, Li Y, Payne-Turner D, *et al.* Targetable kinase-activating lesions in Ph-like acute lymphoblastic leukemia. *N Engl J Med* 2014; **371:** 1005–1015.
27. Huynh T-K, Meeus P, Cassier P, *et al.* Primary localized rectal/pararectal gastrointestinal stromal tumors: results of surgical and multimodal therapy from the French Sarcoma Group. *BMC Cancer* 2014; **14:** 156.

SUPPLEMENTARY MATERIAL ON THE INTERNET

The following supplementary material may be found in the online version of this article:

Table S1. Molecular and clinicopathological features of the GIST series analysed in this study

Table S2. *ETV6–NTRK3* alternative chimeras identified in different tumour types (from Cosmic Database; http://cancer.sanger.ac.uk/cosmic)

Table S3. Detailed information about antibodies employed in the study

Table S4. Potential fusions involving protein-coding genes and supported by at least one spanning and two encompassing reads identified in the five 'quadruple-negative' GISTs analysed